



Politecnico
di Torino

ScuDo

Scuola di Dottorato - Doctoral School
WHAT YOU ARE, TAKES YOU FAR

Doctoral Dissertation

Doctoral Program in Metrology (34th cycle)

Instrumentation for daily-life brain-computer interfaces

**Applied metrology for assistive devices relying on
steady-state visually evoked potentials and motor
imagery**

By

Antonio Esposito

Supervisor(s):

Prof. Marco Parvis, Supervisor

Prof. Pasquale Arpaia, Co-supervisor

Doctoral Examination Committee:

Prof. Claudio Narduzzi (Reviewer), University of Padua

Prof. Mauro D'Arco (Reviewer), University of Naples Federico II

Prof. Guido Perrone (President), Polytechnic of Turin

Prof. Vincenzo Ferrari, University of Pisa

Prof. Fabien Lotte, University of Bordeaux

Politecnico di Torino

2022

Declaration

I hereby declare that, the contents and organization of this dissertation constitute my own original work and does not compromise in any way the rights of third parties, including those relating to the security of personal data.

Antonio Esposito
2022

* This dissertation is presented in partial fulfillment of the requirements for **Ph.D. degree** in the Graduate School of Politecnico di Torino (ScuDo).

to those who strive for a better future

心臓を捧げよ

Acknowledgements



At the end of this doctoral journey, an unusual for many reasons, I need to thank so many people. It may appear obvious to thank supervisors first, but I do so genuinely: it is only thank to them if I am an aspiring academic, they taught me how to be concrete in a world that speaks too much, and they passed on their love for metrology. Although I usually call them "professors" for the respect they deserve, this time I want to thank them for the humanity behind their role: thank you Pasquale Arpaia, thank you Marco Parvis. I would also like to thank Professor Coyle, whom I have been knowing since the beginning of this journey. I had the pleasure of meeting him in person recently, and I thank him for having welcomed me with great affection into his group.



Ringrazio tutti i colleghi, presenti e passati, che condividendo anche solo un pezzo di strada con me mi hanno lasciato qualcosa e sono parte di ciò che sono oggi. In particolare voglio ringraziare Mirco, Giovanna, Federica, Isabella e Luigi per i momenti trascorsi da amici più che da colleghi. Ringrazio Antonella, per la sua dolcezza e la sua professionalità. Ringrazio Angela, che affronta tutti i problemi con una passione da cui ho solo da imparare. Ringrazio Nicola, perché nel confronto con lui ho sempre avuto occasioni di crescita. Ringrazio Egidio, che nonostante i mille impegni mi offre sempre un supporto profondo e sincero. Ringrazio Umberto, che per primo mi ha fatto avvicinare al mondo delle misure grazie alla sua grande capacità tecnica. Ringrazio infine tutti quei colleghi che non riesco a citare qui, ma che fanno il loro lavoro con passione, disciplina, e soprattutto onestà.

Desidero ringraziare quelli che sono miei amici da sempre: Antonio, Genny, Ferdinando, Vincenzo, Ilaria, e Chiara, per i momenti di spensieratezza di cui tanto c'è bisogno quando si diventa grandi. Desidero poi ringraziare profondamente la mia famiglia, che è il mio porto sicuro in ogni tempesta, ed in particolare mio padre, mia madre, Francesco, Gennaro e Marianna. Desidero infine ringraziare Sabatina, che mi è stata vicinissima in quest'ultimo intenso periodo anche quando ci separavano troppi chilometri. Se è vero che ho concluso bene, lo devo anche a lei.



In ultimo spendo qualche parola influenzata dal lato nerd che in un ingegnere raramente manca. Niente paura, non scrivo in giapponese, non sono capace purtroppo. Ne "l'attacco dei giganti", il comandante Erwin Smith incitava i membri del corpo di ricerca con la frase 心臓を捧げよ (Shinzō o sasageyo), letteralmente "offrite i vostri cuori". Al di là dello stile violento che caratterizza la serie, il significato profondo di questa frase è da capire nel suo contesto: mentre esseri giganteschi divorano il genere umano, il desiderio di Erwin è quello di scoprire "la verità che si cela dietro questo nostro mondo", arrivando anche ad offrire la vita per il desiderio di conoscere e, soprattutto, per il bene dell'umanità. Ringrazio quindi tutti quelli che lottano per un mondo migliore, non con le armi e con la guerra, ma mettendo sé stessi in tutto quello che fanno. Spero di riuscire a farlo anch'io in prima persona, seguendo la strada che mi indica sempre il comandante del mio commando (di ricerca, sia ben chiaro):

- "non problemi, ma opportunità"
- "non preoccupazioni, ma azioni"
- "un passo alla volta, un piede dietro l'altro"

a cui aggiungo la regola d'oro del Vangelo che mi accompagna da sempre

- "fate agli altri ciò che vorresti fosse fatto a voi"

Abstract

This doctoral work focuses on bringing brain-computer interface technologies closer to daily life by means of a metrological approach. In particular, applied metrology appears essential because these interfaces enable non-muscular communication through the measurement of brain signals, and even because their components must be characterized to fully understand system operation. Many challenges are associated with daily-life applications, namely non-invasive measurement, wearability, portability, user friendliness, and low cost. Thus, electroencephalography was a key choice for designing the systems. The usage of few acquisition channels was also considered, and proper processing had to be studied to detect the phenomena of interest. Finally, consumer-grade equipment was taken into account in the implementation. Two paradigms were investigated: a reactive interface relying on steady-state visually evoked potentials, and an active paradigm relying on motor imagery.

A metrological characterization of the consumer-grade equipment was first proposed. Characterization results show that a low-cost electroencephalograph can be successfully employed due to its linearity and limited gain error. Also, for the reactive paradigm, the characterization of flickering icons generated by smart glasses demonstrated that the harmonic content of such stimuli can be meaningfully different from the nominal one. This characterization pointed out that their harmonic content should be carefully measured before addressing the brain response to flickering lights, though exploiting commercial smart glasses in the operation of a reactive brain-computer interface is feasible.

Next, a wearable system based on steady-state visually evoked potentials was built by integrating commercial augmented reality glasses with the low-cost electroencephalograph. The power spectral density associated with the evoked potentials was measured to detect the neural phenomena of interest. An experimental campaign conducted with 20 subjects pointed out that mean classification accuracy among

subjects can be as high as 95 % at 10 s stimulation time, but it drops to about 75 % when a 2 s stimulation is considered. Thus, the system can be accurate enough for some industrial and healthcare applications, but further studies are needed to increase the system speed.

Finally, a wearable system based on motor imagery was proposed. A filter bank common spatial pattern algorithm was used for classification. The minimum number of acquisition channels needed for the detection was investigated. Results demonstrated that a single channel is not suitable for the detection of motor imagery, but the number of channels can be as low as three. The exact channels to exploit do depend on the involved tasks and subjects and they can vary from session to session. Nonetheless, the locations of selected channels were compatible with the sensorimotor area reported in the scientific literature. It was then noted that the wearability and portability of such a system could be still achieved, but neurofeedback had to be considered to improve motor imagery detection. The proposed system adopted an extended reality multi-sensory feedback. Results of a further experimental campaign conducted with eight subjects demonstrated that neurofeedback is effective in improving the detection of motor imagery for most subjects. The mean classification accuracy resulted about 70 %, which is an empirical threshold for an acceptable performance of motor imagery brain-computer interfaces.

As a whole the work demonstrated that reactive brain-computer interfaces are close to daily-life applications, though they still deserve an engineering phase, while research and development is needed for an active interface relying on motor imagery, and a deeper study of neurofeedback has been addressed for enhancing the detection of motor-related neurophysiological phenomena.

Contents

Acknowledgement	iii
Abstract	vi
List of Figures	xi
List of Tables	xviii
Introduction	1
1 Brain-computer interface technology	4
1.1 Brief history	5
1.2 Taxonomy of BCI systems	8
1.3 Measurement system	11
1.3.1 Signal acquisition	11
1.3.2 Features extraction	14
1.3.3 Features translation	16
1.3.4 Applications	18
1.4 Daily-life neural interfaces	18
1.4.1 Requirements	19
1.4.2 Implementations	20
1.4.3 Perspectives	21

2	Designing wearable brain-computer interfaces	23
2.1	Acquisition hardware	24
2.2	Processing approaches	27
2.3	Metrological considerations	30
2.3.1	Signal quality	33
2.4	Electroencephalograph calibration	36
2.4.1	Experimental setup	37
2.4.2	Data analysis	39
2.4.3	Results	42
2.5	Smart glasses characterization	47
2.5.1	Experimental setup	48
2.5.2	Results	51
2.5.3	The human brain as a transducer	55
3	A wearable BCI based on evoked potentials	58
3.1	Steady-state visually evoked potentials	59
3.2	System design and prototyping	61
3.2.1	Augmented reality glasses	63
3.2.2	Single-channel electroencephalography	64
3.2.3	Detection of evoked potentials	66
3.3	System performance	68
3.3.1	Experimental campaign	68
3.3.2	Classification results	71
3.3.3	Latency versus accuracy	76
3.3.4	Comparison with literature	78
3.4	Applications	81

4	A wearable BCI based on spontaneous brain activity	89
4.1	Motor imagery	90
4.2	Filter bank common spatial pattern	92
4.2.1	Filter bank	93
4.2.2	Spatial filtering	94
4.2.3	Features selection	96
4.2.4	Classification of mental tasks	98
4.3	Acquisition channels	102
4.3.1	An attempt with a single channel	103
4.3.2	EEG channels selection	104
4.4	Neurofeedback in MI-BCI	113
4.4.1	Measuring MI-related phenomena	115
4.4.2	Measurement system	121
4.4.3	Experimental results	126
	Conclusions	134
	References	138
	Appendix A Measuring brain activity	152
A.1	Measurement techniques	152
A.1.1	Electroencephalography	153
A.1.2	Magnetoencephalography	154
A.1.3	Functional magnetic resonance imaging	154
A.1.4	Functional near-infrared spectroscopy	155
A.1.5	Other techniques	155
A.2	Measuring the electrical brain activity	157
A.3	Measurand brain signals	159

List of Figures

1.1	The German psychiatrist Hans Berger, inventor of electroencephalography [1].	6
1.2	Francesco Bettella and the Italian team WHi won the BCI race at Cybathlon 2020.	8
1.3	Different degrees of invasiveness for a brain-computer interface, typically related to the brain activity measurement technique.	9
1.4	Measurement scheme of a brain-computer interface	11
1.5	EEG electrodes locations according to the international standard framework 10-20 [2]; the positions <i>Fpz</i> and <i>Oz</i> are highlighted in black at the scalp frontal region and at the occipital region, respectively.	13
1.6	Feature extraction allows for a convenient representation of signals in trying to maximize separability.	14
1.7	Two different datasets in which each element is represented with two features. <i>First row</i> : due to a linear boundary, the best approach must assume linear separability. <i>Second row</i> : the boundary is non-linear, thus a non-linear approach like random forest guarantees better separation [3].	17
2.1	The Olimex EEG-SMT acquisition board with two active dry electrodes connected to channel 1 for a single-channel differential acquisition and a passive dry electrode connected to “drive right leg” (DRL) reference terminal.	25

2.2	The EEG cap Helmate by ab-medica with ten dry electrodes in different shapes and bluetooth connection to ensure high wearability and portability.	26
2.3	The FlexEEG system by Neuroconcise Ltd with seven electrodes needing conductive gel. Bluetooth connectivity ensures portability other than wearability.	27
2.4	Example of a support vector machine with linear kernel. Note that some training data are misclassified, but this is permitted in finding an optimal separation with soft margin [3].	29
2.5	Wearable BCI system based on SSVEP. From left to right: the BT200 AR glasses for stimuli generation, the human user, the Olimex EEG-SMT data acquisition board with dry electrodes.	31
2.6	Comparison between simulated nominal amplitude spectrum of the visual stimuli and measured EEG spectrum corresponding to visual stimulation.	32
2.7	A typical electroencephalographic signal recorded through dry electrodes during experiments with SSVEP. Artifacts related to eyeblinks are clearly visible.	35
2.8	Signal conditioning circuit being part of the Olimex EEG-SMT acquisition board. The connections to the CH1 pins and the DRL are shown, as well as the input ADC line.	37
2.9	Coaxial schematic diagram of the EEG calibration setup realized at the “Istituto Nazionale di Ricerca Metrologica” (INRIM).	38
2.10	Physical realization of the measurement setup for the EEG calibration.	40
2.11	Linearity of the EEG-SMT electroencephalograph measured at 20 Hz (inset: sine wave acquired with for $V_{CAL,rms} = 100 \mu V$).	43
2.12	Magnitude (gain) error of the EEG-SMT electroencephalograph measured at frequencies up to 100 Hz.	44
2.13	Analog conditioning circuitry of the Olimex EEG-SMT board replicated in LTspice for executing a Monte Carlo analysis.	44

2.14	Simulated gain error obtained with a Monte Carlo analysis (gray line and shaded areas) and compared to the measured gain error (black line with bars). The different gray levels correspond to three different probability of occurrence for simulated values.	45
2.15	Relative error between the measured frequencies and the generator ones in percentage.	46
2.16	Schematic diagram of the setup for characterizing the BT-200 optical output, based on an OPT101 amplified photodiode with increased gain [4].	49
2.17	Picture of OPT101-based circuit implemented on a matrix board; note that PD is the OPT101 photodiode.	49
2.18	Measuring the luminous intensity of Epson Moverio BT200 smart glasses nominally flickering at about 10 Hz.	51
2.19	Measuring the luminous intensity of Epson Moverio BT200 smart glasses nominally flickering at about 12 Hz.	52
2.20	Comparing the harmonic amplitudes normalized at the first harmonic for two representative flickering frequencies.	52
2.21	Measuring the luminous intensity of Epson Moverio BT350 smart glasses nominally flickering at 10.7 Hz.	53
2.22	Measuring the luminous intensity of Epson Moverio BT350 smart glasses nominally flickering at 16 Hz.	54
2.23	Comparing the harmonic amplitudes normalized at the first harmonic for two representative flickering frequencies.	54
2.24	Measures associated with Hololens white flickering icon represented in the time domain.	55
2.25	Repeated measures for the flickering icons and corresponding EEG spectra. Mean spectra are compared as well as the standard deviation of the peaks.	57
3.1	Architecture of the AR-BCI system based on steady-state visually evoked potentials.	62

3.2	An example of a signal measured with the Olimex EEG-SMT after placing all the dry electrodes for SSVEP detection. Note that some artifacts related to eye-blinks are present.	70
3.3	Scatter plot of EEG signals in the PSD features domain, associated with 10 s-long stimulation and for a different number of simultaneous stimuli. Both axis are in logarithmic scale.	72
3.4	Scatter plot of EEG signals in the PSD features domain, associated with 2 s-long stimulation and for a different number of simultaneous stimuli. Both axis are in logarithmic scale.	73
3.5	Mean classification versus SSVEP stimulation time (almost coincident with system latency). The standard deviation of the mean is also reported as a shaded area. The "1 stimulus" case is compared with the "2 stimuli" one.	77
3.6	Median classification versus SSVEP stimulation time (almost coincident with system latency). The interquartile range is also reported with a shaded area as a measure of dispersion around the median. The "1 stimulus" case is compared with the "2 stimuli" one.	78
3.7	Classification accuracy versus stimulation time in the four PSD features case.	79
3.8	Median classification versus SSVEP stimulation time (almost coincident with system latency). The interquartile range is also reported with a shaded area as a measure of dispersion around the median. The "1 stimulus" case is compared with the "2 stimuli" one.	80
3.9	AR-BCI system based on SSVEP proposed for accessing data from a wireless sensor network.	82
3.10	Android application diagram for an inspection task in industrial framework: smart transducers and related measures are selected by staring at corresponding flickering icons.	83
3.11	Example of inspection with the wearable SSVEP-BCI: measure selection menu, with flickering white squares for options (as usual in AR glasses, background image is blurred to focus on the selection).	84

3.12	Example of a bridge inspection with smart glasses and a distributed wireless sensor network for measuring static and dynamic mechanical quantities.	85
3.13	AR-BCI system based on SSVEP communicating with a sensor stack through Bluetooth low-energy.	86
3.14	User interface realized in Android for bridge inspection during a load test. In the first activity (up) the smart glasses automatically connect to multiple wireless transducers. In the second activity (middle) the user visualizes environmental data. The third and fourth activities (down left and down right) can be accessed by selecting the data to visualize. The black background is equivalent to transparency when the application is running on smart glasses.	87
3.15	Application of the wearable SSVEP-BCI in the rehabilitation of children with ADHD through a behavioural therapy, as documented in [5].	88
3.16	Distinction between voluntary and involuntary eye-blinks in time domain with an empirically determined threshold.	88
4.1	Map of the primary motor cortex associated with different motor processes according to the anatomical divisions of the body.	91
4.2	Time-frequency representation of EEG patterns associated with three motor imagery tasks and their spatial distribution [6].	92
4.3	Architecture of the filter bank common spatial pattern algorithm for both the train and evaluation phases [7]. The transverse arrows highlight the blocks needing training before their usage.	94
4.4	Classification accuracies for the 12 subjects from dataset 2a and dataset 3a. The six possible classes pairs are considered as well as the four classes case.	101

4.5	Results of motor imagery classification with single channel data from dataset 2a of BCI competition IV. The six possible pairs of classes are considered for the 9 subjects: left hand vs right hand (blue), left hand vs feet (red), left hand vs tongue (yellow), right hand vs feet (magenta), right hand vs tongue (green), feet vs tongue (cyan).	104
4.6	Representation of the channel selection algorithm exploiting the FBCSP approach for the classification of EEG signals.	105
4.7	Classification performance (cross-validation) for progressively selected channels and for each pair of classes.	108
4.8	Classification performance (cross-validation) for progressively selected channels in the four-class problem.	109
4.9	Mean classification performance obtained to validate the respective sequence of the channel selection procedure in the binary classification cases.	111
4.10	Mean classification performance obtained to validate the respective sequence of the channel selection procedure in the four-classes case.	112
4.11	Classification performance in validating the channel sequences found on dataset 3a.	113
4.12	Most predictive information on the scalp for each pair of classes.	113
4.13	Time course of ERDS for subject A03 (session T) from BCI competition IV dataset 2a.	117
4.14	Analysis of MI-related phenomena for subject A03 (session T) from BCI competition IV dataset 2a.	118
4.15	Time course of ERDS for subject A05 (session T) from BCI competition IV dataset 2a.	118
4.16	Analysis of MI-related phenomena for subject A05 (session T) from BCI competition IV dataset 2a.	119
4.17	Time course of ERDS for subject A02 (session T) from BCI competition IV dataset 2a.	119

4.18	Analysis of MI-related phenomena for subject A02 (session T) from BCI competition IV dataset 2a.	120
4.19	Time course of ERDS for subject AE data acquired with FlexEEG while no neurofeedback was provided.	121
4.20	Analysis of MI-related phenomena for subject subject AE data acquired with FlexEEG while no neurofeedback was provided.	122
4.21	Blocks and sub-blocks of the proposed neurofeedback protocol employed in the closed-loop motor-imagery-BCI.	123
4.22	Block diagram of the closed-loop BCI system based on motor imagery and neurofeedback.	124
4.23	Wearable and portable EEG acquisition system employed in experiments with neurofeedback during motor imagery.	125
4.24	Timing diagram of a single trial in the BCI experiment with neurofeedback.	125
4.25	Visual feedback consisting of a mentally-controlled virtual ball.	126
4.26	Wearable and portable haptic suit with 40 vibration motors.	127
4.27	An example of the permutation test for the subject SB1 executed on the time course of classification accuracy in different experimental conditions. The blue curves correspond to the accuracy calculated with true labels, the red curves correspond to the accuracy obtained with permuted labels.	130
4.28	Time varying decoding accuracy associated with motor imagery. The classification accuracy of subject SB1 is compared to the one of a trained subject (A03 from BCI competition IV).	131

List of Tables

3.1	Classification performance of SSVEP-related EEG signals. For each subject, the "1 stimulus" case is compared with the "2 stimuli" case, and the results of a 10 s-long stimulation are compared with a 2 s-long one. Performance is assessed with cross-validation accuracy and its associated standard deviation over 4-folds. The mean accuracy among all subjects is reported too, as well as the accuracy obtained by considering all subjects together (row "all"). The SVM classifier considers two PSD features.	74
3.2	Comparison of classification performance for an SVM classifier considering two PSD features (2D SVM) and one considering four PSD features (4D SVM) of SSVEP-related EEG data. The mean cross-validation accuracies and their associated standard deviations are reported for the "1 stimulus" and the "2 stimuli" case, and a 10 s-long stimulation is compared with a 2 s-long one.	75
4.1	Mean and standard deviation of the cross-validation accuracy obtained on dataset 2a with a Bayesian classifier.	100
4.2	Classification accuracies for the 12 subjects from dataset 2b and dataset3b. Subject-by-subject accuracies are reported for cross-validation (CV) and hold-out (HO).	102
4.3	Comparison between NBPW, SVM, and kNN classifiers for different classification problems. Mean cross-validation accuracy and associated standard deviation were calculated among 9 subjects (dataset 2a) by taking into account all channels.	107

4.4	Mean and standard deviation of the classification accuracy obtained during channel selection, for both 8 and 22 channels.	110
4.5	Mean and standard deviation of the classification accuracy obtained during channel sequences validation.	112
4.6	Questionnaire provided to the participants at each experimental session	133
A.1	Summary of the main characteristics concerning neuroimaging methods.	156

Introduction

Brain-computer interfaces are powerful systems enabling non-muscular communication and control. Such systems rely on the measurement of brain activity, from signals acquisition to processing, thus aiming to associate a meaning to voluntarily or involuntarily modulated brain waves. A main application of these interfaces is the replacement of lost function for people with severe impairments. In addition to that, they can also help in restoring lost natural outputs of the central nervous system, as well as improve, enhance, or supplement the nervous system functions. Hence, brain-computer interfaces can also be employed as assistive devices for people with no impairment. Typical examples are gaming, entertainment, education, or novel tools for workers. Whether these kinds of neural interfaces are sought for able-bodied people or impaired ones, the need to move from laboratory environments to daily-life has recently emerged.

The quest for daily-life brain-computer interfaces has thus led to new challenges and requirements. Surely, the first requirement is to adopt non-invasive neuroimaging techniques to acquire brain activity. This is trivially justified by the need to avoid surgical risks and because of the poor social acceptance of an invasive implant inside the skull. Nonetheless, from a strictly metrological point of view, a relevant drawback is the unavoidable degradation of the signal quality if compared to invasive neuroimaging techniques. Such a degradation is even more present when wearability and portability constraints are considered. For instance, these typically imply that the electroencephalography should be preferred to the magnetoencephalography, although the magnetic field would not be affected by the presence of the skull as it happens for the electric field associated with brain activity. Furthermore, wearability is correlated with the usage of few acquisition channels, thus requiring to extract the neurophysiological phenomena of interest by less available information. On the other hand, portability implies that motion artifacts could greatly affect the acquired

signals, and again this requires a proper processing to remove such artifacts without diminishing the amount of available information about brain activity. Lastly, it is worth mentioning that a user-friendly interface for daily-life applications requires an ergonomic acquisition system and minimal calibration time for the system to work. Overall, the challenges associated with this technological trend are related either to the hardware and software part constituting a brain-computer interface. Nowadays, it is still unclear to what extent BCIs can be ported to everyday life given the degradation of their performance associated with the abovementioned requirements and constraints.

On the road to daily-life brain-computer interfaces, the work reported in this thesis concerns the investigation of two different paradigms. Firstly, a reactive paradigm was investigated, namely a brain-computer interface relying on external stimulation. Steady-state visually evoked potentials were particularly considered as they have been largely investigated in the scientific community with respect to more classical architectures. Next, an active paradigm was considered, whose operation relies on spontaneous and voluntarily modulated brain activity. Notably, motor imagery was exploited, i.e. the act of imagining a movement without actually executing it. Although more interesting because of the possibility to avoid external stimulation, the detection of motor imagery is usually more critical than detecting evoked potentials. A third paradigm could be possibly considered, namely passive brain-computer interfaces relying on the measurement of involuntarily (spontaneously) modulated brain activity. They are indeed very interesting for monitoring the mental state of a user, but such a paradigm goes beyond the scope of the present thesis and it will not be considered in the following.

The thesis has been structured as follows. Chapter 1 gives an essential background on brain-computer interface technology. Its history is briefly retraced from electroencephalography invention to brain-races, then these systems are categorized according to their different characteristics, and finally a general architecture is presented by highlighting the main blocks. The chapter ends by extensively discussing the requirements and reporting some implementation examples pointing to daily-life neural interfaces. Moreover, some perspectives are outlined as possible developments addressed to a near future. Chapter 2 focuses on the design of daily-life interfaces that, with an abuse of notation, are referred to as "wearable". This keyword stresses the need to use little cumbersome hardware for both signal acquisition and actuation, and this is even related to low cost and user-friendly equipment. The chapter aims to

describe devices that can be employed in aiming to realize wearable brain-computer interfaces, as well as the processing approaches that are more suitable for systems with limited computing capability. Then, the chapter also considers metrological aspects, particularly focusing on the characterization and calibration of consumer-grade electroencephalographs, as well as the characterization of smart glasses that have been exclusively employed in the reactive paradigm. After these general chapters, the discussion of Chapter 3 and Chapter 4 is devoted to the specific realization of wearable interfaces based on visually evoked potentials or based on motor imagery, respectively. Both chapters report some considerations on the neurophysiological phenomena of interest, and then they present the design, prototyping, and experimental validation of such systems. Finally, applications are even discussed in order to better justify the relevance of the work presented hereafter.

Chapter 1

Brain-computer interface technology

A brain-computer interface (BCI) is a system allowing direct communication between the brain and the external world. It typically involves communication with or control of electronic devices, and it does not depend on the normal brain output channels [8]. Such a technology relies on measuring brain activity, induced or evoked both involuntarily or voluntarily from the subject [9]. BCIs can exploit a single type of physiological signals, or different types of physiological signals at once (hybrid or multimodal BCIs) [10, 11]. Although most researchers have been focusing on helping people with motor disabilities [12, 13], some companies now offer BCI-based games for healthy users [14, 15], while other research groups are developing applications in fields like human-machine interaction and robotics [16, 17]. It is not rare to call such systems “brain-machine interfaces” (BMI) or even “brain-robot interfaces” (BRI). Though they have different nuances, these terms will be used interchangeably. The European “BNCI Horizon 2020” project [18] identified six application scenarios for BCI systems in relation with the central nervous system (CNS) natural output:

- replace lost natural CNS output;
- restore lost natural CNS output;
- improve natural CNS output;
- enhance natural CNS output;
- supplement natural CNS output;

- research to investigate CNS functions.

Among the possible fields, this thesis mainly focuses on daily-life applications of BCIs. A main objective is to improve wearability and portability of such systems with respect to both signal acquisition and processing, as well as to guarantee relatively low-cost implementations. As case studies, industry and healthcare will be mostly considered.

The current chapter provides an essential background for the ensuing discussion, thus an effort was made to point out the major aspects of this vast technological field. Therefore, the history of BCI is briefly retraced in Section 1.1. A categorization of BCI technologies is attempted in Section 1.2 by taking into account their major attributes. Then, in Section 1.3, a general BCI architecture is introduced and discussed. Finally, Section 1.4 presents some requirements for building daily-life neural interfaces, reports some examples from the literature or from the market, and outlines some future perspectives for BCIs. Then, novel designs are proposed in the following Chapters. The interested reader is also addressed to Appendix A for more details on measuring brain activity, while just the most relevant aspects for wearable BCIs will be treated in the chapters.

1.1 Brief history

In 1924, the German psychiatrist Hans Berger (1873 - 1941) was able to record for the first time the electrical activity of the human brain. After 1924, neurophysiologists recorded a big amount of brain signals in several conditions. In 1929, Berger published a report with data from 76 subjects obtained by introducing electrodes in their skull [19] (Fig. 1.1). Moreover, some researchers focused on voluntarily control of the brain rhythms [20, 21]. The expression “brain-computer interface” (BCI) was first introduced in 1973, with the famous article by Jacques J. Vidal *Toward Direct Brain-Computer Communication* [22]. In particular, his research at University of California demonstrated the feasibility of a communication relying on the information extracted from brain waves. In a further article, *Real-Time Detection of Brain Events in EEG* [23], Vidal showed that, in some situations, it was possible to detect and reliably classify in real-time evoked responses or event-related potentials. The proposed system required a stimuli generator for the elicitation of

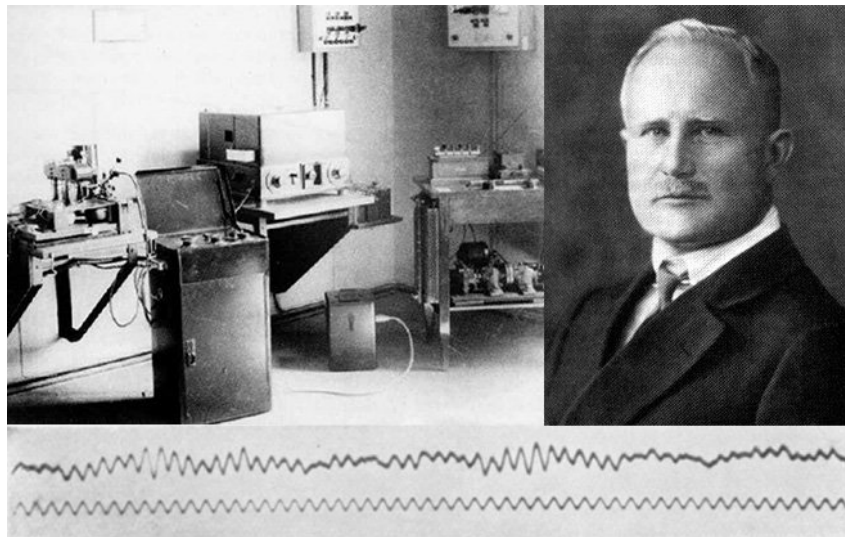


Fig. 1.1 The German psychiatrist Hans Berger, inventor of electroencephalography [1].

brain potentials: an intermittent stimulus pattern shared the display with a fixed maze in which the BCI user had to drive a mobile cursor. The electric potentials to classify were related to four different fixation points, through which the user could move the cursor.

The first international meeting on BCI research was organized by IEEE, the Institute of Electrical and Electronic Engineers, more than 25 years later, in 1999 [12]. The need of a meeting arose from the rapid growth of BCI research groups. Its scope was to review the state of the art of BCI technology at that time and establish common definitions, methods, and procedures. Worldwide, the BCI research groups were more than 20. Essentially, all BCI systems were based on electroencephalography (EEG), and their performance was assessed with a parameter called “information transfer rate” (ITR), whose maximum value was reported to be 5–25 bit/min. It was also highlighted that the central element in each BCI system is the *algorithm translating electrophysiological input from the user into output that controls external devices*. These considerations were mostly confirmed in the second international meeting, held in 2002 [24]. After 30 years from the first proposal of a brain-computer interface, the results were already poor, though advancing technology and more powerful computers were unlocking new horizons. The achievement of higher speeds and greater classification accuracies, both implying greater ITRs, was led back to the need for improvements in signal acquisition and processing, but also to a better user training. It was clear that such improvements depended (and depend

today) on a synergy between different disciplines and on the adoption of common criteria and strategies among the ever-growing research groups.

As mentioned above, the BCI research field has always been related to medical applications, promising solutions for people affected by amyotrophic lateral sclerosis or by the locked-in syndrome [25], as well as new rehabilitation possibilities [26, 27], e.g. in post-stroke recovery. At the same time, BCIs can be used by able-bodied people in leisure activities, such as gaming and entertainment [28], or in other daily-life applications like smartphone control [29]. In the last decade, BCI technologies have seen considerable acceleration in their development, mainly because of the advances in processing algorithms [30] but also because of the progress in neuroimaging techniques [31]. Some BCI paradigms are currently reaching 100 bit/min, though there is a trade-off between such a performance and ease-of-use [32]. For instance, high ITRs are typically reached with a BCI relying on external stimulation, and this might not always be desirable. Furthermore, the ITR is not necessarily an appropriate metric to describe the performance of a BCI system, and the definition of ITR itself has been questioned in some contexts [33]. As technological development goes on, BCI communities are growing over the world, and many researchers involved in the field belong to the “BCI society” founded in 2013. Several scientific disciplines cooperate in research and development, and among them it is worth mentioning neuroscience, psychology, engineering, and computer science. In addition, ethics is another important concern that is accompanying the field. Thanks to conferences and other events, the BCI culture is spreading around the scientific and non-scientific communities. Notably the BCI international meeting is currently held every two years, and the Graz BCI conferences are also held every two years in an alternative manner. It is also worth mentioning that “BCI competitions” were held in the recent past (2000-2008) as an occasion for different research groups to compete and interact, and today these events have still an echo because the datasets originated by them are often considered as benchmarks in the BCI literature [34]. Finally, starting from 2016, a BCI-related contest is held as one of the disciplines of the Cybathlon (Fig. 1.2), an international multi-sport event in which people with disabilities compete by exploiting assistive technologies [35] (Fig. 1.2).

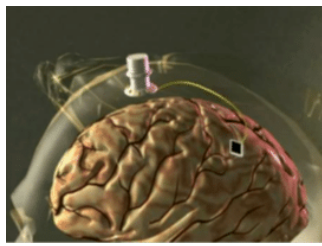


Fig. 1.2 Francesco Bettella and the Italian team WHi won the BCI race at Cybathlon 2020.

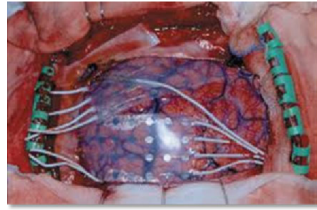
1.2 Taxonomy of BCI systems

It is not easy to establish well-defined categories in sorting out systems or technologies, especially for a field like “brain-computer interfaces” that is complex and continuously evolving. Most probably, such well-defined limits between different things do not even exist. However, the attempt to set those boundaries is an essential task for a better comprehension of the topic. Taxonomy allows to highlight the major differences between various systems and technologies, and this leads to focus on the better solution for a specific problem.

BCI systems can be divided into categories according to several aspects. The first distinction concerns the invasiveness of the technique employed to acquire brain activity (Fig. 1.3). When sensing elements are placed outside the skull, the BCI is categorized as *non-invasive*. This guarantees an easy and safe utilization, but detection reliability is affected by the tissues interposed between the actual signal source and the acquisition system. On the other hand, *invasive* techniques may produce highly reliable control signals with high-speed information transfer. However, there are risks related to the need of surgery for implanting the sensors inside the skull, they are difficult to use, and they potentially lead to infection and long-term viability [11]. These invasive BCIs are often distinguished from *partially invasive* BCIs. The difference is that neural probes are not placed inside the grey matter of the brain, but outside the grey matter though inside the brain, e.g. on the



(a) Representation of an invasive intracortical sensing.



(b) ECoG as an example of partially invasive measurement.



(c) A classic non-invasive technique for measuring brain activity, the EEG.

Fig. 1.3 Different degrees of invasiveness for a brain-computer interface, typically related to the brain activity measurement technique.

cortical surface. It is important to highlight that the difference between these two does not merely reside in the level of risk for the user, but also in different measurement reliability. Indeed, long-term signal variability in invasive BCIs is induced as a result of neuronal cell death, cicatrization, and increased tissue resistance [36]. For these reason, a partially invasive technique like the electrocorticogram (ECoG) reduces the risks and instabilities of an intracortical electrogram while preserving the advantages of a more invasive approach with respect to a non-invasive EEG, such as greater spatial resolution, temporal resolution, and immunity to noise.

BCIs can also be distinguished according to the nature of the signals they use as input [12]. Notably, *endogenous* control modules respond to spontaneous control signals from the user, e.g. a motor imagery task generating sensorimotor rhythms (SMRs), while *exogenous* control modules respond to control signals evoked from the user by a stimulus, e.g. event-related potentials such as the P300 response potential, or visually-evoked potentials (VEPs) [36]. At this level, the distinction is thus between stimulus-related paradigms (exogenous) versus non-stimulus-related (endogenous). If a stimulus is needed, a further distinction can be done among evoked and induced potential. *Evoked potentials* are oscillations that are phase-locked to the stimulus, and they can be detected by analyzing the average among different trials or with a spectral analysis. On the other side, *induced potentials* are not phase-locked to the stimulus, and they are detected by first removing the average component among trials and then analyzing trials in time-frequency [37]. In these same regards, a similar distinction was proposed in [38] between reactive, active, and passive BCIs. In a *reactive BCI*, the brainwaves are produced in response to external stimuli, and this clearly coincides with the ‘exogenous BCI’ case. It is also worth saying that the subject can consciously or unconsciously be exposed to the

external stimuli, and this implies a further distinction between a reactive BCI for control applications versus a monitoring application. Secondly, in an *active BCI* the subject voluntarily produces a modulation of the brain waves for controlling an application, independently of external events. Finally, in a *passive BCI* the user does not directly and consciously control his/her electrical brainwaves. Such paradigms are generally used for monitoring the user's mental state. The last two BCI types can be associated with the 'endogenous BCI' category, but of course some aspects of their are better focused.

Another distinction is made between dependent and independent BCIs [8]. A *dependent* BCI relies on other normal brain outputs, usually a muscular activity. An example could be a BCI based on the steady-state visually evoked potential (SSVEP). This evoked potential is generated in the occipital area of the brain when the user stares at a flickering icon. In order to work, this usually requires that the user moves his/her eyes to gaze at a specific icon. On the other side, an *independent* BCIs provide a completely new communication channel, because it does not depend on already existing pathways. As an example, P300 is again a visually evoked potential, but it only requires that the user is concentrated on an icon without moving the eyes. The potential is evoked in relation to the flashing of this icon [39]. To make things more confusing, a study suggested that also SSVEP can be used without a gaze shift, and in that case such a system would be considered as an independent BCI [40].

Finally, a last functional distinction is worthily mentioned. A BCI system is *synchronous* if the interaction between the user and the system occurs over a specific period of time, which has also a well-defined initial time (referred to as 'cue'). Therefore, only in that period the device can receive biomedical signals and process them. Instead, if the user wants to interact at any time, there is the need of an *asynchronous* BCI, which is able to react to the mental activities coming from the patient at any time without any restrictions. The last aspect is quite important in daily-life applications, but the asynchronous mode clearly introduces more difficulties because the system must be not only capable of discriminating "a what" but also "a when" [41].

1.3 Measurement system

A general purpose BCI architecture is represented in Fig. 1.4. Signals are acquired from the user's head, and then they are processed to retrieve a command for the application of interest. The signal processing can be divided in two stages: (i) features extraction derives a meaningful synthetic description of the signals, and (ii) features translation interprets them by giving back an output command. A feedback is finally given to the user depending on the application.

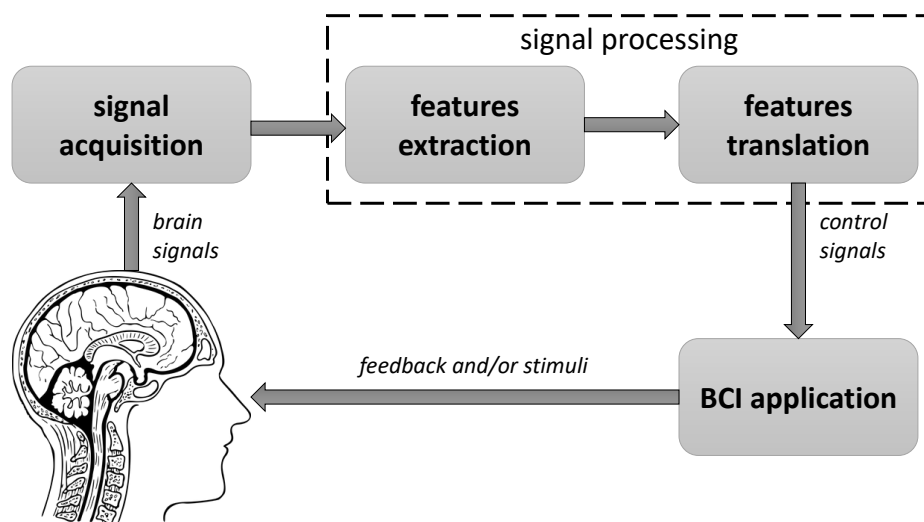


Fig. 1.4 Measurement scheme of a brain-computer interface

In the following, the blocks introduced for the BCI architecture are discussed in more detail. The purpose is to give a deeper understanding for the different elements constituting such systems, with a particular emphasis on EEG-based systems. Meanwhile, further details are addressed to the specific implementations that are treated in the next chapters.

1.3.1 Signal acquisition

Different neuroimaging techniques can be used in BCI systems [42]. The electromagnetic activity is typically measured, but there are also other physiological phenomena that are related to brain activity, e.g. blood dynamics. The interested reader is addressed to Appendix A for an extensive discussion of the major neuroimaging

techniques. Concisely, the brain activity is described by means of signals in time domain related to different neurophysiological phenomena. The probes for acquiring these brain signals can be put inside or outside the user's scalp, and they define the degree of invasiveness of the BCI system. In the present thesis, the focus is on electrodes placed outside the scalp to acquire the cortical electrical activity. Therefore, a non-invasive electroencephalography (EEG) will be considered. Despite the enormous advantages that EEG non-invasiveness has for practical applications, its spatial resolution is limited (order of magnitude: 1 cm) because the signals measurable from the scalp surface can only be related to populations of active neurons [43]. This is indeed one of the major factors that are limiting neuronal activity decoding in EEG-based systems. Furthermore, the electrical activity is attenuated by the layers between the brain and the electrodes, thus it is more sensible to noise.

Electrode types can be distinguished between wet and dry, depending on whether conductive gels are used or not at the electrode-scalp contact. Gels used in wet electrodes have the advantage to enhance the contact with the skin and hence improve the signal quality. They are used in conventional systems, notably in clinical application. On the other side, dry electrodes guarantee higher comfort for the user and they are more suitable for daily-life applications. A recent comparison between these two technologies showed that signal quality complies with the needs of clinical applications even when dry electrodes are used [44]. However, particular attention must be made since these electrodes have a poorly stable contact and hence they are more affected by artifacts during recording. For both electrode types, pre-amplification or simply buffering can be considered for impedance matching: such electrodes are thus referred to as "active". In contrast, passive electrodes (no pre-amplification) are simply conductor and they are usually employed for signal referencing. Electrode placing was standardized with the 10-20 system [2]. According to it, locations are identified by considering inter-electrodes distances equal to the 10% or the 20% of the nasion-inion distance. Therefore, the distances are relative to the dimensions of the specific user's scalp. The standard electrode locations of the 10-20 system are shown in Fig. 1.5, where the positions *Fpz* and *Oz* are highlighted as an example. These specific positions will be considered in Chapter 3 for the measurement of visually evoked potentials. It is also worth mentioning that more electrode locations can be identified with the 10-10 system, which defines a finer spatial grid for the placement.

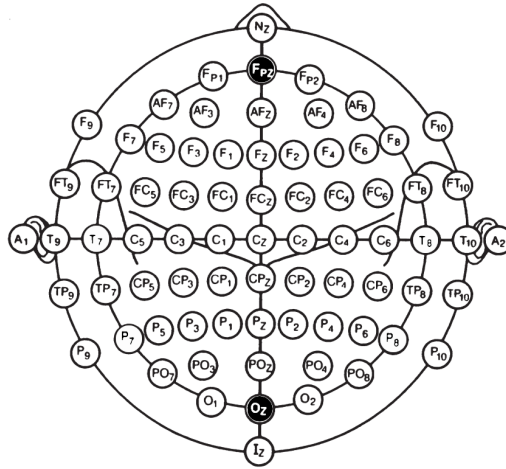
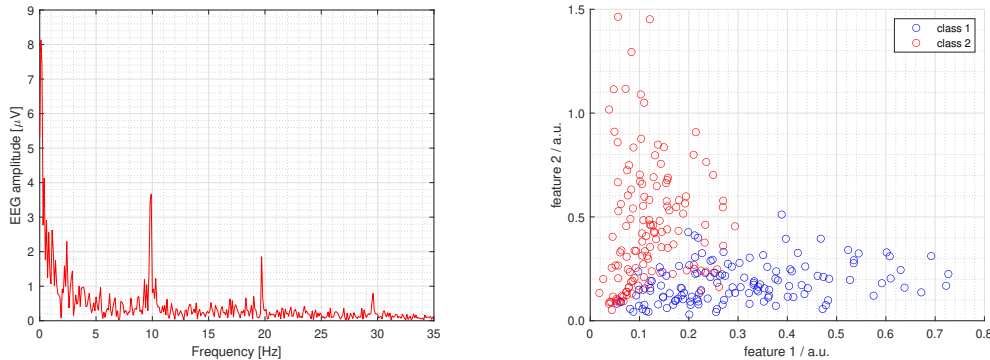


Fig. 1.5 EEG electrodes locations according to the international standard framework 10-20 [2]; the positions Fpz and Oz are highlighted in black at the scalp frontal region and at the occipital region, respectively.

With particular regards to EEG acquisition, signal amplitudes normally span the $0.5 \mu V$ to $100 \mu V$ range [43]. Therefore, amplification is another crucial part of the acquisition system. Together with filtering, it contributes to the signals conditioning needed before voltage acquisition. Frequency bands of interest are typically limited to about 100 Hz, but this higher limit can be lowered depending on the actual case. Clearly, filtering should always consider the only frequencies of interest in trying to maximize the signal-to-noise ratio, which is quite limited in EEG measurements. Moreover, since the advent of digital electronics, the voltage acquisition consists of an analog-to-digital converter, so that the digitized signal can be better processed by following stages and stored in digital memories. In few cases, analog EEG acquisitions are still taken into account. They consist of voltage-controlled deflections of pens writing on a paper tape. Such analog EEG machines are certainly a historical heritage that could be popular among clinicians, but they are definitely not used in an engineering context. In either case, the vast majority of EEG acquisition systems consider multi-channel devices with 64 or more electrodes. Acquisitions are often triggered in order to synchronize measurand signals with an external event. This is typically the case when event-related potentials (ERP) are measured, while, generally speaking, there is the need to provide timing of data points in most BCI applications. More details on the measurand signals are recalled in the Appendix A with respect to classical frequency bands and common paradigms.



(a) Frequency domain representation of a signal. (b) Representation of signals from two different classes in a features domain.

Fig. 1.6 Feature extraction allows for a convenient representation of signals in trying to maximize separability.

Nonetheless, other relevant aspects will be better treated in the following chapters proposing specific BCI systems design.

1.3.2 Features extraction

Once the signals are acquired, the decoding of neural activity requires proper processing. In the first processing step, peculiar features must be extracted from available signals in order to synthetically describe the signals while trying to emphasize the informative content. This is useful for the interpretation of the user intention or mental state. An example of features extraction is represented in Fig. 1.6. When the signal to analyze is represented in frequency domain (Fig. 1.6a), the plot shows some harmonic components that could characterize the signal. However, in aiming to distinguish this signal from another one, a suitable choice could be describing the signal in terms of the power associated with the harmonics. Assuming that these signals can be described with two power features, each one corresponds to a dot in a plane. Such a *features domain* representation can highlight a separability between two classes of signals (Fig. 1.6b).

Since digitized EEG signals are affected by noise, either electrical or biological interferences, pre-processing is often considered before the features extraction. This phase usually consists of spatial and/or frequency filtering and decomposition, so to allow artifacts removal, or at least reduction. They mostly require multi-channel

acquisitions, or even additional signals coming from electrooculography and/or electromyography [45]. For instance, eyes and muscular movements affecting the EEG signals can be identified with a proper decomposition in order to remove the artifacts-related components. Indeed, in doing that, there is also the risk of removing relevant information. After the pre-processing, commonly used features in representing EEG signals are frequency band power features and time point features [30]. Band powers represent the signals for a fixed frequency band and a fixed channel with respect to its mean power or mean energy over time. The time windows considered for this calculation are referred to as “epochs”. On the other hand, time point features concatenate samples from available channels. Band power features are mostly used when the amplitude of EEG rhythms are related to the neurophysiological phenomenon of interest, while time point features aim at describing temporal variations. Such considerations suggest knowledge-driven processing approaches. Notably, exploiting the knowledge about neurophysiological phenomena is desirable when there is a limited amount of available data to train a model for feature extraction. This prevents the risk of overfitting the model on training data, which would lead to poor performance on independent data. For instance, a deep neural networks could be more prone to overfitting since it typically involves many parameters to be determined, while available EEG data could be not sufficient for that. In this context, an interesting research trend is also attempting to explain artificial intelligence, so to validate the training of the features extraction models while providing an interpretation of the measurand signals features. This appears particularly relevant in medical and biomedical applications.

Another crucial step is features selection. This step allows to reduce the number of predictors, which represent the signals under analysis, to a subset of mostly informative features. The aim is again to reduce the risk of overfitting the signal processing model on training data by excluding non-relevant features, thus enhancing the predictive accuracy and the interpretability of the model. Three main selection methods include subset selection, shrinkage, and dimension reduction [3]. Subset selection can consider all possible subsets of features to find an optimal one by relying on an objective function. However, since computational burden is often prohibitive, stepwise selection is typically considered, since it allows to add or remove a single best feature at time. In shrinkage methods, the selection is conducted by shrinking coefficients associated with each feature toward zero: this method inevitably involves the features translation step, in which a functional relationship between features and

model response is attempted. Lastly, in dimension reduction methods, the directions of maximum variance in the features space are typically derived, e.g. with a principal components analysis. It is worth noting that the feature selection step is often integrated within the feature extraction itself, or it can be carried out in conjunction with the training of the features translation model (regression or classification). Broadly speaking, there could be no clear distinction between the blocks of signal processing: the current discussion considers separated blocks for simplicity, but features extraction, selection, and translation can be conducted simultaneously, such as in deep neural networks.

1.3.3 Features translation

In the general BCI architecture discussed here, the last part of signal processing consists of translating the features describing brain signals into control signals for an application. The goal is to derive a functional relationship between the features (predictors) and the output control signals (response), usually by regression or classification. In this thesis, classification is mostly considered, because in most cases there is no logical order among the possible output values. In particular, the measured brain signals can be associated to a specific class between 2 or more choices. Modern classification methods mostly rely on machine learning. As a first classification attempt, a simple approach is typically considered, such as *linear discriminant analysis* (LDA) or *k-nearest neighbors* (KNN) [3]. Successively, a more complex approach can be adopted to enhance the classification according to the features statistical distribution. In this sense one can also speak of *statistical learning*, and common approaches are *decision trees*, *random forest*, or *support vector machine* with linear or non-linear kernels. Fig. 1.7 shows two different datasets represented in bi-dimensional features domains to highlight that the most suitable classification approach depends on the shape of the boundary between different classes. Furthermore, in the last years, novel approaches have been developed starting from the abovementioned classical methods [30]. Notably, adaptive classifiers are used to deal with signal non-stationarity, tensor-based classifiers are used to analyze data in a geometrical space allowing better manipulation, or transfer learning techniques are explored in order to generalize a trained model to data with a different statistical distribution. Deep learning has also attracted many researchers in the BCI field, but it will not be considered hereafter since it typically requires more data.

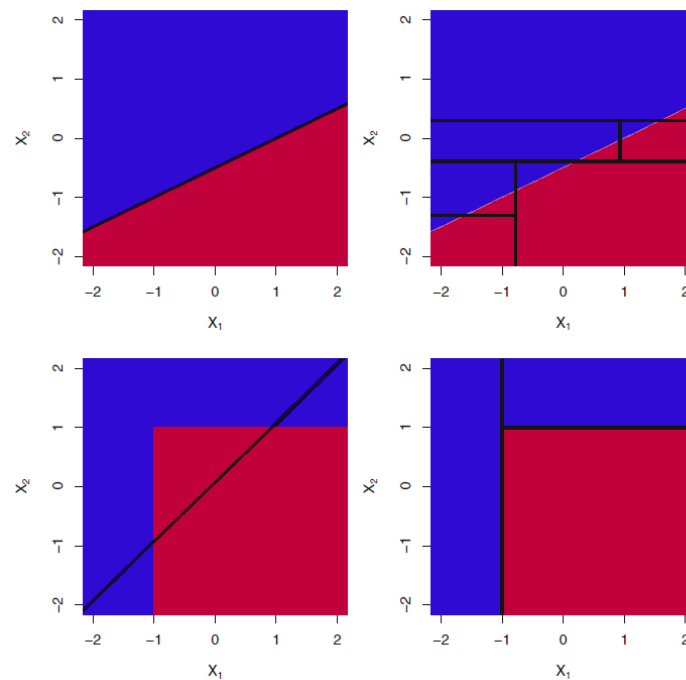


Fig. 1.7 Two different datasets in which each element is represented with two features. *First row*: due to a linear boundary, the best approach must assume linear separability. *Second row*: the boundary is non-linear, thus a non-linear approach like random forest guarantees better separation [3].

Classification performances can be assessed by different metrics depending on the final application. A largely considered parameter is the *classification accuracy*, which is calculated as the ratio between correctly classified signals divided by the total number of classified ones. This accuracy is actually a success rate, and it quantifies how many times the BCI system correctly recognizes the user's intention. Classification accuracy is also a common objective function in training the features selection part of the model. Its calculation requires that test data, independent of the training data set, are available. However, during the training procedure, classification accuracy can be estimated with *cross-validation*. This procedure consists of randomly splitting training data into training and validation subsets, so to estimate the classification accuracy by averaging the accuracies on the validation subsets across different iterations. Cross-validation is thus extensively used in model selection during training and for estimating the model performance on independent data [46].

1.3.4 Applications

BCI technology has been exponentially growing over the current decade. Especially in early researches, this was associated with clinical applications due to the possibility to guarantee alternative communication paths for people with motor disabilities [12]. A direct interface with the brain is meant to help overcoming eventual functional disabilities, and indeed common application examples are the control of a robotic prosthesis or wheelchair [47, 48]. However, the usefulness of BCI has been explored in further fields. In recent years, applications have been identified in gaming and entertainment, in education and training, as well as in industrial contexts [49]. As mentioned before, the European community has addressed the usefulness of BCI systems as assistive devices, not only to replace or restore lost natural outputs of the central nervous systems, but also to improve, enhance, and supplement such natural outputs in able-bodied people [18]. To this aim, many paradigms were developed and they are still studied today, such as the possibility to exploit motor imagery in spontaneous activity-based BCIs, or the possibility to provide an external stimulation for the user and detect the potentials elicited by a voluntary exposure to these stimuli.

In the next chapters, some applications will be presented with respect to either the SSVEP reactive paradigm, i.e. BCIs rely on steady-state visually evoked potentials, and the motor imagery active paradigm, which instead relies on spontaneous brain activity. Though the focus is on fundamental research regarding daily-life neural interfaces, it will be useful to discuss the applications attempted for different case studies. In all cases, the application itself will provide a feedback to the user. This feedback may simply consist of the result of the control action, or it can be a functional feedback that allows the user to better focus the mental task to carry out.

1.4 Daily-life neural interfaces

In the last section, application examples have been reported to better highlight the power of brain-computer interfaces as assistive devices for impaired or able-bodied people. Many efforts have been made to bring BCI technology out of the laboratory [50], and many attempts are still ongoing to make this possible, but applications in everyday life are nowadays limited due to technological and practical issues. The work discussed in this thesis would like to contribute to the spreading of such

neural interfaces in daily-life activities by providing a more accessible technology. Therefore, the present section first discusses some requirements that a daily-life brain-computer interface should have, and then reports some practical considerations devoted to the implementation of such systems. The overall aim is to introduce the reader to the proposal of the thesis, whose general aspects will be treated in Chapter 2, while the details will be extensively discussed in Chapters 3 and Chapter 4 with specific regard to a BCI based on evoked potentials and based on motor imagery, respectively. Some future perspectives are also mentioned at the end of the present chapter.

1.4.1 Requirements

The first requirement for a daily-life neural interface is non-invasiveness. There are two main reasons for such a design choice: the risk of surgical intervention for an invasive device, and its poor acceptance by a large audience of users. Indeed, despite the risks, an invasive BCIs could be essential for users with severe disabilities. However, their employment does not comply with daily-life usage. Though such considerations may sound trivial, it is worth stressing that the choice of non-invasive neuroimaging techniques limits the brain activity measurement. Next, wearability and portability are required. Often these two aspects are confused, and the only keyword "wearable" is employed. Actually, also this thesis refers to the treated systems as "wearable brain-computer interfaces" for the sake of brevity. However, it is to remark that a device may be easy to wear but not portable, and still that a portable device/system may be not wearable. For instance, an electronic device acquiring biosignals may be worn on the head, but it could be not portable if it does not have a battery supply independent from the main supply. The wearability and portability requirements comply with the need to leave the user as free to move as possible, and in general the aim is to provide high user-friendliness to avoid fatigue in long-term usage. These constraints are right away translated into the need for using a lightweight signal acquisition system, as well as into the usage of gel-free electrodes. Notably, these constraints not only affect the hardware part, but they pose some constraints on signal processing too. As an example, motion artifacts diminish the signal-to-noise ratio of the acquired brain signals and proper processing is needed for artifacts removal. Moreover, since wearability typically implies the usage of few channels, classification algorithms can exploit less information than usual brain-

computer interfaces. Another obvious requirement is low cost. Moreover, the BCI system is supposed to exploit as few components as possible to also guarantee easy reproducibility. The requirements stated above justify the large employment of electroencephalography (EEG) as brain activity acquisition technique [42], since it is non-invasive and relatively low-cost, as well as it can be wearable and portable. For the same reasons, EEG was also considered as a main design choice for the systems discussed hereafter.

As a last aspect considered here, there is the possibility to have minimal training (or ideally no training), namely to avoid long periods in which the system must be tuned before the user can use it. Unfortunately, this aspect is critical because of (i) inter-subject variability, which would require the system to be tuned on each specific user, and even more because of (ii) intra-subject variability, which would require a re-tuning every time the user would like to use the device or even during the usage itself. As discussed later on, such issues are harder to address for active BCIs when compared to reactive BCI paradigms. Indeed, when the paradigm relies on spontaneous brain activity, there is the need of a proper training protocol for the user to learn how to voluntarily modulate his/her brain signals, while the detection of evoked potentials is usually more robust. In brief, this thesis will suggest that today's reactive BCIs are far more suitable for daily-life applications since they are performant enough even with little user training, while active BCIs require proper user training protocols and further investigation in transfer learning techniques for addressing algorithm pre-training and signals non-stationarity.

1.4.2 Implementations

The interest in wearable brain-computer interface as daily-life assistive devices has been recently increasing. In a recent review on BCIs used in games [28], the progresses in EEG-based devices for video games were reported by showing that the gaming field greatly contributes to orienting BCI issues and concerns. For instance, since user motivation is crucial in BCI functionality, games are a good research tool for testing daily-life usage. This review highlighted how BCI are far from applications for healthy people, and that, even though the interest in using commercially available devices is increasing, widespread adoption of such a technology has not yet been triggered. Notably, it was also remarked that motor imagery paradigms are not usually implemented with commercial devices. Among commercial devices, indeed

the *Emotiv EPOC* is one of the most exploited in BCI implementations. For instance, a wearable BCI based on steady-state visually evoked potentials was implemented to control a quadcopter [51]. In that work, the attempt was to integrate in a single head mounted device both the EEG recording system and a virtual reality visor, by following the idea that the “smart glasses” can replace the conventional displays of visual stimuli. This concept will be also adopted in part of the work described below [49].

Other commercial devices indeed exist as interesting solutions for daily-life applications. Among them, it is worth mentioning EEG caps from *g.tech*, which are more devoted to clinical applications, and EEG caps from *Neurosky* and *Bitbrain*, whose designs are more prone to user-friendly implementations. Moreover, open hardware solutions are also quite interesting due to the possibility to customize the acquisition system [52]. In these regards, some ongoing studies are trying to assess the quality of signals measured by such commercial devices, and their performance is often compared to EEG systems with wet electrodes, which are de facto standards [53, 44]. In following this trend, Chapter 2 will report the characterization of the *Olimex* EEG acquisition system that has been mostly employed in the development of our wearable BCIs.

1.4.3 Perspectives

Today’s society is data hungry. The possibility to have at our disposal a huge amount of data has disclosed new possibilities in many technological fields, such as image processing. Once the “big data” are properly stored, which is itself a challenge, their analysis is not trivial, but deep learning has demonstrated an extraordinary capability in identifying unimaginable patterns in data, thus giving new insights on many phenomena. Therefore, the interest in adopting novel deep learning techniques even in the BCI field is clearly justified. A model identified by means of deep learning could give many new insights in the complex behaviour of brain activity, thus opening up new possibilities both in terms of more powerful interfaces and more understanding of the human brain. Nonetheless, the application of such techniques to brain signals analysis is still struggling because of the limited amount of structured brain data. Data augmentation and artificial data synthesis are also under study, as well as transfer learning has been recently considered to enable the usage of powerful processing techniques requiring big data. In this context, daily-life usage

of brain-computer interfaces would allow to acquire much more real data related to the brain.

Exiting the laboratory environment will indeed be a big change for the BCI field, and its impact on society is still under discussion. Hence, such a contingency poses both technological and ethical issues. From the technological point of view, the scientific and technical communities already understand the need to have standardized measurement procedures, both for acquisition and processing, without which the mere availability of much brain data would not be enough [54]. Unfortunately, the efforts in this direction are still at an early stage. Another interesting initiative has risen in the last few years in trying to also standardize the processing of brain signals and build a common platform to share and compare the results of different research groups [55]. The standardization needs could indeed benefit from that, but today this is still poorly diffused. Beyond that, the possibility to share standardized procedures is still facing an intensive and hard discussion phase. Lastly, the tremendous potential of brain-computer interfaces clearly poses ethical issues. Although BCI are still very far from “mind reading”, privacy issues are already present in acquiring and storing brain data [56], especially when applications like neuromarketing are sought. Hence, ethics will probably follow and guide the development of BCI technologies even more.

Chapter 2

Designing wearable brain-computer interfaces

Research and development in the BCI field is an ever-growing topic, and it is recently attracting more and more investment from the scientific community. The previous chapter tried to depict a general overview of this technology, and it already underlined the most relevant aspects in aiming to build devices for daily-life applications, which is indeed the focus of this thesis. In particular, the current discussion looks at brain-computer interfaces as a mean for control and communication with the external world. The final scope is to propose BCI technology for daily-life assistive devices, in targeting both able-bodied and impaired people. Therefore, the present chapter will translate the requirements identified for daily-life BCIs into design choices, and it will propose a possible implementation approach. As in every engineering topic, there will be the need to find an optimal balance between the several trade-offs that characterize the BCI technology. The work reported in this thesis has thus attempted to keep the system as performing as possible while concentrating on user-friendliness.

In the following, Section 2.1 will introduce acquisition approaches for recording EEG signals by relying on components off the shelf. Section 2.2 will instead propose processing approaches in trying to balance performances with computational burden. Metrological aspects will be treated in Section 2.3, with particular regard to the importance of properly recording brain signals before they can be processed. The characterization of the employed off-the-shelf instrumentation is then treated

in Section 2.4 and Section 2.5, concerning the electroencephalograph calibration and smart glasses characterization, respectively. The aim is to stress the need for calibration that especially arises when employing commercially available devices. In contrast, laboratory setups typically guarantee higher metrological performances by design. Basing on the results of this chapter, specific implementations will be treated in the following chapters by considering steady-state visually evoked potentials and motor imagery, respectively.

2.1 Acquisition hardware

In designing the signal acquisition for neural activity, the hardware part is mainly concerned. Key aspects for the proposed architectures are indeed high wearability and portability of the head mounted device, and this is especially feasible by choosing electroencephalography (EEG) as acquisition technique (see Appendix A). As a further aspects, also EEG non-invasiveness has already been indicated as essential for everyday-life usability. In addition, user-friendliness is enhanced by adopting a limited number of dry electrodes to place on the scalp. This is in contrast with more classical approaches, where many EEG electrodes are exploited and conductive gels are used to provide a good skin-electrode contact. To translate these design choices into an actual implementation, a low-cost acquisition system relying on components by Olimex Ltd was firstly adopted. In detail, the Olimex EEG-SMT is an acquisition board with up to two differential channels [57] providing signals conditioning for the signals recorded by electrodes. For each channel, two active electrodes are connected to the positive and to the negative input terminal, respectively. These electrodes are active since a buffering circuit is integrated onto the electrode, so to enhance impedance matching between electrode and skin (scalp). Meanwhile, a passive electrode without buffer must be connected to the reference input, which is shared by both channels and serves for common mode noise rejection. Fig. 2.1 shows this acquisition channel in single-channel configuration.

The signals acquired through the electrodes are amplified and filtered before being digitized. According to the circuit schematic by Olimex Ltd, the nominal bandwidth is 0.16 Hz to 59 Hz, while the nominal gain equals 6427.2 V/V assuming that the gain of the second stage is set at 40 V/V through the trimmer (see [57]). After signal conditioning, the ATmega16 microcontroller provides the analog-to-digital



Fig. 2.1 The Olimex EEG-SMT acquisition board with two active dry electrodes connected to channel 1 for a single-channel differential acquisition and a passive dry electrode connected to “drive right leg” (DRL) reference terminal.

conversion. The resulting 10-bit codes are finally sent through UART (USB connector) to an external device, for example a personal computer. Note that when only one differential channel is considered (e.g. CH1), the other channel should be short-circuited. Also note that silver pins were added to one of the active electrodes (noticeable in Fig. 2.1). This helps to overcome the hair and reach the scalp during EEG acquisition, while pins are not necessary for the other electrodes placed on hairless parts of the scalp/body. It is worth remarking that the Olimex EEG acquisition system is open hardware. This makes such a solution very attractive for designers, since they have full control of hardware, firmware, and software. Further details about the internal structure of the Olimex acquisition board will be given in the context of its metrological characterization. In that framework, there will also be the opportunity to better understand the working principles of this EEG amplifier as a representative example of the main principles shared with more sophisticated amplifiers.

The acquisition system has been here introduced in a single-channel configuration for the sake of simplicity, and this configuration was indeed used in recording brain activity related to steady-state visually evoked potentials. Nonetheless, the double-channel configuration was also exploited in some preliminary attempts with motor imagery signals acquisition. Despite that, in motor imagery applications two channels are generally too few. Therefore, using the Helmate by ab-medica [58] was also attempted. This is a wireless device conceived for higher quality EEG (Fig. 2.2)

and it exploits ten dry electrodes to provide up to eight single-ended channels. The electrodes are dry, made of conductive rubber, and they have Ag/AgCl coating. Three different electrode shapes can be installed for an optimal contact with the scalp, and a skin-electrode impedance check is also implemented. Acquired signals are transferred through Bluetooth communication to a personal computer with the proprietary software “Helm8 Software Manager”.



Fig. 2.2 The EEG cap Helm8 by ab-medica with ten dry electrodes in different shapes and bluetooth connection to ensure high wearability and portability.

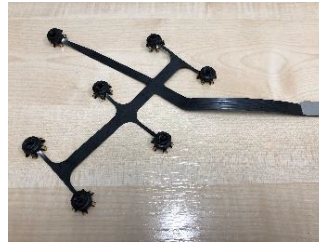
Hence, for the Helm8 EEG cap, the hardware implementation details are not available because of IP protection. In a similar vein, also the software is proprietary. During the thesis work, some experiments were conducted with this device, though no significant results are reported hereafter. However, this kind of solution appeared very interesting for future developments of wearable and portable BCIs.

Lastly, the FlexEEG system from Neuroconcise is here introduced [59]. This wireless device uses Bluetooth communication to guarantee portability other than wearability. It consists of a flexible electronic board for signal conditioning and transmission (Fig. 2.3a), and two possible electrodes configurations can be exploited, for visually evoked potentials and motor imagery, respectively. The sensorimotor electrode array shown in Fig. 2.3b has been considered hereafter for experiments with motor imagery. It comprises seven star-shaped electrodes (Fig. 2.3c) for a configuration with three bipolar channels, i.e. CP3-FC3 and CPz-FCz and CP4-FC4, as well as a reference electrode at the AFz standard location. These placing allows to map the sensorimotor area of the scalp. The usage of conductive gel is suggested to ensure a proper skin-electrode contact during EEG measurement. In standard settings, electrical brain activity is sampled at 512 Sa/s with 16-bit resolution. Data are received in Simulink and online processing is also possible. In terms of user comfort, the only disadvantage is the need of conductive gel, though this solution

was successfully employed in neurofeedback experiments with motor imagery, as discussed in Chapter 4.



(a) flexible board and electrode array



(b) sensorimotor electrode array



(c) star-shaped electrodes

Fig. 2.3 The FlexEEG system by Neuroconceive Ltd with seven electrodes needing conductive gel. Bluetooth connectivity ensures portability other than wearability.

2.2 Processing approaches

Processing acquired signals is unquestionably a crucial step in the measurement of neural activity. The specific approach to adopt strongly depends on the kind of activity to decode. Therefore, in this section the attempt is to discuss some general aspects for the investigated processing approaches, so to give a general overview of them before addressing the details to further sections of this thesis. Especially for motor imagery, processing approaches were first tested on benchmark datasets available online. Then, the more promising ones were adopted to process the data acquired in dedicated experiments.

In describing the processing approaches, features extraction is distinguished from classification as discussed in Chapter 1. In accordance with the taxonomy of a recent review [30], the techniques explored for features extraction fall into the *band power-based* category. As the definition suggests, the basic idea is to retrieve the signals power associated with the frequency bands of interest. In preliminary studies preceding this thesis, algorithms based on the “fast Fourier transform” (FFT) were compared to assess the amplitude of specific harmonic components, notably in measuring evoked potentials [60]. However, as it will be clarified later, a more suitable choice for features extraction was the assessment of power spectral density (PSD). For instance, when the user is stimulated with a flickering icon at 10 Hz, it is well known that a visually evoked potential is elicited in the brain at corresponding

harmonics [61] (see Fig. 1.6a). A band-power based features extraction consists of calculating the PSD in the neighbourhood of 10 Hz and eventually higher harmonics.

Broadly speaking, the band-power features are not only restricted to evoked potentials, but they are also used in other BCI paradigms, such as in motor imagery. Obviously, the frequency bands to consider do depend on the specific case. Differently from the evoked potentials case mentioned above, the harmonics or bands to consider can be hard to determine a-priori for motor imagery. Therefore, machine learning techniques were exploited to identify the functional relation between signals features and signals class. It is also worth noting that, in multi-channel acquisitions, the relation of band-power features across different channels must be considered. Hence, the machine learning approaches adopted in this work process both frequency and spatial information. Notably, by relying on training data, an optimal model is identified in separating different EEG patterns. In the present study, this operation can be decomposed in (i) identifying an optimal projection for spatial information, and (ii) select the best features for the ensuing classification step. Again, the details are addressed to specific system implementations. However, it is to remark that, in order to cope with the minimal training requirement introduced at the end of Chapter 1, the processing approaches described here are mainly *knowledge-based*. This means that the machine learning-based models were built by also integrating neurophysiology notions. On the contrary, a deep learning-like approach would have required much more training data since it is not based on previous knowledge. Such an issue could be mitigated by means of *transfer learning*, which has been also investigated in this thesis work. Ultimately, these processing approaches were also chosen by taking into account their computational burden, which had to be minimized especially when online processing was required.

Clearly, classification was also considered after features extraction as a crucial part of model identification. Nevertheless, it should be noted that the classification itself is useless if features are poorly separable. For this reason, the main focus was on features extraction. Then, the best classification approach could be selected depending on the boundary between different classes in the features space. Considered classifiers were chosen among supervised machine learning approaches. Firstly, “support vector machine” (SVM) [3] was exploited for two-classes discrimination. In the SVM approach, a boundary is identified for optimal separation of training data in the features space. For instance, data in the features space could be separated by a hyperplane (SVM with linear kernel), or the boundary could have a more

complicated shape (SVM with non-linear kernel, e.g. Gaussian or polynomial). The SVM was chosen since it is a very versatile approach: other than a proper kernel, the optimal separation allows for some misclassification in training data (soft margin) to avoid overfitting (Fig. 2.4). In addition to the class, a score can be also assigned to the signals to classify. That class score corresponds to the probability that the assigned class is correct. On an intuitive level, if each measure is represented as a dot in the features space, the farther the dot is from the margin (on the correct side), the higher is the score. This concept is important from a metrological perspective, because it means that an uncertainty can be associated with the assigned class. In this context, it was also interesting to consider another kind of classifier, namely a *Bayesian classifier*. Indeed, for such a case, the concept of class probability is more natural because a Bayesian classifier calculates the probability for a measure to belong to a class and then assigns the most probable class. Among the possible implementations, the “naive bayesian parzen window” (NBPW) classifier was considered [62]. This approach will be better described in discussing the motor imagery-based BCI implementation in Chapter 4. For both classifiers, multi-class extensions are possible when more than two classes are of interest.

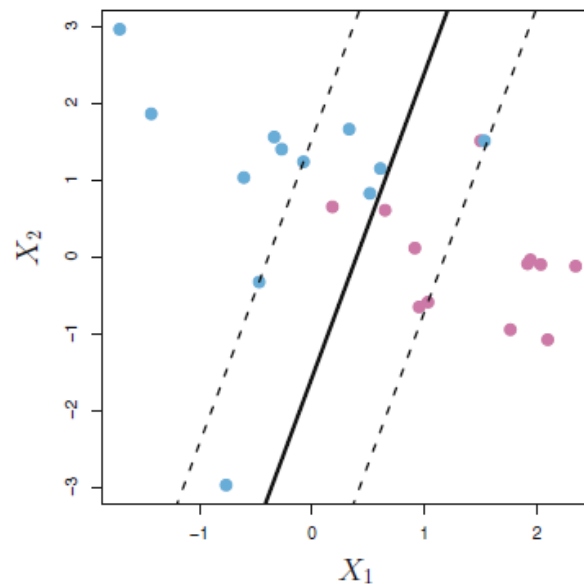


Fig. 2.4 Example of a support vector machine with linear kernel. Note that some training data are misclassified, but this is permitted in finding an optimal separation with soft margin [3].

Other classification approaches considered in developing BCI systems were the “k-nearest neighbors” classifier, “linear discriminant analysis”, or “random forests” [3]. These classifiers usually led to performances compatible with SVM and NBPW, thus they are not explicitly considered later on. However, attempting different approaches confirmed the idea that features extraction plays a major role before the best classifier can be selected and trained.

The performance of a classifier can be assessed by different metrics, and indeed the most common one is classification accuracy. The concept of accuracy in this context refers to the number of successfully classified trials related to the total number of trials to classify. Such a metric is not always the optimal one for assessing the performance of a system, but this is largely considered in the current thesis in order to easily compare the presented results with literature results. In addition to that, Cohen’s kappa has been also considered as it normalizes the accuracy value by the number of classes to discriminate. Finally, the “information transfer rate” (ITR) is another common metric that also involves information about the time needed to classify, and thus it can be useful in assessing the system speed and accuracy simultaneously.

2.3 Metrological considerations

In designing a BCI that is wearable, portable, and relatively, low-cost off-the-shelf components are a suitable choice. In a reactive BCI, such a choice is not exclusively limited to the EEG acquisition, but it is also extended to the stimuli generator. For instance, in the BCI based on steady-state visually evoked potentials (SSVEP) treated in Chapter 3, smart glasses are exploited to generate the flickering lights needed to elicit SSVEP signals. Though many literature studies have been based on commercially available components, the possibility to employ such instruments was not properly justified. Indeed, several studies proved that employing smart glasses for generating visual stimuli and commercial or custom EEG for measuring brain activity is feasible, at least from an operational point of view [49, 51, 63]. Nonetheless, off-the-shelf components are much different from laboratory instrumentation, and they could affect the BCI system performance in an uncontrolled manner if a proper characterization is not carried out.

In better understanding the limiting factors deriving from the usage of off-the-shelf components in a BCI system, a metrological analysis of its building blocks was conducted. The SSVEP-based BCI is here taken into account as case study. This is particularly useful for highlighting the aspects of interest for the characterization. Nevertheless, the electroencephalograph calibration discussed in §2.4 is useful for EEG-based BCIs in general, and hence for an active paradigm too, such as the motor imagery (MI) BCI treated in Chapter 4. Instead, the characterization of smart glasses applies only to systems requiring external stimuli. Note that characterizing EEG devices by exploiting evoked potentials has been already proposed in literature studies [64, 65]. However, in those approaches, the characterization depends on the subjects' response to the external stimuli because the experiments consist of measuring the brain activity during a user task. In our discussion, instead, each component is characterized separately and independently from the BCI user. Then, the functionality validation for the whole systems will be reported in Chapter 3 and Chapter 4.

The building blocks of the SSVEP-BCI are represented in Fig. 2.5: smart glasses are used for generating flickering icons, the human user transduces this visual stimulation into a SSVEP oscillation, and the EEG device measures the brain activity containing the SSVEP. Meanwhile, the smart glasses will not be considered for the MI-BCI. The need for a characterization of the components arose from BCI experiments pointing out discrepancies between the expected system response and the measured response. In details, in experiments with SSVEP, the user was stimulated with a flickering light that should have followed a square-wave path (Fig. 2.6a), but the resulting EEG spectra showed some unexpected harmonic components with unexplained amplitudes (Fig. 2.6b).

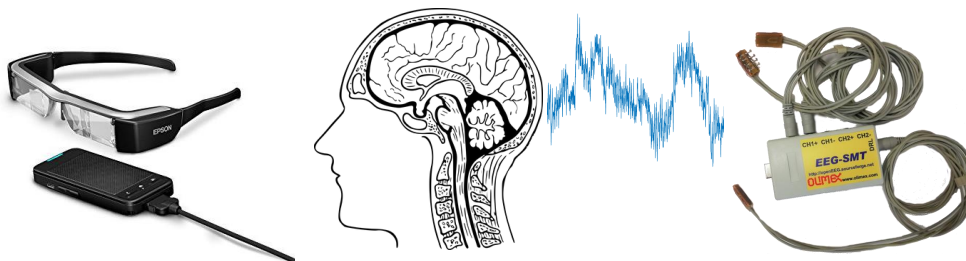
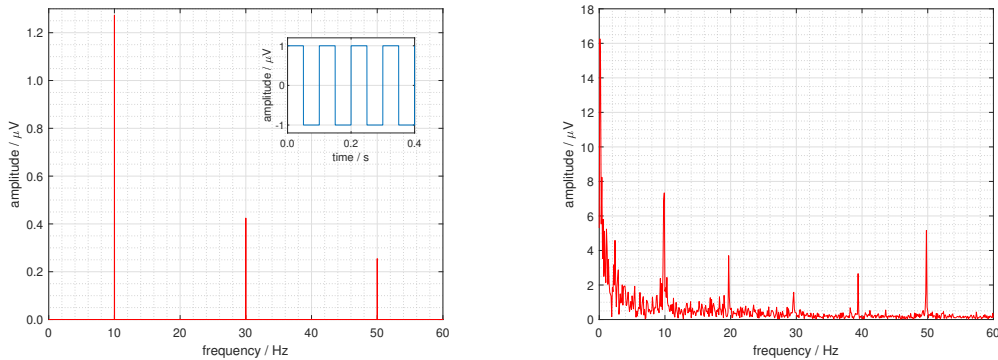


Fig. 2.5 Wearable BCI system based on SSVEP. From left to right: the BT200 AR glasses for stimuli generation, the human user, the Olimex EEG-SMT data acquisition board with dry electrodes.



(a) ideal 10 Hz square wave spectrum (inset: time domain) (b) EEG spectrum corresponding to a 10 Hz visual stimulation

Fig. 2.6 Comparison between simulated nominal amplitude spectrum of the visual stimuli and measured EEG spectrum corresponding to visual stimulation.

Indeed, the major limitation to the system performance comes from the human user because of the poor signal-to-noise ratio, non-linearity, and non-stationarity of the measurand [66]. In metrological terms, the human vision system could be seen as a transducer with high intrinsic uncertainty and, in analysing the whole system, the uncertainty associated with the other two blocks should be negligible. This is particularly true in laboratory or clinical applications, where it is possible to choose the stimuli generator and in the signal acquisition system, without caring much about wearability, portability, and/or cost. On the other side, such considerations do not necessarily hold in the consumer-grade context. Therefore, the following sections report the studies conducted for each block separately to quantify uncertainties and errors introduced by the the EEG acquisition device and the smart glasses. This metrological analysis appears essential in justifying the approach adopted in designing wearable interfaces and address future improvements. It is to remark that the proposed system focuses on user-friendliness with the aim to spread BCI technology. This should imply a better understanding of brain mechanisms thanks to the possibility of acquiring a large amount of data. Precisely for this scope, studying the metrological performance of such systems cannot be avoided in guaranteeing the reliability of the acquired data. Before entering into the details of the equipment characterization, further general considerations are needed about signal quality.

2.3.1 Signal quality

The quality of the recorded EEG signal is indeed a crucial factor for the BCI operation and the possibility of evaluating the acquisition quality is typically related to the detection of artifacts. Such artifacts can be divided into internal, such as eye blinks, muscular contraction, or heart beat noise, and external, such as electromagnetic interferences, or power line noise. Indeed, proper EEG electrodes are critical for measuring artifacts-free brain activity. Unstable positioning and deterioration are two important aspects related to that, and these issues are worsened in case of dry electrodes, i.e. when conductive gels are avoided in contacting the user's scalp. In this regard, some studies have been conducted to compare different electrodes applications, namely wet, semi-wet, and dry. Main findings are well resumed in [67]. In there, the magnitude and stability of the electrode-skin impedance was investigated. Reasonably, the contact impedance associated with dry electrodes resulted the highest and most unstable one. This can clearly lead to a distortions of the actual brain signals and, in some cases, no satisfactory EEG can be obtained. Nonetheless, the results of the review suggest how to lower the electrode-skin contact impedance. First of all, the usage of active electrodes is recommended to improve the measure quality by pre-amplifying the brain signals as soon as they are picked up. Then, the forearm resulted the worst skin location in comparison with hairy scalp and forehead, so it should be avoided. For instance, one can place the reference electrode on the ear instead of the forearm. As already mentioned above, silver pins were added to the active electrode of the Olimex EEG-SMT when contacting the skin in hairy scalp areas. A dense set of pins is also suggested since increasing the contact area is beneficial for reducing the contact impedance. Also recall that, if an Helmate-like EEG cap is used, the electrodes shape is also optimized to overcome the hair and reach the scalp. Finally, the contact impedance is lowered by applying pressure to the electrodes. The values reported in [67] for the impedance are also compatible with the case of skin abrasion, thus indicating no need to scrub the scalp surface. In our work, tight headbands were used in aiming to apply a sufficient pressure to the electrodes while avoiding discomfort for the user.

The above-mentioned precautions are indeed useful in daily-life EEG applications because they would require gel-free electrodes. In addition, monitoring the electrodes contact impedance during EEG measurement would be desirable. Impedance check is typically implemented with an active measurement method,

in which a small current is injected and the resulting voltage is measured [68, 69]. Unfortunately, this is not always possible. For example, the commercial EEG setup from Olimex does not include an impedance check circuitry, and this should be purposely added. Given that, the possibility of different quality checks on the measured signal was considered during our work. In [44] it is suggested that the line noise (50 Hz in Europe) is not properly rejected if there is a difference between the contact impedances associated with the reference electrode and the measuring electrodes. In particular, in experiments with the Olimex EEG-SMT, it was observed that the 50 Hz harmonic was emphasized when the two electrodes of a differential channels were applied with different pressures. By noting that one of the electrodes was placed on the forehead (no hair), this eventuality suggested to adjust the electrode in the hairy scalp area, usually by tightening the headband. Actually, even if this was done during the user preparation, the electrodes placement slightly changed during the experiments due to their long term instability. This was also detected by the appearance of a higher 50 Hz harmonic in the recorded signals, but at least in experiments with SSVEP, such an event rarely compromised the brain signals classification. In accordance with such experimental experiences, it appears that contact impedance constraints are not always tight, since the system functionality remained despite some instabilities. Nonetheless, this can be true for the SSVEP detection, while it was not possible to observe a similar phenomenon in the experiments with motor imagery.

As a further check for signal quality relying on the measured EEG signals, artifacts were visually inspected. Indeed, it is generally accepted that a normal EEG is characterized by the absence of identifiable abnormalities. Hence, a statistical definition of a “clean EEG” signal can help to set threshold values so to determine artifact levels in an EEG recording. These thresholds are generally based on amplitude, skewness, and kurtosis of the EEG signal. Threshold-based approaches are commonly used to reject EEG segments, they require to manually define the thresholds, and distinguishing between high and low level of contamination is not trivial. In such a framework, classifier-based methods have also been proposed to this aim. As an example, some authors chose to divide the quality of the EEG in three classes [70], i.e. low quality, medium quality, and high quality, and then they employed more than a hundred features to classify the EEG quality of the segments. The considered features were generally extracted from EEG signals filtered in different frequency bands. Meanwhile, only three signal quality indicators were used in [71]: the ratio of

alpha power to the total EEG power, the variance of each EEG signal, and the power at the line frequency (50 Hz or 60 Hz). These parameters were motivated by the fact that, when the eyes are closed, the power of alpha rhythm becomes dominant and it can occupy a large part of the frequencies of interest. Moreover, it appears useful to check line noise because in daily-life settings this is the most prevalent noise source. Overall, there is no unambiguous standard for evaluating the quality of EEG signals, and detecting artifacts typically relies on empirical experience. In the case of dry electrodes, this is even more challenging since the recording is more sensitive to artifacts and the acquired signals would be typically discarded by a clinician used to EEG recording with wet electrodes. As a representative example, Fig. 2.7 shows a 4 s-long EEG signal recorded during experiments with SSVEP. The pronounced valleys in the recording correspond to the movement of the electrodes due to eye blinking, and such artifacts would lead to discarding this trial. However, such signal can be easily classified as corresponding to a 12 Hz stimulation and it should be not discarded at all. In this sense, the empirical experience conducted with dry electrodes differs from the one associated with classical recording methodologies.

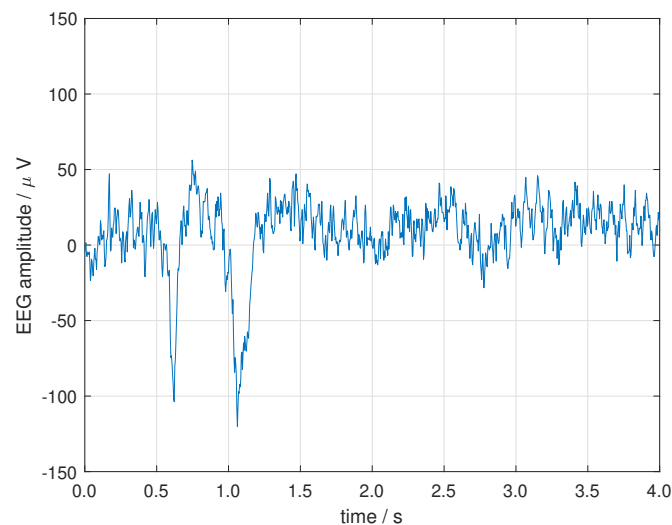


Fig. 2.7 A typical electroencephalographic signal recorded through dry electrodes during experiments with SSVEP. Artifacts related to eye-blinks are clearly visible.

Apart from artifacts detection and eventual rejection of a whole trial, artifacts could be also removed from a trial. In [72], a comparison between the most common techniques of artifact detection and removal have been presented, e.g. regression, filtering, and independent component analysis (ICA). Regression requires the record-

ing of electrooculographic (eyes) and/or electromyographic (muscles) activity in addition to the brain signals recording, thus this is typically undesirable in enhancing wearability and portability of the system. Analog and digital filtering is instead quite simple and effective, and it only requires that the identifiable artifact-related bands do not overlap with the signal-related band. Finally, ICA is a typical technique for separating signal sources from noise sources in trying to remove the noisy part, but it requires multi-channel acquisition. Also, a similar technique is based on "artifact subspace reconstruction" (ASR) and it also typically involve multiple channels [73]. Hence, in the BCI systems with a single or few channels, filtering or ICA extensions are typically considered. As it will be detailed in the respective chapters, filtering was sufficient in the SSVEP-BCI, while an extension of ICA was investigated for motor imagery. However, artifact removal techniques should be better investigate for the few channels cases. As a general consideration, artifact removal did not appear essential in the case of SSVEP, given that precautions were taken in properly measuring the EEG. Instead, evaluating the signal quality in motor imagery was more challenging due to concomitant unexplained phenomena.

2.4 Electroencephalograph calibration

An electroencephalograph is a specialized voltmeter measuring the electrical activity of the brain. Peak-to-peak amplitudes in normal EEG typically range from $0.5 \mu\text{V}$ to $100 \mu\text{V}$ and the frequency band of interest is 0.5 Hz to 100 Hz [43], though the exact band depends on the considered application. Especially for off-the-shelf components, there is the need to calibrate the gain of an EEG acquisition system at different nominal frequencies. Nowadays, in clinical applications, some guidelines exist for EEG calibration prior to the measurement of brain-activity [74]. However, there is a lack of standardization in assessing the metrological performances of EEG instruments. These are often validated by acquiring the brain activity of a user with eyes open, or closed, or even by evoking brain potentials [64, 65]. Nonetheless, merely validating by means of evoked potentials could be not appropriate since the human response to stimulation is not yet fully understood (e.g. see [75] for SSVEP). It is worth noting that, in this context, the IEEE Standards Association has indicated a roadmap for neurotechnologies by considering standardized calibration procedures in addition to validation based on user tasks [76]. The work reported hereafter aimed

to give a small contribution to the topic. An EEG calibration procedure has been proposed to assess errors and uncertainties related to the instrument, and also to give basic traceability to the international system of units. In doing that, one can exclude or take under control errors in the EEG measurement, so as to achieve valuable results with the acquired data.

The device under test, which was taken into account as a case study in this section, consists of the Olimex EEG-SMT plus dry electrodes [57] (Fig. 2.1). This instrument has been employed during the thesis work to acquire electroencephalographic signals from a single differential channel in the SSVEP-BCI case and its usage was also attempted with two bipolar channels for the MI-BCI case. Particularly for the SSVEP detection, the band of interest spanned from 1.0 Hz to 60.0 Hz. In processing EEG data, the focus was on amplitude spectra, while the phase response was not considered. Therefore, only asynchronous measurements were carried out for the calibration, while synchronous measurements are eventually addressed to future works.

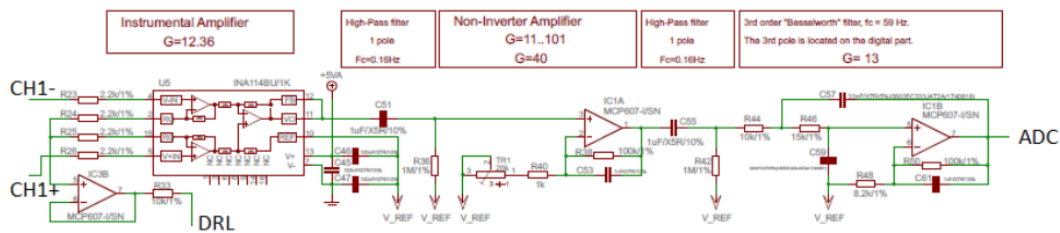


Fig. 2.8 Signal conditioning circuit being part of the Olimex EEG-SMT acquisition board. The connections to the CH1 pins and the DRL are shown, as well as the input ADC line.

2.4.1 Experimental setup

The internal structure of the electroencephalograph under test is similar to a typical EEG amplifier, but it was simplified by the manufacturer to be less cumbersome and low-cost. It consists of an instrumentation amplifier with two differential channels followed by further filtering and amplifying stages. Active electrodes are connected to the positive and negative terminals of each channel. Meanwhile, a passive electrode must be connected to the "drive right leg" (DRL) input to act as a reference potential for common mode rejection. The distinction between active electrodes and passive electrodes is that the former have an operational amplifier-based buffer to improve the electrode-skin contact impedance, while the latter are simply conductors. Passive

electrodes could also be employed as input to the differential channels, but this is not recommended for the sake of signal quality. After amplification and filtering, the signals are digitized with an ATmega16 microcontroller: this provides the timing for the analog-to-digital conversion (ADC), and the resulting 10-bit codes are sent through USB to an external device, such as a personal computer. The sampling rate was set at 256 Sa/s. In the present case, only one differential channel (CH1) was considered, while the other (CH2) was internally short-circuited to avoid cross-talk noise. Fig. 2.8 shows a part of the EEG acquisition board devoted to signal conditioning before the ADC. Note that a trimmer can be used to adjust the variable gain of the second amplifying stage. In the present calibration, the trimmer was set to 1.66 k Ω to achieve a gain $G_2 = 38.6$ V/V. According to nominal specifications, the bandwidth should go from 0.16 Hz to 59 Hz, while the nominal gain should equal 6202.25 V/V (given the value set for G_2). Nonetheless, calculations conducted thanks to the circuit schematic already highlighted a gain that was 20 % higher (about 7510 V/V).

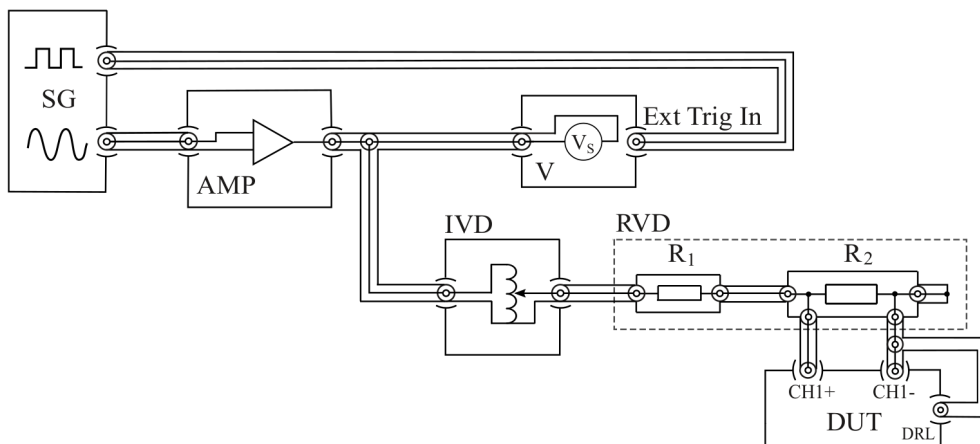


Fig. 2.9 Coaxial schematic diagram of the EEG calibration setup realized at the “Istituto Nazionale di Ricerca Metrologica” (INRIM).

In order to calibrate the gain of the EEG-SMT, a calibration setup was adapted from a setup for calibrating lock-in amplifiers [77], designed and realized at the Italian national institute for research in metrology (“Istituto Nazionale di Ricerca Metrologica”, or INRIM). This is represented in Fig. 2.9. The signal generator SG provides both (i) a large-amplitude, low-distortion sine wave V_S and (ii) an isofrequential reference square wave V_{REF} for triggering a calibrated voltmeter. Two

output channels are employed. This generator is based on the PCI-6733 board from National Instruments. The signal V_S is buffered by a unity-gain amplifier (based on INA111) with differential input, thus providing electrical decoupling from SG as well as the drive current for the following stages. The buffered voltage is fed to a calibrated voltmeter, the Hewlett-Packard 3458A (used in synchronous sub-sampling mode), which is externally triggered by V_{REF} in order to provide an accurate measurement of V_S . Meanwhile, V_S is also scaled by means of cascaded inductive voltage divider (IVD) and resistive voltage divider (RVD) stages. The measured scaling factor for IVD (k_{IVD}) goes from 0.0 to 1.0 with 50 ppm relative uncertainty, while for the RVD the measured scaling factor is

$$k_{RVD} = \frac{R_2}{R_1 + R_2} = 9.999317 \cdot 10^{-5} \quad (2.1)$$

with relative uncertainty equal to 13 ppm. The calibration voltage in input to the EEG-SMT, applied between CH1+ and CH1-, results

$$V_{CAL} = k_{IVD}k_{RVD}V_S. \quad (2.2)$$

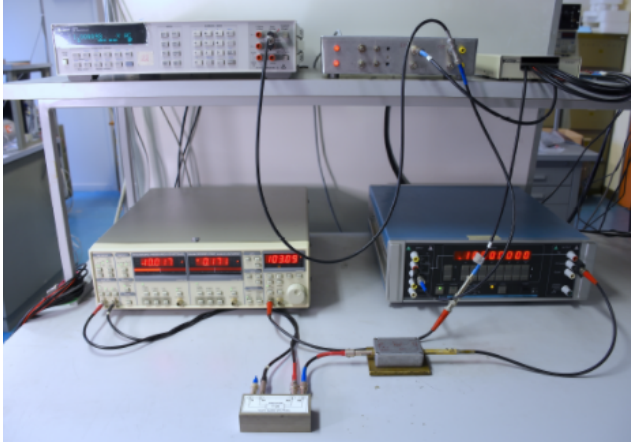
The instrumentation employed in realizing the calibration setup is reported in Fig. 2.10, together with a detail of the connection to the EEG electrodes. The input voltages are digitized and the output codes are sent through USB to a PC with MATLAB®, which acquires the data in order to process them. The connections to the electrodes are realized with a copper plate and conductive carbon tape. In this way, CH1 is connected to the terminals of the resistance R_2 , while the DRL electrode is connected to the generator common, which is also equipotential to the shield of the coaxial cable connected to the generator itself, as shown in Fig. 2.9.

2.4.2 Data analysis

The acquired codes were scaled according to

$$V_{EEG}(K) = \frac{KQ - SH}{GA}, \quad (2.3)$$

where K is an acquired code, $SH = 2 \text{ V}$ is the internal level shifting, $GA = 7509.7 \text{ V/V}$ is the conditioning circuit nominal gain calculated from the Olimex Ltd schematic,



(a) instruments connected according to the coaxial scheme of Fig. 2.9



(b) detail of the connection to the electrodes

Fig. 2.10 Physical realization of the measurement setup for the EEG calibration.

and the ADC resolution Q is calculated with the nominal full scale range value $FS = 4\text{ V}$ and the nominal bit resolution $N = 10$:

$$Q = \frac{FS}{2^N} \quad (2.4)$$

According to the IEEE-1057 standard (see Sec. 4.6 in [78]), the sinefit algorithm was applied to fit the acquired waveforms. In particular, the four-parameter method was exploited: this calculates the values of amplitude (A), offset (O), phase (φ) and frequency (f) of a sinus that give the best fit, in the least squares sense, to the recorded signal. Hence, the sinefit algorithm fits a function of the form

$$V(t_n) = A \cos(2\pi f t_n + \varphi) + O. \quad (2.5)$$

The 4-parameter sinefit is actually an iterative procedure in which an initial guess is needed for the signal frequency. Per each signal to fit, the frequency guess was set equal to the respective nominal frequency set on the generator. The MATLAB function employed for the fit is available online [79] and it was implemented according to the IEEE-1057 standard referenced. The root means square (rms) values were calculated for both the V_{EEG} and the calibration signal. In particular

$$V_{EEG,rms} = \sqrt{\frac{A_{EEG}^2}{2} + O_{EEG}^2}, \quad (2.6)$$

while the rms of V_{CAL} was calculated by scaling the rms of V_S , namely

$$V_{CAL,rms} = k_{IVD}k_{RVD}\sqrt{\frac{A_S^2}{2} + O_S^2}. \quad (2.7)$$

Indeed, the concept behind the present calibration method is to generate a large and highly accurate signal and then scale it down to the measurement range of interest. Such an approach is reflected into the (2.7) employed for data analysis, and this allows to obtain a great accuracy and a well-defined traceability, in contrast with a case in which one would directly generate a small calibration signal [77].

The uncertainties associated with $V_{EEG,rms}$ and $V_{CAL,rms}$ were also calculated. To this aim, uncertainties had to be estimated for the four parameters of the sinefit. Firstly, the uncertainty associated with the frequency was estimated by considering that the 4-parameter sinefit iteratively employs a 3-parameter sinefit to find A , O , and φ while progressively adjusting f . Starting from the guess value, the frequency is increased or decreased by a fixed amount in each iteration, so as to reduce the error between measured samples and the fitted sine. The iterative procedure stops when the frequency difference between two adjacent iterations is small enough. In the present case, the stopping criterion was set so that the frequency difference was less than 100 ppm. Reasonably, the relative frequency uncertainty is assumed equal precisely to 100 ppm. After that, the uncertainty of the other parameters can be estimated with the variance of the respective estimators as discussed in [80]. In that work, the author analyses the statistical distribution, bias and variance of the coefficient estimators for a 3-parameter fit. Under the assumption of Gaussian distribution for the parameters, the variances associated with A and O were estimated to be equal to

$$\sigma_A^2 = 4\frac{\sigma^2}{N} \quad \text{and} \quad \sigma_O^2 = \frac{\sigma^2}{N},$$

respectively, with σ^2 equal to the sample variance associated with fit residuals. Hence, at the end of the fit, the sample-by-sample difference between the measured data and the fit sine of (2.5) can be used to estimate amplitude uncertainties. Given that, the law of propagation of uncertainties is applied [81] to achieve the type A uncertainty

$$u_{V_{EEG,rms}} = \frac{1}{V_{EEG,rms}}\sqrt{\frac{A_{EEG}^2}{2}\sigma_{A_{EEG}}^2 + O_{EEG}^2\sigma_{O_{EEG}}^2}. \quad (2.8)$$

An analogous expression is obtained for the type A uncertainty of V_S . Then, the type B uncertainty derived from the specifications of the voltmeter is combined to achieve

$$u_{V_S,rmsC} = \sqrt{u_{V_S,rms}^2 + \frac{t_{V_S}^2}{3}}, \quad (2.9)$$

where $t_{V_S} = 110 \mu\text{V}$ is the tolerance resulting from the datasheet for the voltage measurement; by assuming a uniform distribution associated with the tolerance value, it must be divided by $\sqrt{3}$ to achieve a standard deviation associated with a Gaussian distribution. Note that this normalization is mandatory before combining the two uncertainty contributions. Finally, the uncertainty of $V_{CAL,rms}$ is obtained by propagating the uncertainties in (2.7), i.e.

$$u_{V_{CAL,rms}} = V_{CAL,rms} \sqrt{\left(\frac{u_{V_S,rmsC}}{V_{S,rms}}\right)^2 + \left(\frac{u_{k_{RVD}}}{k_{RVD}}\right)^2 + \left(\frac{u_{k_{IVD}}}{k_{IVD}}\right)^2}, \quad (2.10)$$

where the relative uncertainties of RVD and IVD have been also taken into account.

2.4.3 Results

The characterization of the EEG device was performed at frequency up to 100 Hz with the described setup. Both the linearity and the magnitude error were measured. In addition, frequency errors were also detected. Linearity was first assessed through measures conducted with $V_{CAL,rms}$ at 20 Hz and seven different amplitudes: 10 μV , 20 μV , 30 μV , 40 μV , 60 μV , 80 μV and 100 μV . Fig. 2.11 shows the result obtained by plotting $V_{EEG,rms}$ as a function of $V_{CAL,rms}$. Clearly, linear behavior is visible. This was confirmed by executing a linear fit and then a Fisher test for the goodness of fitting (p-value $< 1 \times 10^{-13}$). The ideal response with unitary gain and zero offset is also reported with a dashed line to better highlight linear errors. Notably, the sought magnitude error is actually a gain error, and from these measures it resulted in about 9.5%. Meanwhile, the offset error resulted in less than $-0.08 \mu\text{V}$.

The magnitude error as a function of the frequency was calculated according to the expression

$$\varepsilon = \frac{V_{EEG,rms} - V_{CAL,rms}}{V_{CAL,rms}}, \quad (2.11)$$

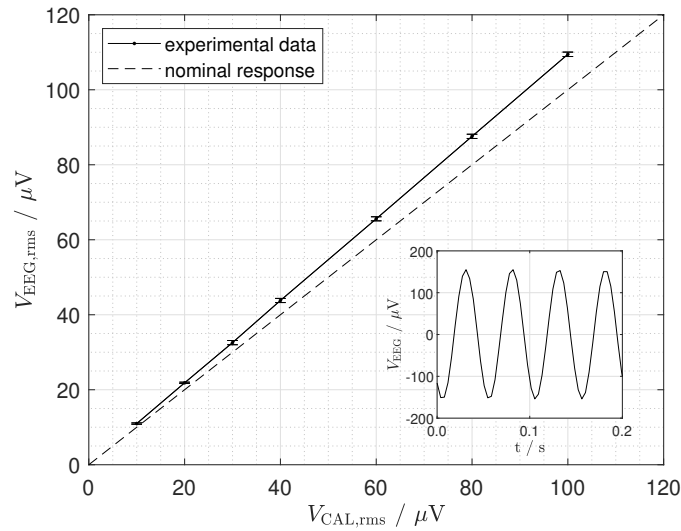


Fig. 2.11 Linearity of the EEG-SMT electroencephalograph measured at 20 Hz (inset: sine wave acquired with for $V_{CAL,rms} = 100 \mu V$).

and the associated uncertainty was calculated by propagating the uncertainty of the two rms voltages according to the law of propagation of uncertainties [81]. By doing that, the obtained curve is reported in Fig. 2.12. The error bars associated with each measuring point represent the propagated uncertainty, expanded with coverage factor $k = 4$. The largest uncertainty on this gain error is 0.3 % and it is associated with 100 Hz.

In explaining the measured gain error, circuit simulations were performed thanks to the possibility to replicate the EEG schematic [57], which is open source. The software LTspice® by Analog Devices was then used to set a Monte Carlo analysis. In doing that, nominal values were assigned to the passive components constituting the conditioning circuitry, and then their declared tolerances were also taken into account. The circuit implemented in LTspice, together with the analysis setting, is represented in Fig. 2.13. The circuit simulation was executed by repeating an AC sweep analysis more than 32 000 times. In each repetition, a pseudo-random value was selected for each component by considering the set of possible values defined by the respective tolerance. The AC sweep instead consisted of calculating the amplitude of the output voltage for different frequency values in the range 1 Hz to 100 Hz. Then, the circuit gain was obtained by the ratio of these voltage values and the input voltage, here set at 1 V. The gain error was finally obtained in relative terms to the nominal gain declared by the manufacturer (7510 V/V). The results are

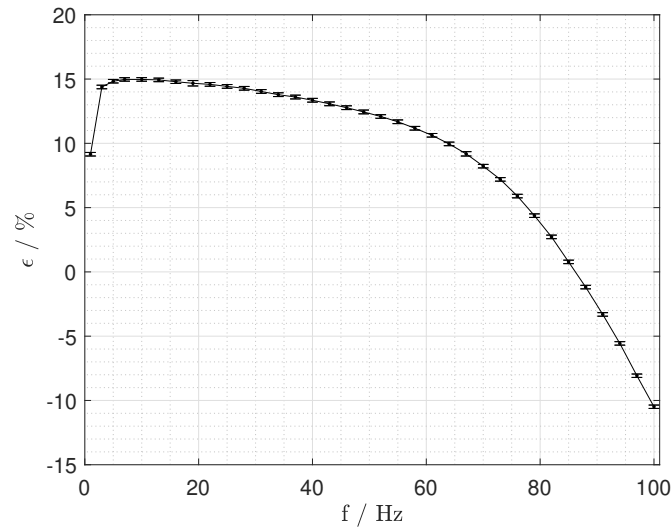


Fig. 2.12 Magnitude (gain) error of the EEG-SMT electroencephalograph measured at frequencies up to 100 Hz.

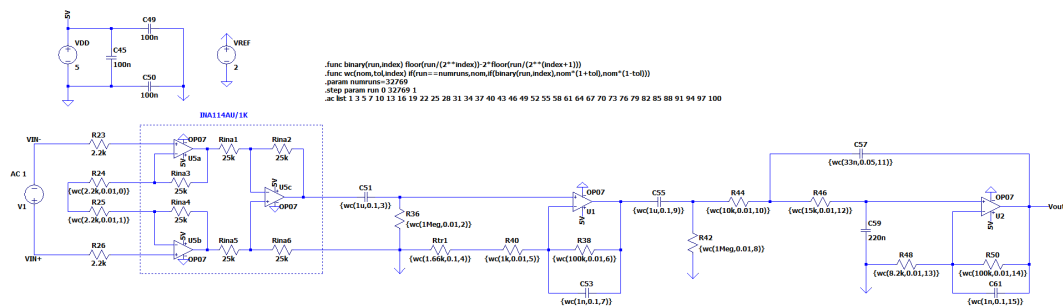


Fig. 2.13 Analog conditioning circuitry of the Olimex EEG-SMT board replicated in LTSpice for executing a Monte Carlo analysis.

reported in Fig. 2.14 and compared with the measured gain error. The thick grey line corresponds to the simulated gain error when all components assume their nominal value. The gray levels are related to different probabilities of having a certain gain error. In particular, these were arranged in three levels:

- the inner 50% range, or mid-range, refers to the interval from the 25th to the 75th percentile and it is represented in dark gray;
- the inner 90% range, which refers to the interval from the 5th to 95th percentile, is represented in gray;
- the range of all possible values is instead represented in light gray.

Interestingly, the measured gain error lies at the limit of the mid-range and it is in principle explained by tolerances associated with circuit components. Nonetheless, the measured curve is almost constantly shifted with respect to the simulated gain error corresponding to nominal values. Therefore, the most probable reason for the 10 % gain error is a drift in the variable gain stage (second stage, i.e. G_2), and calibrating the EEG may be as simple as adjusting the trimmer for setting a different G_2 value.

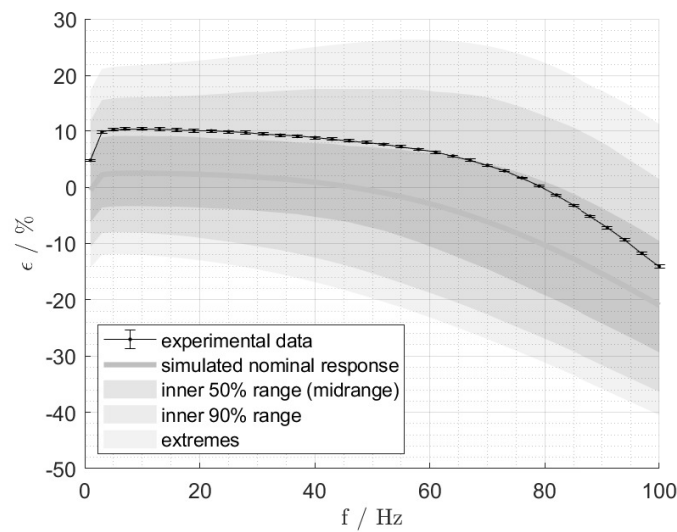


Fig. 2.14 Simulated gain error obtained with a Monte Carlo analysis (gray line and shaded areas) and compared to the measured gain error (black line with bars). The different gray levels correspond to three different probability of occurrence for simulated values.

During experiments with brain-computer interfaces, the uncertainty associated with the brain signals themselves (intrinsic uncertainty) and the electrodes-scalp contact impedance are usually higher than the measured gain error. However, the gain error can be corrected by calibrating the EEG with the results reported above. The uncertainty associated with this correction is negligible in typical electroencephalographic measures. This implies that even a low-cost device like the Olimex EEG-SMT can properly measure electrical brain activity. Nonetheless, it is worth remarking that a highly relevant aspect in EEG measurement is the skin-electrode contact, which must be stable enough during the measurement. Unfortunately, the procedure introduced in this section was not appropriate to investigate this issue, and further measures are needed.

To conclude, the frequency errors detected in calibrating the EEG device under test can be addressed. Recall that the nominal sampling frequency of the EEG-SMT is 256 Sa/s. However, as a result of the sinefit algorithm, all frequencies resulted slightly less than the respective set ones when the nominal sampling rate was considered. The relative frequency error was thus assessed by defining

$$\varepsilon_f = \frac{f_{EEG} - f_{CAL}}{f_{CAL}}, \quad (2.12)$$

where f_{EEG} are the frequencies measured with the EEG device under test, while f_{CAL} are the nominal generator frequencies. Since the frequency stability of the generator is in the order of ppm, the whole frequency error should be led back to the EEG-SMT. This error is plotted in Fig. 2.15 as a function of the f_{CAL} values. These errors were reasonably explained with a sampling frequency of the EEG different from the nominal one. In particular, it was derived that the actual sampling frequency equals 257 Sa/s with 1 Sa/s uncertainty. Moreover, instabilities of the internal clock also affect the actual value of the sampling frequency.

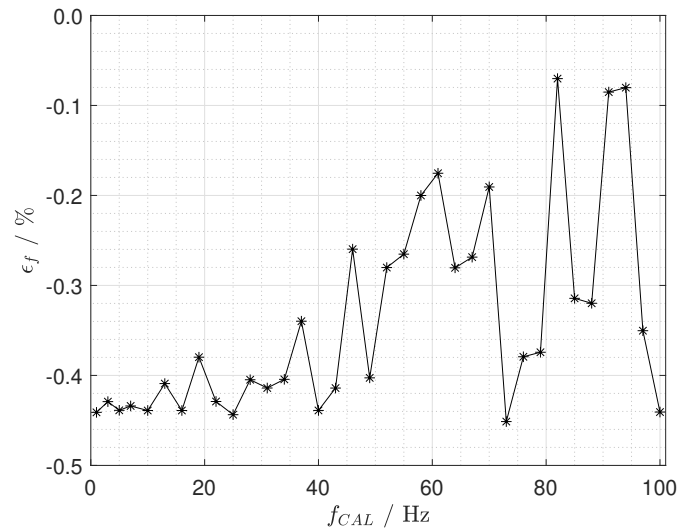


Fig. 2.15 Relative error between the measured frequencies and the generator ones in percentage.

2.5 Smart glasses characterization

In this paragraph, the discussion copes with the possibility to provide visual stimuli through smart glasses. Especially because of their wearability and portability [82], these devices are increasingly exploited in extended reality (XR), which is typically declined into virtual reality (VR), augmented reality (AR), and mixed reality (MR). For a wearable SSVEP-BCI, the user can interact with the AR glasses by merely staring at icons appearing on the display. Previous research has already proved the functionality of wearable XR-BCI systems. However, errors and uncertainties of such a stimuli generator were not quantified. Currently, calibrating smart glasses regards the accurate measurement of both the device physical position and the user's eyes position for properly rendering virtual objects [83]. Even in dealing with display calibration, pixel-wise calibration is needed for spatial objects positioning [84]. Clearly, generating flickering icons with smart glasses is strictly related to the BCI framework, and, even in SSVEP-BCI research, previous works only dealt with the optimal layouts for the stimuli [85]. The current discussion, instead, deals with the display characterization from the view of flickering icons generation.

Commercially available smart glasses exploit different display technologies. A basic distinction is between video see-through and optical see-through [82]. The former relies on an embedded camera to record the surrounding environment and then display virtual objects overlapped to the recorded video. The latter, instead, uses a semi-transparent display that does not hide the real scene while superimposing virtual objects to it. Although the two technologies have many common features, optical see-through devices are mostly considered in this work because they are better suited for augmented reality applications. A first example of optical-see-through device is the Microsoft HoloLens. The HoloLens display consists of a set of transparent screens, each one showing a different image to create a stereoscopic illusion. The displays are planar waveguides: a source transmits image data along the length of the transparent displays, and then the light rays get eventually extracted to reach the user's eyes. To generate a flickering icon, the HoloLens can be programmed by considering that the declared refresh rate is 60 Hz. Therefore, these icons are obtained by switching on and off display pixels. Another family of smart glasses is the Epson Moverio one. Two representative devices are the BT200 and the BT-350. The first has an LCD display with an active matrix of polysilicon thin-film-transistor. The second one, instead, exploits a silicon-based organic LED matrix. Both devices

can be programmed in Android with a dedicated graphic library. The screen refresh rates are 60 Hz and 30 Hz, respectively.

In a straightforward approach, the flickering frequencies are obtained by switching pixels on or off after a fixed number of refresh periods. Thus, the achievable flickering frequencies equal the refresh rate divided by an integer number. More sophisticated approaches could be also adopted to achieve more frequencies, but this would go beyond the scope of this work. In SSVEP applications, higher refresh rates are usually preferred to enable more flickering frequencies. This was a main reason for employing the BT200 in the BCI implementation, and, as a consequence, the stimuli characterization primarily concerns this device. However, further information about the flickering generated with other display technologies is also reported in the following.

2.5.1 Experimental setup

For measuring luminous intensity, a transducer was implemented as shown in Fig. 2.16. It is based on a commercial photodiode integrated with a transimpedance amplifier, the OPT101. An external resistor was used to increase the gain while reducing the bandwidth. In measures with Epson Moverio BT200, the external resistance was 10 M Ω , resulting in a 11 V/ μ A gain and about 1.3 kHz. In order to avoid noise from the mains supply, a 5 V battery was used for supplying the circuit. The output was sampled at 1 kSa/s with the ADC of an STM32F401RE microcontroller and then the data were sent to a PC with MATLAB, thus allowing further elaboration.

Measuring the luminous intensity of light waves emitted by smart glasses aimed to highlight eventual differences between the nominal wave shape and the actual one. Hence, Fourier spectra were calculated to analyse the harmonic content of the flickering icons up to 100 Hz. Harmonic amplitudes were investigated relatively to the first harmonic. Meanwhile, accurate absolute values were not of much interest for the visual stimuli.

A picture of the measurement setup, realized according to the scheme of Fig. 2.16, is shown in Fig. 2.17. The transducer circuit was integrated on a green matrix board, and then the battery supply and the board for signal acquisition were attached. Eventually, the acquisition board could be shielded to avoid electromagnetic interference,

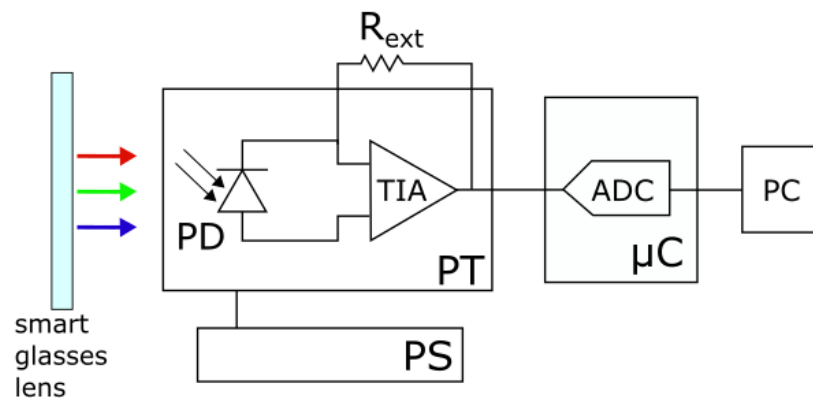


Fig. 2.16 Schematic diagram of the setup for characterizing the BT-200 optical output, based on an OPT101 amplified photodiode with increased gain [4].

while the matrix board was not shielded. In measuring the luminous intensity, the OPT101 sensing element was attached to the display of the BT200 smart glasses (one lens at time). Each acquisition lasted 10 s to offer enough spectral resolution (0.1 Hz) in analysing stimuli spectra. The 10 s-long records were mainly analysed in the

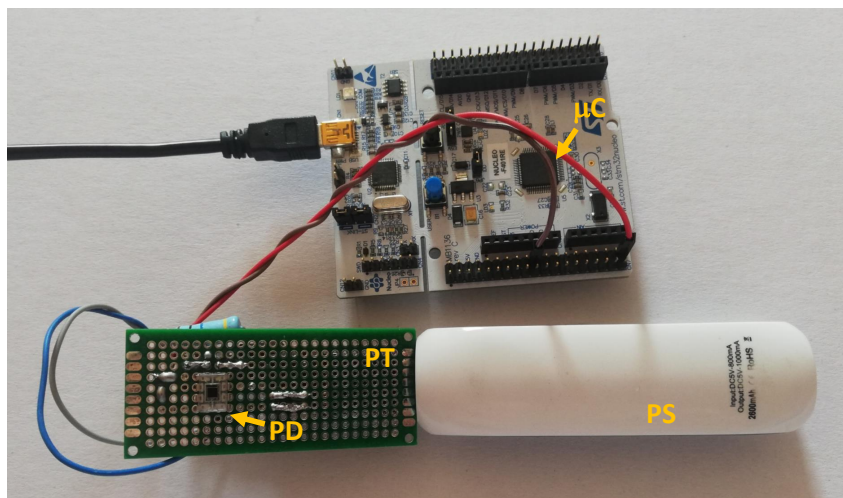


Fig. 2.17 Picture of OPT101-based circuit implemented on a matrix board; note that PD is the OPT101 photodiode.

frequency domain. Hanning windowing was applied before executing a "fast Fourier transform" (FFT) algorithm, thus reducing spectral leakage without greatly affecting harmonic amplitudes. From the FFT results, only the amplitude spectra were derived, while phase response was not of interest. Then, each spectrum was normalized with respect to the amplitude of the first harmonic. Therefore, by scaling the first

harmonic to unitary amplitude, it was easier to evaluate the relative amplitudes of higher harmonics. Despite these considerations on calculated spectra, some hints about the absolute luminous intensity could be derived according to the OPT101 datasheet. In details, the OPT101 datasheet reports scaling factors to apply when the measured light wave has wavelength $\lambda = 650$ nm and the ambient temperature is $T_A = 25$ °C [4]. Note that, because of the external resistor for setting a higher gain, the steps for scaling the ADC voltage to luminous intensity are

1. divide the OPT101 output voltage by the DC gain equal to $11 \text{ V}/\mu\text{A}$ to obtain the photodiode current;
2. divide the photodiode current by $0.45 \mu\text{A}/\mu\text{W}$ to obtain input power;
3. divide the resulting power by the photodiode area, i.e. $5.2 \times 10^{-2} \text{ cm}^2$;
4. by considering that $1 \text{ lx} = 1.4641 \times 10^{-7} \mu\text{W}/\text{cm}^2$, convert power density to luminous intensity.

Although a white light should actually take into account multiple wavelengths, and also other corrections should be applied to achieve accurate measures, these calculations were exploited to give the first estimate of the incident luminous intensity.

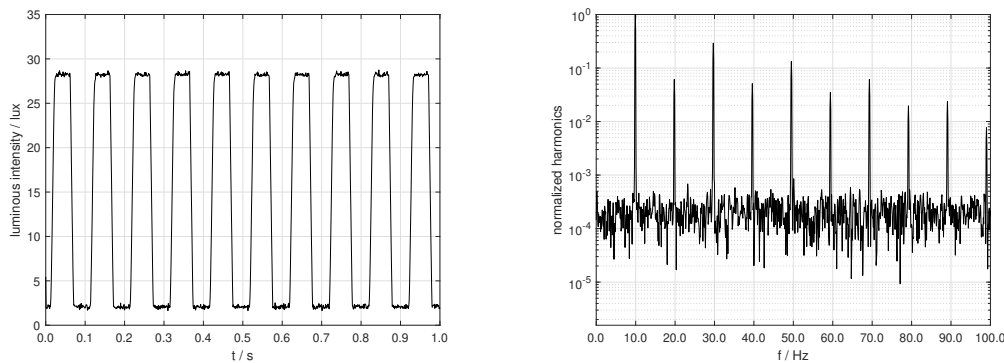
The Epson Moverio BT200 and BT350 were programmed in Android. The application simply switches on and off pixels according to the refresh rate. Notably, achievable flickering frequencies equal

$$f_{flick} = \frac{f_{refresh}}{n}, \quad (2.13)$$

where $f_{refresh}$ is the refresh rate of the smart glasses, nominally equal to 60 Hz and 30 Hz respectively, while n is an integer number. White square icons were considered for both devices. This kind of application was purposely designed for stimuli characterization. Therefore, the icon was centered and enlarged to cover about 80 % of the display. The experimenter could set the desired flickering frequency to test. In case the frequency did not match (2.13), the application automatically set the nearest higher frequency satisfying the conditions of that formula. On the other side, the Microsoft HoloLens 1st gen smart glasses were also tested by programming them with Unity. Similar considerations hold about the adjustable flickering frequency and the size of the squared white icons.

2.5.2 Results

Fig. 2.18 shows the measured luminous intensity for an icon generated by BT200 set at 10 Hz. Both time and frequency domain are shown. Note that the curve in the time domain appears smoother than an ideal square wave. The spectrum, shown in Fig. 2.18b with amplitude in logarithmic scale, shows some spurious even harmonics in addition to the expected odd harmonics. Recall that the spectrum is normalized to the first harmonics in order to focus on harmonic ratios more than absolute amplitudes. By localizing the harmonic peaks, it also emerges that the first harmonic is actually lower than the nominal value, namely it equals 9.9 Hz. This suggests that the refresh rate is actually lower than the nominal value. Fig. 2.19,



(a) OPT101 output voltage in the time domain scaled to lx (b) normalized amplitudes in frequency domain (log scale)

Fig. 2.18 Measuring the luminous intensity of Epson Moverio BT200 smart glasses nominally flickering at about 10 Hz.

instead, shows the measured luminous intensity for an icon generated by BT200 set at 12 Hz. The curve in the time domain appears even more smoothed than before, especially at off-to-on transitions. Asymmetric transitions are typically associated with even harmonics, and these are indeed visible in the spectrum (Fig. 2.19b). In addition, it must be also noted that, by design, a 50 % duty cycle cannot be obtained neither in the square wave case because $12 \text{ Hz} = 60 \text{ Hz}/5$. Henceforth, a period of the ideal flickering lasts for 5 periods of the refresh rate and cannot be split in two equal halves. As a matter of fact, the lower luminous intensity for the measured curve in time the domain lasts for more time than the higher intensity, thus proving that the duty cycle is closer to $40 \% = 2/5$. This is another reason for the presence of even harmonics in the signal spectrum. Again, the first harmonic is localized at 11.9 Hz,

thus giving another hint in believing that the actual refresh rate is close to 59 Hz. The previous considerations are consolidated by comparing the spectra associated

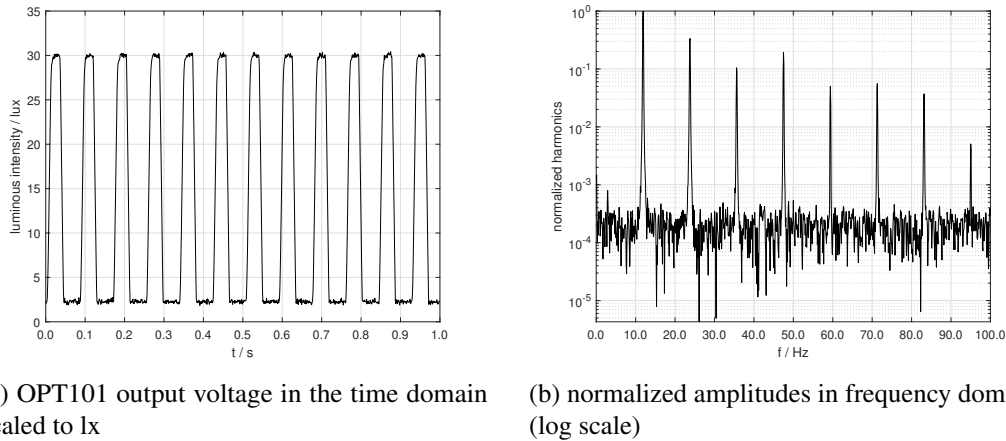


Fig. 2.19 Measuring the luminous intensity of Epson Moverio BT200 smart glasses nominally flickering at about 12 Hz.

with the two flickering icons with a linear scale for amplitudes and by highlighting harmonic ratios. Such comparison is done by means of Fig. 2.20. This shows that even harmonics are more evident in the 12 Hz case, which also suffers from the duty cycle problem. Furthermore, for an ideal square wave, the ratios should follow the scaling low $1/k$ with k odd integer equal to the harmonic order. The plot of Fig. 2.20a is closer to this mathematical law, but in both cases one can say that the spectrum is quite different from the ideal square wave one.

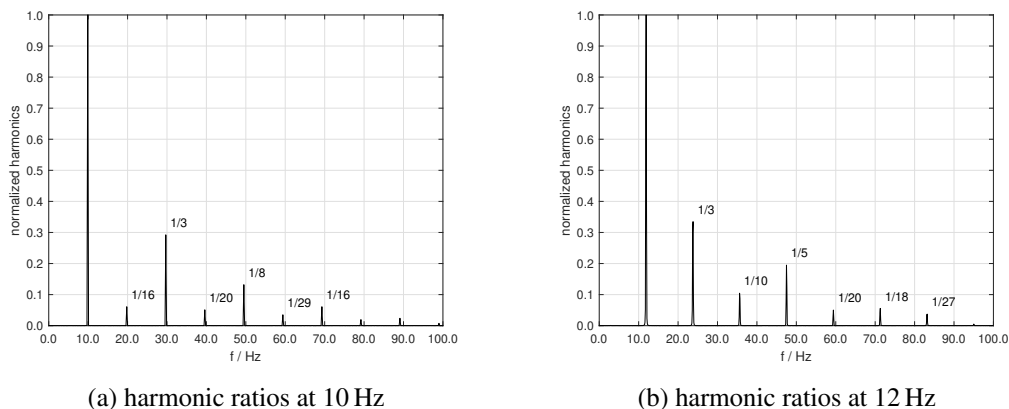


Fig. 2.20 Comparing the harmonic amplitudes normalized at the first harmonic for two representative flickering frequencies.

Similar arguments can be made for the results associated with the BT350. In this case, Fig. 2.21 shows the measured luminous intensity for an icon nominally flickering at 10 Hz. Recalling that the declared refresh rate for this device equals 30 Hz, the flickering frequency should be a third of it. Reasonably, the curve in the time domain appears even smoother than before and the "totally-on time" for the flickering icon is almost null. Again the associated spectrum highlights spurious even harmonics and, by localizing the harmonic peaks, it results that the first harmonic is higher than the expected nominal value (about 10.7 Hz). Hence, this suggests that the refresh rate is higher than the nominal one. This is even more evident in

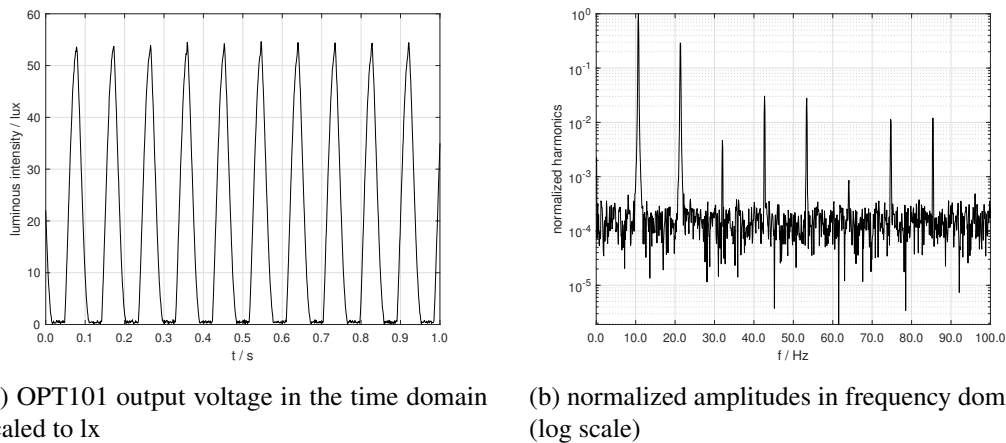


Fig. 2.21 Measuring the luminous intensity of Epson Moverio BT350 smart glasses nominally flickering at 10.7 Hz.

the 12 Hz case reported in Fig. 2.22: the flickering frequency is actually 16.0 Hz = 32 Hz/2. Also note that the curve in the time domain tends to be sinusoidal, and even harmonics appear though they are lower than the 10.7 Hz case. Finally, the plots in Fig. 2.23 better represent the actual harmonic ratios: for the 10.7 Hz case, only the first and second harmonic have meaningful amplitudes, while in the 16.0 Hz case the only first harmonic dominates the other, thus furtherly proving that the wave tends to be a sine wave. In conclusion, these measures reveal that the harmonic content is different from the expected one mainly in terms of spurious even harmonics or attenuation of higher harmonics. Moreover, the actual refresh rates are different from the declared one. From the point of view of SSVEP-BCI functionality, the most relevant issue is the location of the harmonics due to the exact refresh rates. Nonetheless, this aspect can be taken into account and it is suggested to also consider a 0.1 Hz uncertainty associated with the flickering frequencies. Further

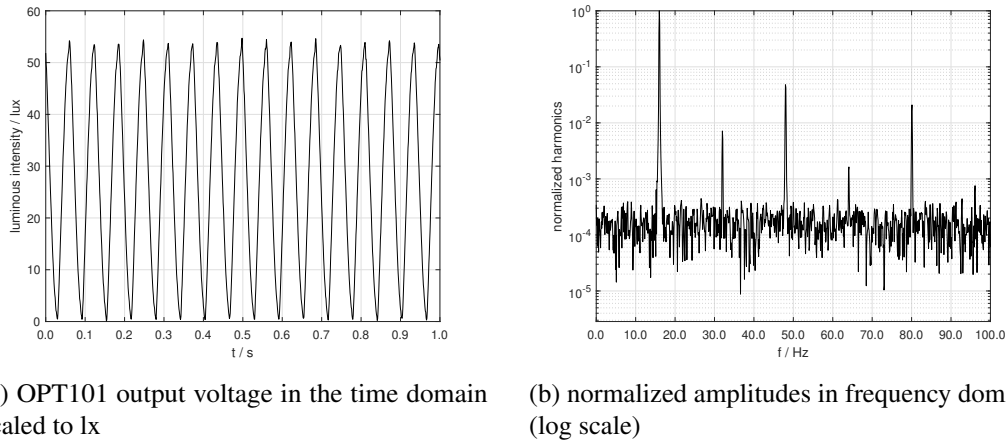


Fig. 2.22 Measuring the luminous intensity of Epson Moverio BT350 smart glasses nominally flickering at 16 Hz.

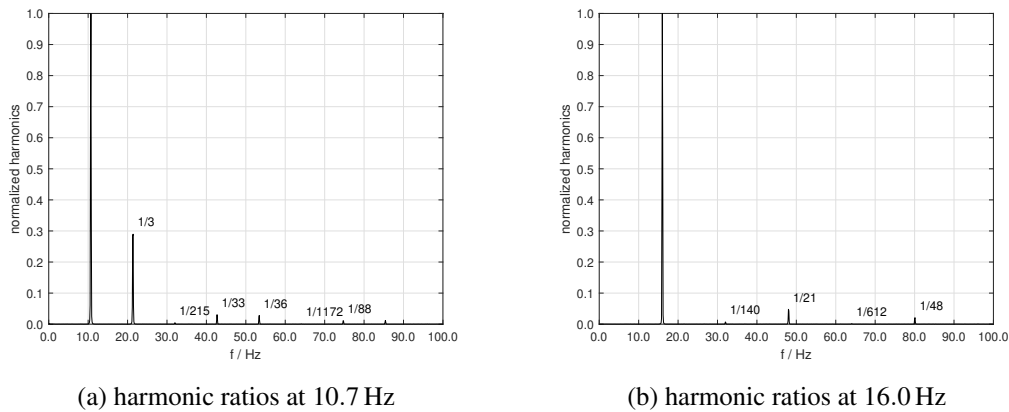


Fig. 2.23 Comparing the harmonic amplitudes normalized at the first harmonic for two representative flickering frequencies.

considerations concerning the harmonics to be detected in the EEG spectra are conducted in the following, and this is another relevant aspect for the SSVEP-BCI functionality.

In addition to the measurements conducted on the Epson Moverio devices, which are representative kinds of smart glasses for augmented reality, the Microsoft HoloLens (1st Gen) were also considered as an example of a mixed reality device. The emitted luminous intensity was still measured with the photodiode-based transducer, but measures revealed a different working principle. To highlight that, Fig. 2.24 represents the measures corresponding to a 3 Hz flickering and a 10 Hz flickering. Note that the HoloLens were programmed in Unity by replicating the Android application

already used for the Epson Moverio. Measures thus reveal that there is no definite "on period" or "off period". Instead, there are light pulses with different frequencies: when the icon is off, there are less pulses in the unit time, while the number of pulses is greater when the icon must be on. Such a behavior is evident from the time domain, while it is not possible to analyse these measures in the frequency domain as done before. Although light modulation is different from the Epson Moverio case,

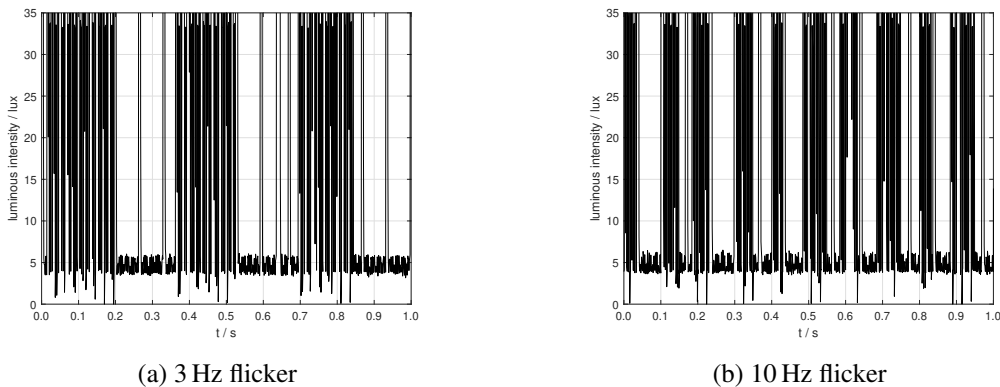


Fig. 2.24 Measures associated with Hololens white flickering icon represented in the time domain.

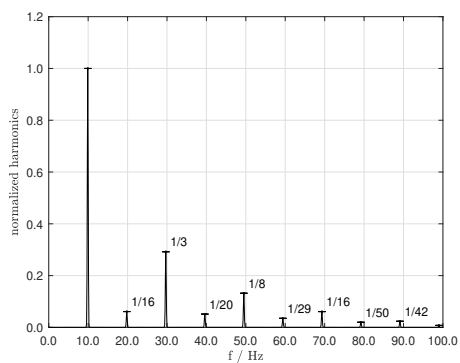
the human eye does not see any difference. Then, it will be interesting to point out eventual differences in the corresponding electroencephalographic signals. This is briefly discussed in the next section.

2.5.3 The human brain as a transducer

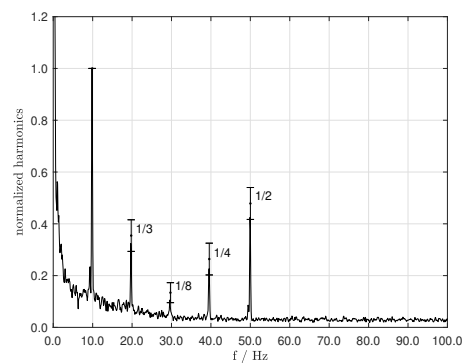
Characterizing the components of a brain-computer interface is an essential step in willing to understand how the human brain works. Indeed, once instrumental errors are excluded or corrected, one can isolate the user's contribution to the BCI measurement chain in terms of generated or transduced signals. Surely, many different brain activities could be investigated, and they actually are in many laboratory settings. In this section some considerations are specifically reported for SSVEP as a representative case of reactive paradigms. Indeed, evoked potentials have been widely studied and the response of the brain to external stimulation is understood, though not completely explained. For instance, in literature the non-linear origin of SSVEP spectra has been investigated in trying to explain the harmonics associated with the measured electroencephalographic signals in relation to visual stimulation

[75]. Moreover, in [86] it was shown that stimulating a user with a square wave, the SSVEP response in the frequency domain will have 2^{nd} , 3^{rd} and 4^{th} harmonic. There, usually the first one and second one are with the highest amplitude, so that these two are mostly considered in signal classification. Nevertheless, in their work, the authors focused more on interpreting the brain signals than classification, and they already noted that, due to the limited frequency of the displays, some issues arise in the design of stimulus applications.

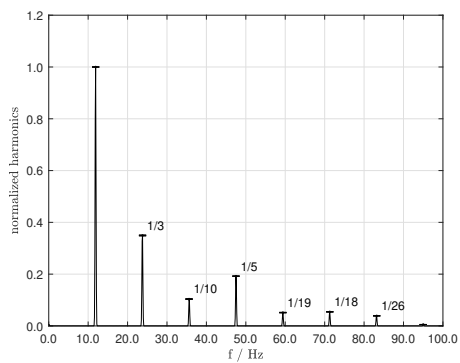
As a matter of fact, previous results of the present thesis have shown that novel technologies and off-the-shelf components for wearable BCIs can introduce some errors. Therefore, it is interesting to analyse the results of some preliminary experiments with the SSVEP-BCI after correcting the instrumental errors. It is to remark that such corrections are not mandatory in the SSVEP-BCI operation, where the focus is on classifying the brain signals to understand which icon must be activated. Instead, they are needed in investigating how the visual system of a human transduces light into electrical signals. Preliminary EEG data from BCI experiments with SSVEP has been thus used in comparing the spectra of the flickering icons discussed above and the EEG spectra. Fig. 2.25 compares the results of repeated measurements with the BT-200 smart glasses and the EEG spectra of a trained subject using the SSVEP-BCI. In details, Fig. 2.25a and Fig. 2.25c report the mean spectra across repeated measurements with the 10 Hz and 12 Hz flickering, respectively. The standard deviation of the peaks is reported as well. Thanks to that, it is clear that the optical output of the BT-200 has a quite stable behavior. Meanwhile, Fig. 2.25b and Fig. 2.25d report the mean EEG spectra obtained with 12 measures each, along with the standard deviation of the peaks. There, the amplitudes were corrected by considering the measured gain for the Olimex EEG-SMT. In this case, the error bars representing standard deviations are relatively high, thus proving an intrinsic uncertainty arising from the brain transduction effect. It can be also seen that there is not a clear correspondence between the peaks observed in the flickering icons and the ones observed in the EEGs. However, an exhaustive analysis of the neurophysiological response to flickering lights goes beyond the scope of this thesis. Indeed, this brief discussion was used to better tune the classification strategy for the SSVEP-BCI, and it appears also useful to point out the presence of instrumental error that must be taken into account when studying the brain as a system. Nonetheless, this interesting and non-trivial analysis is addressed to the specialized literature.



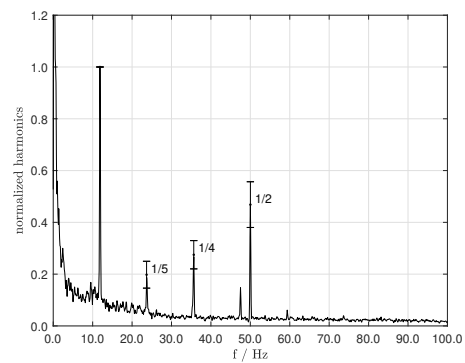
(a) mean spectrum for a 10 Hz flickering icon with standard deviation of the peaks



(b) mean EEG spectrum and standard deviation of the peaks for 10 Hz stimuli



(c) mean spectrum for a 12 Hz flickering icon with standard deviation of the peaks



(d) mean EEG spectrum and standard deviation of the peaks for 12 Hz stimuli

Fig. 2.25 Repeated measures for the flickering icons and corresponding EEG spectra. Mean spectra are compared as well as the standard deviation of the peaks.

Chapter 3

A wearable BCI based on evoked potentials

Reactive brain-computer interfaces are the most performant in terms of brain pattern recognition. At the current technological state, training and detection time are generally low, though they can be still unsuitable for many practical applications. The performance achievable by a reactive BCI is due to the presence of an external stimulation, which generates a neurophysiological response to detect and classify. By classifying such brain patterns, the system understands the user's intention and generates a command for the desired application. Nonetheless, the need for external stimuli is probably the main drawback of reactive BCIs. The current chapter discussed the possibility to realize a highly wearable BCI by relying on steady-state visually evoked potentials, or SSVEPs for short. Such an interface requires flickering lights as external visual stimuli, which can lead to eye fatigue and affect long term performance. Nonetheless, SSVEP-based BCIs are trainingless or require minimal training, and their classification accuracies are above 90% even with 1 s to 2 s visual stimulation.

The remainder of the chapter is organized as follows. Section 3.1 resumes the notions required in building a BCI based on steady-state visually evoked potentials. Section 3.2 proposes a SSVEP-based BCI realized by integrating the already introduced electroencephalograph with augmented reality glasses. Section 3.3 presents the results of an experimental campaign conducted with such a system to assess its performance. This discussion comprises the statistical analysis of the acquired

EEG measures in order to highlight both intra-subject and inter-subject variability. Evidently, this variability affects the system performance, and it is traced back either to physiological phenomena and instrumentation uncertainties. Finally, application examples are reported in Section 3.4 with respect to the industrial framework and healthcare. Those solutions were investigated as a consequence of the reactive BCI realization discussed hereafter.

3.1 Steady-state visually evoked potentials

Evoked potentials are electrical brain signals caused by sensory stimulation. The related brain patterns reflect brain mechanisms and measuring them can either provide further understanding of such mechanisms or an alternative communication way for the user. Visually evoked potentials (VEPs) have been largely exploited in developing EEG-based BCIs [40, 87, 88]. Certainly, investigated paradigms also involve acoustic [89] or tactile stimulation [90], especially when dealing with people with vision impairment. Nonetheless, the visual channel is the most intuitive one and hence the most studied. Different types of VEPs can be distinguished [91]. Notably, *steady-state visually evoked potentials* are elicited by lights flickering so that the effects of consecutive flashes overlap, thus giving rise to a steady state. The minimum flickering frequency for eliciting SSVEPs is about 6 Hz. Meanwhile, an upper limit is not explicitly determined: human response to flickering was studied up to 100 Hz, but most studies do not overcome 60 Hz [88, 92].

The operating principle of SSVEP-based BCIs is rather simple. If the user gazes at a flickering light with frequency f , the evoked potential has fundamental frequency equal to f . Therefore, if multiple lights are flickering at different frequencies, the SSVEP frequency detected from the measured EEG is associated with what the user is gazing at. Actually, different flickering lights could also be distinguished by means of their phase other than their frequency. Though this principle is quite interesting, such a possibility was not considered in the present work. Ultimately, SSVEP allows a user to communicate by merely staring at a light or an icon on a display. The advantage is that, at least in principle, no training is required neither for the system operation nor for the BCI user [93]. Despite that, the system can be tuned on a specific subject to enhance detection performances with minimal adjustments. For instance, the processing algorithm can be trained for a specific user with little

training, or the electrodes position could be personalized for each user. These aspects will be better discussed next with specific regard to our SSVEP-BCI.

As mentioned above, the main drawback of reactive BCIs is the need for external stimuli. In the SSVEP case, the previously underlined advantages are thus counter-balanced by the need for the user to stare at a screen and keep his/her eyes fixed for a certain time. Nevertheless, many studies showed that SSVEPs are very reliable owing to good reproducibility and superior classification accuracy if compared to other BCI paradigms [94–96]. One could also argue that, since the working principle involves shifting the eye gaze, a SSVEP-based BCI could be replaced by an eye tracker, which has higher performance in recognizing eye position. This appears true when considering that most BCI studies concede eye movements. However, it was shown that in a SSVEP-BCI user can shift attention rather than gaze [97], so that it is not necessary nor sufficient to move eyes, but the user must focus his/her attention on the flickering light. Given that, SSVEP-BCIs can solve a major issue in eye tracking technology, where the system cannot distinguish an unintentional fixation from intentional ones. Also, SSVEP applications can be addressed to both healthy people and to people with no oculomotor control, such as patients in advanced stages of amyotrophic lateral sclerosis (ALS) [98].

In this thesis, smart glasses are exploited for visual stimuli generation. Relevant research solutions were resumed in [99] by reporting that the main application field for VEP-based BCIs is robotics, and that video see-through glasses are mostly considered. However, many limitations still prevent the usage of these systems in daily life, especially artifacts [100, 101] and the trade-off between SSVEP detection speed and classification accuracy [87]. These issues are exacerbated when dry electrodes are employed to increase user comfort. Hence, even recent works turn out to be feasibility studies [51, 63]. As a first example of competing SSVEP-BCIs, in 2018 a single-channel BCI was proposed [92] as a speller relying on high-frequency stimuli. Only five subjects participated in the experimental campaign. Each user had to stare at the icon for 10 s and they reached a mean classification accuracy equal to 99.2 %. However, the reproducibility of the results is not assured given the limited number of subjects. As a further example, another speller was proposed in 2019 [102] by exploiting a single acquisition channel, dry electrodes, and a deep neural network for signal processing. The mean classification accuracy among eight subjects was 97.4 % when each subject starred at the flickering lights for 2 s. Despite the good performance, still a few subjects were involved in the campaign

and many trials (about 500) were needed to train the deep network. Finally, it is worth reporting that [51] proposed a BCI integrated with AR glasses for controlling a quadcopter. In this solution, 16 dry electrodes were used, and the mean classification accuracy on five subjects resulted in 85 % while executing a flight task. It should be noted that this accuracy is lower than the previously reported ones, although more electrodes were used. This probably happens because of the flight task that lowers users' attention. Hence, this is a representative example of how leaving controlled laboratory conditions can affect the BCI performance.

3.2 System design and prototyping

The SSVEP-BCI discussed in this thesis has been already introduced in the previous chapter to conduct a metrological characterization of representative building blocks for a wearable neural interface. In that context, the overall working principle was anticipated to justify the investigation of specific phenomena concerning such components off-the-shelf. Conversely, the present discussion deals with the realization of the SSVEP-BCI system, given that the performance of the building blocks are already individually assessed. The architecture of the proposed SSVEP-BCI is shown in Fig. 3.1. Its building blocks are

- AR glasses employed as a visual stimuli generator;
- EEG transducer acquiring the brain signals;
- computing unit to process brain signals and achieve a control command.

Note that the input interface for the system is made of either the EEG transducer, the computing unit for processing, and also the visual stimulation. Moreover, the computing unit and output interface of the AR glasses manage the BCI application also in terms of the visual information resulting from the user's control. Another picture of this SSVEP-BCI system was already presented in Fig. 2.5, while the system worn by a user will be shown next. The implementation of each system block is instead discussed hereafter.

The proposed system allows the user to control augmented reality glasses with his/her brain activity. As already discussed, SSVEP-based BCIs require visual stimulation with flickering icons. The display of AR glasses can provide this stimulation

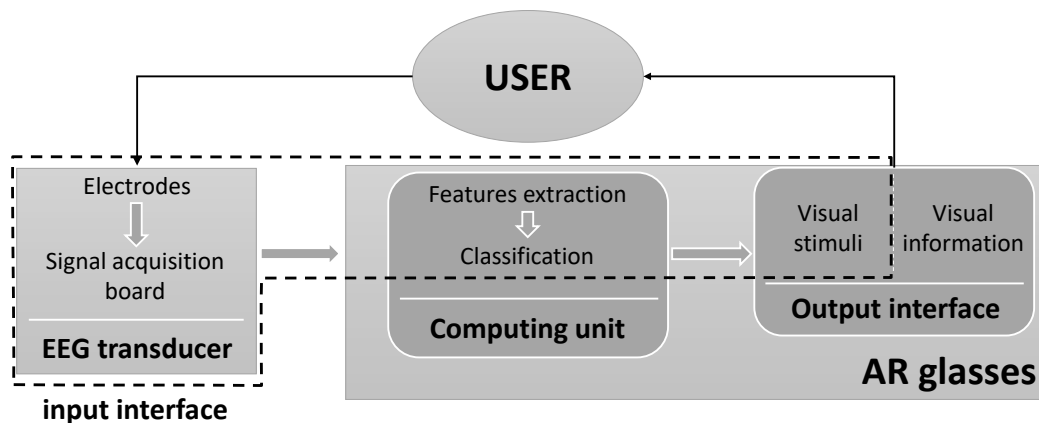


Fig. 3.1 Architecture of the AR-BCI system based on steady-state visually evoked potentials.

while being wearable, in contrast with mostly adopted solutions based on LEDs. The flickering icons on AR glasses display correspond to choices for the user during the usage of an application, and thus they substitute a more traditional interface based on a touch-pad. The potentials evoked by the flickering are then measured with an electroencephalography.

In signal acquisition, different aspects were taken into account. Firstly, brain activity had to be measured with a single-channel non-invasive EEG, due to the practical reasons discussed at the end of Chapter 1, notably user-friendliness and low cost. Secondly, dry electrodes were chosen because electrolytic gels would pose some issues in long-term usage, for instance the need to repeatedly apply the gel that dries out. Dry electrodes are easier to be worn and they might still provide proper EEG measures. On the other hand, avoiding conductive gels poses a severe issue on electrode-skin contact: if the contact impedance is too poor, the EEG activity is not present in the recorded signals. To this aim, tight bands were used to ensure a good electrode-skin contact.

Finally, in order to recognize the user's intention, EEG signals must be processed. The final aim is to assign a class to each signal recorded for a certain time, and that class should be associated with the user's intention, i.e. the control command for the application. Two main parameters will be used to characterize the performance of the system: the classification accuracy, namely the success rate in classifying the brain signals, and the latency for the system to react, consisting of acquisition time plus elaboration time required to make a choice. One may guess that there will be a

trade-off between classification accuracy and latency. The details of the proposed system are discussed in the next subsections.

3.2.1 Augmented reality glasses

As a reactive paradigm, the SSVEP-BCI requires flickering icons on the AR glasses display for visual stimulation. In particular, the specific VEP exploited in this work regards the generation of an oscillation at the same frequency of the flickering stimulus. Hence, when staring at a specific icon, the user's intention is easily retrieved from the frequency domain. Each icon flickers at a specific frequency, and these frequencies must be carefully chosen. Also note that an amplitude modulation could not be considered to encode the information of each possible choice. The reason for that lies in the inter-subject and intra-subject variability of SSVEP signals, but also because of the poor amplitude accuracy of the off-the-shelf components adopted in the system implementation. A phase modulation, instead, would have required a higher stability of the flickering stimuli, but the AR glasses characterization suggested that this is not the case for a typical commercial device. In conclusion, these techniques would have required further investigations, which were beyond the scope of this work.

In its original implementation, the SSVEP-based BCI exploited only two icons. A custom Android application was developed so that these icons could be placed on the opposite corners of the AR glasses display. Moreover, referring to literature studies, white squared icons were implemented to optimize the stimulation. The flicker frequencies were chosen in the *alpha* band (8 Hz to 13 Hz) according to a study indicating this range as the one associated with maximum amplitude of elicited oscillations [95]. Specifically, the nominal flickering frequencies were set at 10.0 Hz and 12.0 Hz. By exploiting the results of Section 2.5, the related uncertainty was estimated to be in the order of 0.1 Hz. The Android "open graphic library" (*OpenGL*) was used in implementing the icons so that the GPU could manage the flickering. Indeed, avoiding the use of CPU in this thread aims to maximize flickering stability, which could be affected by operating system interruptions.

To make a choice through a flickering icon, the user has to stare at (or simply focus on) the desired icon for some seconds. This interval corresponds to the EEG acquisition time. As a first implementation, such a time was fixed a-priori, while

a variable time window can be also used by exploiting a stopping criterion for the flickering. Such a possibility will be recalled later on as a possible variant of the basic system functionality. It was already anticipated that the Epson Moverio BT-200 was used as an output interface, namely the AR devices for both visual stimulation and visual interface with the application. The Android application running on such glasses acquires the EEG signals in parallel to visual stimulation, while the processing of those signals is conducted at the end of the acquisition window. An attentive reader could guess that the processing should be instead conducted in real-time when the acquisition time is not fixed a-priori. Acquisition and processing are detailed next. At the end of those steps, the user's intention is retrieved, short of misclassification errors. The control command triggers an action in the application, e.g. one could request to read data from a sensor. The chosen AR device is capable of communicating with external devices through Bluetooth or WiFi. Hence, the information of interest for the user can be requested without using hands thanks to the EEG transduction, and wireless communication and control is possible.

3.2.2 Single-channel electroencephalography

In the architecture presented in Fig. 3.1, the input interface of the AR-BCI system is a non-invasive single-channel EEG transducer. Only two dry electrodes are employed for a differential acquisition of brain signals. This allows one to have an utmost wearable system. The electrodes are placed on the scalp, according to the 10-20 system [2] at the points "*Fpz*" and "*Oz*", as it was already highlighted in black in Fig. 1.5. This choice was done by considering that "*Oz*" is located at the occipital region of the brain, the one associated with visual activity, while "*Fpz*" is at the frontal region, where it is reasonable to assume limited visual activity. Therefore, a differential acquisition aims to emphasize the only visual activity by subtracting part of the ongoing brain activity. To mitigate the contact impedance issues, silver pins were soldered on the occipital electrode, which needs to overcome the hair to reach the scalp. Furthermore, the use of active dry electrodes eases impedance matching by buffering recorded signals on the electrode itself. In particular, the active electrodes include a circuitry based on an operational amplifier for impedance matching. A third passive electrode, i.e. without active buffering, acts as a ground for the measurement. This ground electrode is usually placed on the forehead, the ear, or even on a wrist or a leg [43]. In this work two positions were exploited: the

left wrist and the left ear. No meaningful difference was found between these two placements, at least in terms of system functionality. Meanwhile, placing the passive electrode with a clip on the ear guarantees better mechanical stability of the passive electrode, which surely results in a more reproducible measurement.

The Olimex EEG-SMT with dry electrodes was chosen for the implementation of the EEG transducer. One of the main reasons for this choice was the very low-cost if compared to more classical EEG amplifiers. It is worth remarking that the discussion of Section 2.4 assessed the metrological properties of this device, which proved adequate for wearable BCI applications. Nonetheless, the skin-electrode impedance could not be studied with a mere electrical characterization of the device. This had to be proven by experimenting with human users, and such contact impedance issues resulted in the most challenging aspect in EEG acquisition. In the prototyping phase, a good electrode contact was ensured with a tight headband for the active electrodes on the user's scalp.

The electrical brain activity measured with the electrodes is transmitted to the EEG transducer board. The two active electrodes are connected to the differential input of an instrumentation amplifier at channel 1 (CH1). A twin channel (CH2) is available in the Olimex EEG-SMT board, but it was not used in the SSVEP-BCI, so it had to be internally short-circuited. Meanwhile, the passive electrode provides feedback for instrumentation amplifiers to reduce common mode noise. In the Olimex EEG-SMT, this is connected to the input "drive right leg" (DRL) input. Signal conditioning is done with several stages providing amplification and/or filtering. The overall gain from the signal pick-up to an analog-to-digital converter (ADC) was set to 6427 V/V thanks to the second amplifying stage, which grants an adjustable gain. The input signal is analogically filtered with a 3rd order Butterworth filter, whose nominal pass-band is 0.16 Hz to 59 Hz. At the end of the amplification and filtering chain, an ADC with 10-bit resolution provides the conversion to a digital signal with a nominal sampling frequency equal to 256.0 Sa/s. The digital signal can thus be transferred to the computing unit of the AR device to be processed. Note that the Olimex EEG-SMT continuously acquired and sent the digitized signals over UART connection (with an USB cable for instance), so that the Android application can save only the EEG epochs of interest.

3.2.3 Detection of evoked potentials

In the previous discussion, it was largely anticipated that the frequency domain enables an easy and intuitive detection of the SSVEP oscillations. In detail, a power spectral density analysis was considered in this work for brain signal processing. A further reason for that was to guarantee low computational burden in implementing a wearable system. Moreover, the good knowledge on the SSVEP phenomena make it useless to adopt computationally challenging approaches, such as deep neural networks, which would also require much EEG data. To present the processing steps of interest, it is useful to distinguish the *feature extraction* and *classification* steps.

In feature extraction, the digitized signal is pre-processed with a digital pass-band filter based on a FIR (finite impulse response) filter. After some preliminary trials, an optimal band was identified, the 6 Hz to 28 Hz range and order 100 was set to have at least 50 dB attenuation in the stop band. The pass-band was also chosen by considering the need to reduce eye-blinking and muscle artifacts [45]. Indeed, linear filtering could be used to reduce noise introduced by artifacts, while methods like regression would need a higher number of electrodes. After that, zero-padding is applied prior to executing a fast Fourier transform algorithm, the well-known FFT. Zeros are thus added at the end of the signal samples to reach the nearest power of 2, so to speed up the FFT execution and possibly provide better frequency domain resolution. Note that zero-padding can fictitiously enhance resolution only because of interpolation, while the actual spectral resolution depends on the length of the EEG epoch, i.e. the acquisition time window. This step makes it clear the trade-off between system latency and classification accuracy: a longer acquisition time enables better frequency resolution and hence better SSVEP detection, since frequency resolution is the inverse of time window. On the contrary, lower latencies are desirable to avoid long selection times for the icons, but this limits the resolution in detecting SSVEP peaks. Furthermore, the Hamming windowing is applied to reduce spectral leakage, while slightly losing in spectral resolution.

Once the signal under analysis is properly represented in the frequency domain, power spectral density (PSD) analysis is carried out on the discrete amplitude spectrum. For each frequency f_i , the corresponding PSD is calculated as the sum of

the squared amplitudes associated to the k_i -th bin and some nearest bins:

$$P(f_i) = \frac{1}{2k+1} \sum_{n=k_i-k}^{k_i+k} A^2(n), \quad (3.1)$$

where k_i is the bin associated with the frequency f_i , k is the number of bins considered on the right and on the left of the bin k_i , and $A(n)$ the amplitude associated to the n -th bin. The bin number k_i is retrieved from f_i by means of the spectral resolution Δf of the FFT, at least in principle, since $f_i = k_i \Delta f$. The frequency f_i can be equal to the nominal stimulation frequency or a higher harmonic of it (an integer multiple). However, the SSVEP peak could not be exactly located at f_i , and hence there is a preliminary step in which the maximum in the neighbourhood of k_i is found. The considered neighborhood was 0.4 Hz. For the sake of clarity, this bin is referred to as k'_i . Extracting the PSD leads to a new representation of an EEG signal in a features domain. Two possible representations were thus investigated: the first considers the PSD at 10 Hz and 12 Hz, while the second also considers the respective second harmonics, i.e. 20 Hz and 24 Hz. In the former case, each signal is represented as a point in a plane, while in the latter one it is represented as a point in the 4D space. Typically, higher order harmonics were not considered because of the poorer signal to noise ratio, but they could also contribute to signal classification in some cases.

In the features domain representation, a hyperplane was adopted to separate the two classes of signals. Specifically, a support vector machine was used by investigating the linear and the Gaussian kernel. After some preliminary trials on EEG signals, the linear kernel resulted in the optimal solution. Hence, the actually adopted classifier is a support vector classifier (SVC) [3]. The analysis of EEG signals and the training of the classifier was done in Matlab. The training must be conducted with labeled EEG signals, i.e. signals for which one knows the belonging class (in the present case, 10 Hz stimulation or 12 Hz stimulation). Notably, Matlab is really useful in deriving the SVC hyperplane parameter that can be then used to classify new unlabeled signals. However, either the PSD features extraction and the classifier usage after training was then translated in Java per Android. This step was necessary in building a wearable system. For the classification step, implementing the SVC in Android simply consisted in solving an inequality considering the hyperplane parameters and the dot associated with the signal to classify.

3.3 System performance

After the design of the BCI system based on SSVEP, and its prototyping by means of the commercially available components mentioned above, validation was necessary. Indeed, a metrological characterization of each system component was carried out as detailed in Section 2.3, Section 2.4, and Section 2.5, but experiments with human users were of course needed to prove the system functionality and assess its performance. In the following, some details about the experimental campaign are reported with specific regard to the setup, the experimental conditions, the assumptions, and the involved subjects. Then, the results in terms of classification accuracy are discussed, and a particular focus is given to the trade-off between the stimulation time (greatly affecting the system latency) and this classification accuracy.

3.3.1 Experimental campaign

Twenty subjects took part in the experiments, of which 13 males and 7 females with age between 22 and 47 years old. Experiments were conducted in a laboratory with closed blinds, so that luminance could be controlled with neon lights. Illumination was hence monitored during the experiments and it resulted in the 95 lx to 99 lx range. All the electrical and electronic instruments that were present in the room were switched off to avoid interferences with the EEG. Surely a laptop was running to acquire from the EEG transducer during the first experimental phase. However it was unplugged from the mains supply during signal acquisitions. Another electronic device in the room was indeed the AR device, which was also battery-supplied during experiments. Finally, smartphones were present in the room, but their interference did not appear on the recorded signals.

Although the final aim is to build a portable system, each subject under test was asked to sit on a comfortable chair with armrests and limit unnecessary movements. Unfortunately, moving the head or the arm greatly affects the contact of the electrodes with the skin since no conductive gels were used. Therefore, these constraints were necessary in the first experimental phase to exclude motion artifacts and in general to ensure the correct electrodes positioning. Once seated, the user could wear the system. The AR glasses had to be worn first, and then a tight headband could be used to fix the electrodes at the occipital and frontal region of the scalp. Also note that

in these experiments a tight armband was used to fix the ground passive electrode on the left wrist of the user. In connecting the electrodes, the same sequence was adopted for every user while checking in real-time the acquired signal with a proper Matlab script:

1. the passive electrode was connected to the DRL input of the EEG transducer and applied on the subject's left wrist with the armband; the acquired signal had to be null due to the absence of signal at CH1 (or CH2);
2. the first active electrode (without silver pins) was connected to the negative terminal of CH1 and placed on the scalp at "*Fpz*" (frontal region) with the help of the headband;
3. after a transient (lasting a few seconds), the acquired signal had to return to zero again, since CH1 is still an open circuit at this stage; indeed, the internal circuitry reaches a stationary condition with a null output;
4. lastly, the second active electrode (with silver pins) was connected to the positive terminal of CH1 and placed on the scalp at "*Oz*" (occipital region of) with the help of the headband; after another transient of a few seconds, a stationary condition is reached in which the mean signal amplitude is null;

The EEG acquisition board was connected to the laptop to acquire signals with a Matlab script. At the beginning of each test, the EEG signal amplitudes had to be checked: it was empirically determined that proper electrodes placement was associate with signal oscillations with a peak-to-peak amplitude below $100 \mu\text{V}$. However, because of dry electrodes, some artifacts could be occasionally present, notably the ones associated with subject's eyes blinking. Unfortunately those artifacts could not be avoided, and in case of badly placed electrodes they led to amplifier saturation. At least 1 s is typically needed to recover from saturation, and hence such a condition had to be avoided. On the other hand, when an artifact related to eye-blink was present but no saturation occurred, signal disruption appeared not meaningful, as already shown in Section 2.3. A typical signal measured with the worn EEG transducer is represented in Fig. 3.2. The artifact related to eye-blinks is revealed with the presence of negative valleys. Note that this phenomenon is not present in EEG systems employing wet electrodes. Given that, the presence of such valleys was reasonably led back to electrodes movement, while it seems unreasonable to read

those valleys as neural activity associated with eye movements. As a further proof of that, similar artifacts appear on the recorded signal when moving the electrodes in other ways. Nonetheless, this particular aspect would require more investigation and a quantitative assessment that was not conducted during the present work.

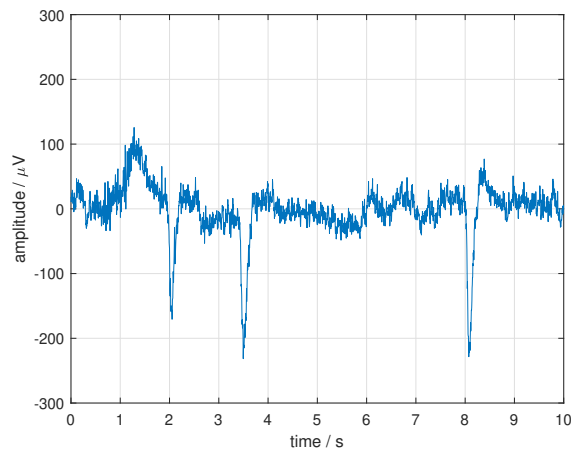


Fig. 3.2 An example of a signal measured with the Olimex EEG-SMT after placing all the dry electrodes for SSVEP detection. Note that some artifacts related to eye-blinks are present.

For each subject, first 24 trials with a single flickering icon were carried out, and then other 24 trials with two flickering icons were conducted. In the first set of trials, the flickering frequency was randomly chosen between 10 Hz and 12 Hz in order to avoid user biases. According to the design, the 10 Hz flickering icon appeared on the bottom-right corner of the AR glasses display, while the 12 Hz appeared on the up-left corner. In each trial, the brain signal was acquired for 10.0 s, and a few seconds passed between consecutive trials. Note that 10.0 s was chosen as an upper limit for user stimulation, which could be already unacceptable in several practical applications. However, smaller time windows can be analysed too by properly cutting the recorded signals and retrieving smaller epochs. The set of trials with two simultaneously flickering icons followed the same principles, but the user had to randomly choose the icon to stare at. In both cases, the only constraint was that the subject had to stare at both icons for 12 times each. At the end of a trial the subject had to declare the choice he/she made, so as to have a class label for each trial. In doing this, there is no guarantee that the user was effectively able to focus the attention on the declared icon for the whole acquisition time. It is also worth noting that the phase of the flickering icon was not synchronized with the acquisition

starting. For this reason, the phase information of the signals is not exploitable for these EEG data.

The data acquired in the described conditions served to train and test the processing of SSVEP signals. This allowed to validate the system design and also to make adjustments where needed. Then, in a later phase, experiments were conducted with the signal processing directly implemented on the AR glasses computing unit, thus avoiding the usage of the laptop with Matlab. In this way, the BCI system is really wearable and portable and it could be exploited in different applications. These applications are described at the end of this Chapter.

3.3.2 Classification results

The EEG data acquired from each subject during the visual stimulation was analysed as described in paragraph 3.2.3, namely by representing each signal in terms of PSD at the stimulation frequencies or their multiple harmonics. Different aspects can be considered in discussing the classification of such signals. First, it is useful to compare the class separability between EEG signals corresponding to 10 Hz stimulation and 12 Hz stimulation. Fig. 3.3 shows the signals of all subjects in the PSD features domain. In particular, each signal is a point in the 2D plane identified with the respective PSD at 10 Hz (x-axis) and 12 Hz (y-axis). A 10 s-long stimulation is currently considered, and the case of a single stimulus is compared with the case of two simultaneous stimuli. The signals corresponding to the two different stimulation frequencies are distinguished by their color. As a general trend, the two classes are quite separated in the features domain. However, there is an overlap between the two classes and some of the signals fall into the “wrong region”: for instance, one of the signals labeled as *class* 12 Hz in Fig. 3.3a is very far from other signals of the same class and much closer to the *class* 10 Hz. Note that better class separability could be expected for the “1 stimulus”, while in the “2 stimuli” case one could foresee an interference of the other stimulus while the user is trying to stare at one of them. Nonetheless, qualitatively speaking, there is no such evidence in comparing Fig. 3.3a and Fig. 3.3b. On the contrary, the classes may seem better separated in the “2 stimuli” case. This will be better assessed in a while by quantifying class separability with classification accuracy.

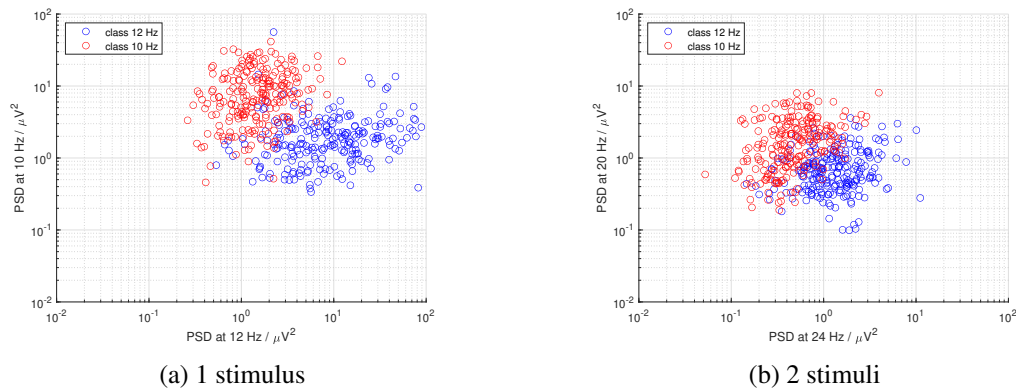


Fig. 3.3 Scatter plot of EEG signals in the PSD features domain, associated with 10 s-long stimulation and for a different number of simultaneous stimuli. Both axis are in logarithmic scale.

It is also interesting to consider a shorter stimulation time: this can be done in post-processing by considering fewer samples of the acquired signals. In doing so, a 2 s-long stimulation time is taken into account. Surely, a shorter stimulation is desirable to speed up communication and/or control with the SSVEP-based BCI, and the trade-off between system latency and classification accuracy will be extensively discussed in the following paragraph. Either way, Fig. 3.4 anticipates that SSVEP classification is less accurate in such a case because, as expected, classes are less separable. It would be also interesting to distinguish between different subjects, so to graphically highlight if there exist "good" and "bad" subjects. Nevertheless, analysing 20 subjects with scatter plots is not manageable and assessing the classification accuracies was needed before further considerations. Finally, as mentioned above, further PSD features can be considered, but a geometrical representation is challenging for a 3D space and impossible for a 4D or higher-dimensional space. Also in this aspect, a metric like classification accuracy is essential.

Several metrics could be used to quantify the separation between classes. As an example, for each class a center could be identified and the Euclidean distance between these centers is a measure of separability. However, hereafter the classification accuracy is considered since it is well related to the BCI system performance. As discussed previously, this metric is obtained as the ratio between the number of correctly classified signals (according to their known class label) over the total number of signals to classify. Therefore, such a metric is directly related to the success rate with which the SSVEP is correctly detected by the BCI system. It is

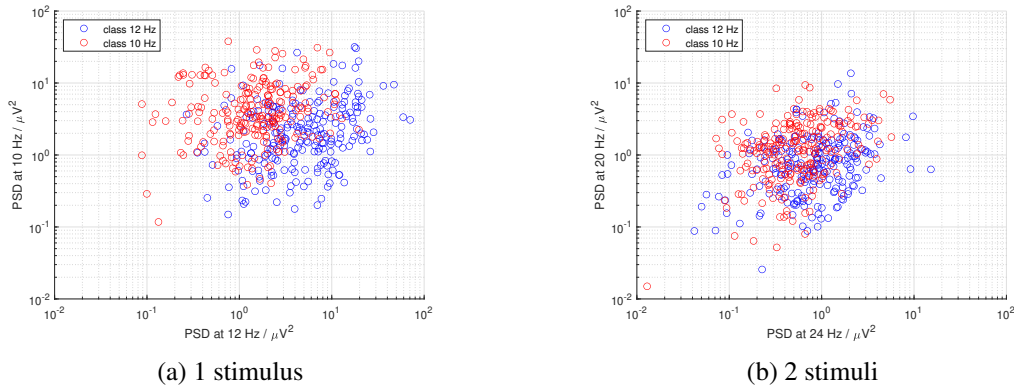


Fig. 3.4 Scatter plot of EEG signals in the PSD features domain, associated with 2 s-long stimulation and for a different number of simultaneous stimuli. Both axis are in logarithmic scale.

even clear that knowing the true labels for all the signals is crucial in assessing the classification accuracy. In the present case, the subject had to declare at the end of each trial the chosen stimulus, so that the probability of a wrongly assigned label is non-null. This is also true for the "1 stimulus" case, where the user could manually select the unique stimulus appearing for each trial and declare the choice at the end of it. Although these errors are possible, it was reasonably assumed that the number of wrong labels is actually very low. Therefore, the main causes for a classification accuracy lower than 100% are poor concentration during some experimental trials, low SSVEP activity, EEG measurement errors, such as temporary electrode disconnection and eye-blink artifacts, or the classification model itself. When identifying the classification model, some trials are needed together with their true labels to tune model parameters: in machine learning, these are referred to as the *training set*. Then, a *test set* is needed to validate the identified model. In the current analysis, cross-validation was used to iteratively split the available data into training and test, so to achieve for each split a classification accuracy on the test set. The mean accuracy between different splits gives an estimate of the model accuracy on unseen data. In particular, a 4-folds cross-validation was considered, thus splitting the data in 75 % for training and 25 % for testing four times. Together with the mean classification accuracy, the standard deviation can be obtained too, so to quantify the precision of this mean. Table 3.1 report the cross-validation accuracy (with associated standard deviation) for the 20 subjects considered as a whole and one-by-one, for either the "1 stimulus" and "2 stimuli" cases, as well as for a 10 s-long and 2 s-long visual

stimulation. Note that the subject "DeLAnn" had no trials for the "1 stimulus" case due to measurement issues, so there is no accuracy to be calculated. It can be seen that, as anticipated, a longer stimulation outperforms a shorter one, while there is no meaningful difference between the "1 stimulus" and the "2 stimuli" case. Hence, in this setup, the non-gazed stimulus is not generally disturbing the focus on the other one. It is worth remarking that in both cases the classification happens among two classes, while increasing the number of total stimuli would indeed reduce the classification performance.

	<i>10 s-long stimulation</i>				<i>2 s-long stimulation</i>			
	1 stimulus		2 stimuli		1 stimulus		2 stimuli	
subject	acc/%	std/%	acc/%	std/%	acc/%	std/%	acc/%	std/%
all	91.2	3.1	94.2	1.8	74.8	4.8	77.5	1.2
EspAnt	100.0	0.0	100.0	0.0	75	12	100.0	0.0
CioAnt	100.0	0.0	100.0	0.0	80	15	98.8	4.4
DasCre	100.0	0.0	100.0	0.0	95.8	7.3	92	10
PasLor	100.0	0.0	100.0	0.0	81	15	92	10
CraFed	100.0	0.0	100.0	0.0	78	16	88	12
ErrErn	100.0	0.0	100.0	0.0	94.6	8.8	87	15
FalGia	100.0	0.0	100.0	0.0	67	19	87	12
CraSim	91.7	8.4	100.0	0.0	58	15	64	17
PetPas	88	10	97.9	7.7	72	16	57	12
DeLAnn			96.7	6.8			88.8	8.8
VasBen	80	15	96	10	68	17	64	17
TeoAle	97.1	6.4	95.8	7.3	74	13	78	13
CapFra	81	14	95.4	8.4	63	15	83	12
SpeMar	75	15	95.4	7.5	48	18	53	18
PesMar	100.0	0.0	94	11	80	15	80	12
FroMir	90	12	92.9	8.3	70	16	61	14
MocNic	97.9	5.6	91	11	78	14	78	14
CanAle	80	14	89.6	9.8	80	15	61	16
DeAGio	65	12	81	17	51	17	52	15
CicMel	88	11	71	15	80	16	49	16
MEAN	91		94.9		73		76	
STD	11		7.4		12		16	

Table 3.1 Classification performance of SSVEP-related EEG signals. For each subject, the "1 stimulus" case is compared with the "2 stimuli" case, and the results of a 10 s-long stimulation are compared with a 2 s-long one. Performance is assessed with cross-validation accuracy and its associated standard deviation over 4-folds. The mean accuracy among all subjects is reported too, as well as the accuracy obtained by considering all subjects together (row "all"). The SVM classifier considers two PSD features.

The results in Tab. 3.1 show that for the 10 s-long stimulation 8 subjects out of 20 reach 100 % accuracy, while only one subject reaches 100 % in 2 s for the "2 stimuli" case. The worst accuracies are about 65 % to 70 % in 10 s, while for 2 s they drop down to about 50 %. Also note that the row "all" corresponds to the case in which the data from all subjects is considered as a whole. Interestingly, the associated accuracies are very close to the mean accuracies, thus indicating that there is no need to train the algorithm subject-by-subject. This aspect is indeed very important in wanting to build a BCI system for daily-life applications, because it indicates that a new subject should not lose time in a training session. Instead, the BCI algorithm can be trained on data from previous subjects. These results can be even enhanced by considering two more features: the PSD at 20 Hz and the PSD at 24 Hz. In doing that, results similar to the ones of Tab. 3.1 can be obtained. It is then interesting to compare the mean accuracies in the four cases, as reported in Tab. 3.2. These accuracies increase (or remain constant in one case), and at least in the 10 s-long stimulation case the associated standard deviation diminishes, thus indicating less variation among classification performance for different subjects. A statistical test (matched paired t-test) reveals that these increases are not statistically significant. However, the improvement is substantial at least for the 10 s case since the minimum accuracy rises from 65 %-70 % to 77 %-85 %. Further considerations about the 2 s case are instead reported in the following discussion about the latency/accuracy trade-off. Finally, note that the accuracy is recalculated for the row "all" in this 4D SVM case, again one finds that they are really close to the mean accuracies already reported in Tab. 3.2.

	<i>10 s-long stimulation</i>				<i>2 s-long stimulation</i>			
	1 stimulus		2 stimuli		1 stimulus		2 stimuli	
classifier	MEAN	STD	MEAN	STD	MEAN	STD	MEAN	STD
2D SVM	91	11	94.9	7.4	73	12	76	16
4D SVM	94.4	7.1	97.2	4.3	75	13	76	15

Table 3.2 Comparison of classification performance for an SVM classifier considering two PSD features (2D SVM) and one considering four PSD features (4D SVM) of SSVEP-related EEG data. The mean cross-validation accuracies and their associated standard deviations are reported for the "1 stimulus" and the "2 stimuli" case, and a 10 s-long stimulation is compared with a 2 s-long one.

3.3.3 Latency versus accuracy

In a SSVEP-based system, performance is typically quantified by simultaneously considering classification accuracy and the stimulation time needed to reach it. The reason is that, as a general trend, the longer the stimulation time is, the better the SSVEP oscillation can be detected. Indeed, a longer stimulation allows to improve the signal-to-noise ratio when considering SSVEP oscillations with respect to the ongoing EEG activity. Nevertheless, a too long stimulation tires the user out, and it would be deleterious for classification accuracy. It is also clear that a short stimulation is desirable to speed up the system. In this context, the system latency corresponds to the time needed to acquire and classify the SSVEP oscillation corresponding to a single icon. If gazing a flickering icon corresponds to selecting it, the shorter the stimulation is and the more commands can be sent in a unit time to the BCI application. In a practical system, system latency and classification accuracy must be balanced to obtain optimal performance, which means a proper success rate in recognizing the user's intention without taking too much time. In order to take into account both aspects simultaneously, a useful metric is the *information transfer rate* (ITR) [8, 103], whose expression is

$$ITR = \frac{1}{L} \left[\log_2 N + A \log_2(A) + (1 - A) \log_2 \left(\frac{1 - A}{N - 1} \right) \right]. \quad (3.2)$$

In there, A is the classification accuracy, L is the system latency, and N is the number of possible choices ($N = 2$ in the present case). This quantity is usually expressed in bit/min.

As said above, the system latency should be calculated by summing stimulation time and EEG processing time. In the present setup, while stimulation is at least 1 s-long, processing requires less than 50 ms once the algorithm is already trained. Therefore, it is reasonable to consider system latency practically identical to stimulation time. In doing this, Fig. 3.5 represents the trade-off under discussion. The two curves represent the "1 stimulus" (blue) and "2 stimuli" (red) case. However, it was already highlighted that there is no statistically relevant difference among them. Hence, the two were mostly represented to have some clues about short-term repeatability of such measures. It can be seen that the two sets of measures are compatible, and that the mean classification accuracy generally increases with stimulation time. The trade-off can be better investigated by first considering the median

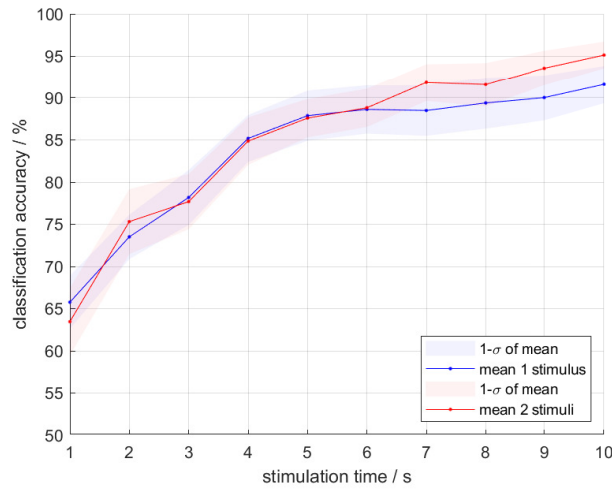


Fig. 3.5 Mean classification versus SSVEP stimulation time (almost coincident with system latency). The standard deviation of the mean is also reported as a shaded area. The "1 stimulus" case is compared with the "2 stimuli" one.

accuracy instead of the mean. The reason relies on the fact that the SSVEP detection performances are diversified among subjects, and the sample mean could be affected by a single poorly performing subject. Along with the median, it seems useful to represent the interquartile range (IQR) as a statistically robust estimate of dispersion. Such quantities are represented in Fig. 3.6 by considering the IQR between the 75th and the 25th percentiles. It can be seen that there is much dispersion around the median classification performance, but in the best cases the accuracy reaches 100 % in a few seconds. Also note that, while the mean and the median accuracies are almost identical at 1 s, the median is typically higher for longer stimulations. This indicates that the accuracy enhancement is actually higher for most subjects, while the performance remains poor for a few subjects. This was somehow anticipated by the results of Tab. 3.1 and Tab. 3.2.

This reasoning was repeated in the case of four PSD features and the results are resumed in Fig. 3.7. These plots confirm that the classification performance is slightly better, but this enhancement is not statistically relevant. Nonetheless, more homogeneous performances can be obtained in some cases, notably increasing the accuracies for the worst subjects. As a prove of that, one can refer to the blue shaded area in Fig. 3.7b, which is noticeable narrower than the one in Fig. 3.6. Finally, it is useful to express the SSVEP-BCI performance in terms of the ITR from eq. (3.2). Note that with $N = 2$ possible choices, the maximum theoretical ITR

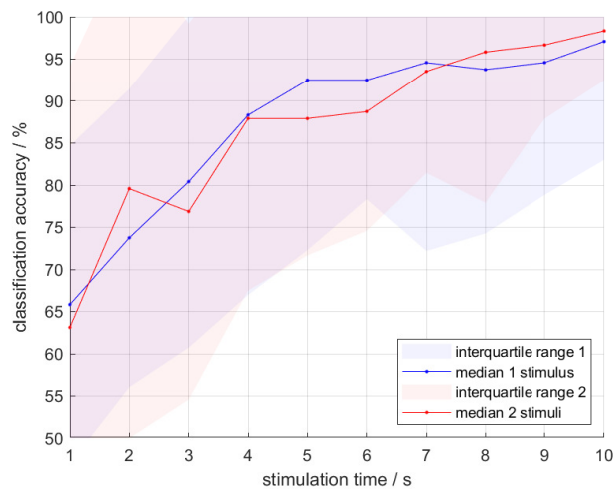


Fig. 3.6 Median classification versus SSVEP stimulation time (almost coincident with system latency). The interquartile range is also reported with a shaded area as a measure of dispersion around the median. The "1 stimulus" case is compared with the "2 stimuli" one.

equals 60 bit/min if at least a 1 s-long stimulation is considered. Then, indeed higher ITRs can be reached for smaller system latencies, but this seems quite unfeasible in the current setting. The ITRs distribution among the 20 subjects is shown in Fig. 3.8 for the "2 stimuli" case as a function of stimulation time. The box-plots show that some subjects overcome 30 bit/min also at short stimulation times, and the same subjects go really close to the maximum possible ITR for longer stimulation times. In general, however, the optimal situation largely depends on the subject: though the median ITR increases almost monotonically with time (red line in the boxes), the ITRs are not always increasing for all subjects and an optimal situation is hard to identify when considering all subjects.

3.3.4 Comparison with literature

The SSVEP-based BCI discussed in this Chapter was designed in order to be low-cost, wearable, and possibly trainingless in order to be closer to daily-life applications. The performance of the system was assessed by means of the experimental results shown above. However, to highlight the contribution of the present work to the ongoing development in this field, it is essential to compare our results with the other ones published in literature. To this aim, some representative examples are here reported by mainly taking into account the last five years of research and development on

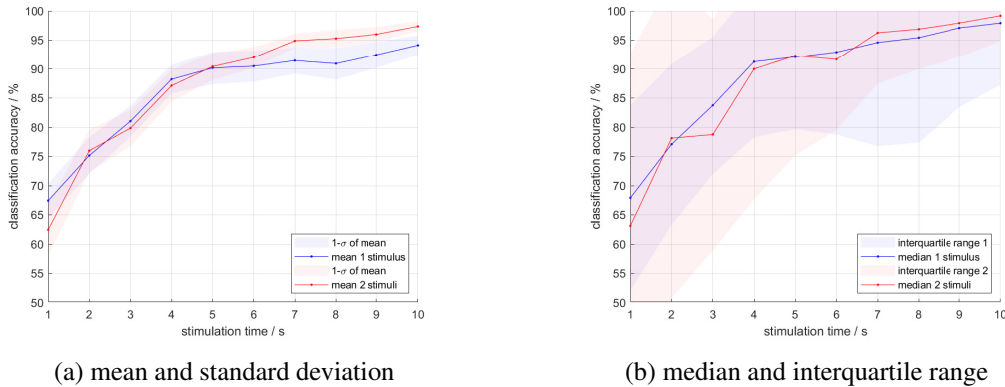


Fig. 3.7 Classification accuracy versus stimulation time in the four PSD features case.

non-invasive SSVEP-BCI. Moreover, another key point is the use of dry electrodes, which are receiving more interest in recent works but they pose some metrological challenges. In this regard, a useful summary is reported in [104]. Focusing on SSVEP literature, it is highlighted that detection algorithms are based on FFT, PSD, or canonical correlation analysis (CCA). System calibration is not typically needed but it can be exploited to increase performance. As an example, the authors of [104] propose a variant of CCA that requires task-related calibration. The classification accuracies of those works are in the 83 % to 93 % range, while the ITR goes from 14 bit/min to 92 bit/min. It is worth noting that the highest ITR is obtained with the task-related CCA and by exploiting 8 dry electrodes. Meanwhile, the ITR reported for the SSVEP-BCI with 1 electrode are about 38 bit/min [105, 106].

SSVEP has been largely exploited in building "mental spellers". In [92], a BCI employing three stimuli and single-channel EEG was proposed. As a performance indicator, a classification accuracy equal to 99.2 % was reported for a 10 s-long stimulation, and the calculated ITR was about 67 bit/min. However, the reproducibility of this result is not foreseeable since only 5 subjects participated in the experiments. Moreover, the system was not completely trainingless since there was the need to optimize the stimulation per each subject. A further speller based on single-channel EEG acquisition and dry electrodes was proposed in [102]. In this case, a deep neural network was used and the classification accuracy reached 97.4 % with a 2 s-long visual stimulation. The assessed information transfer rate was 49.0 ± 7.7 bit/min, but only 8 subjects were considered in the experiments and there is no indication about the cost of the setup. It is also clear that much data are required for the training of the deep net.

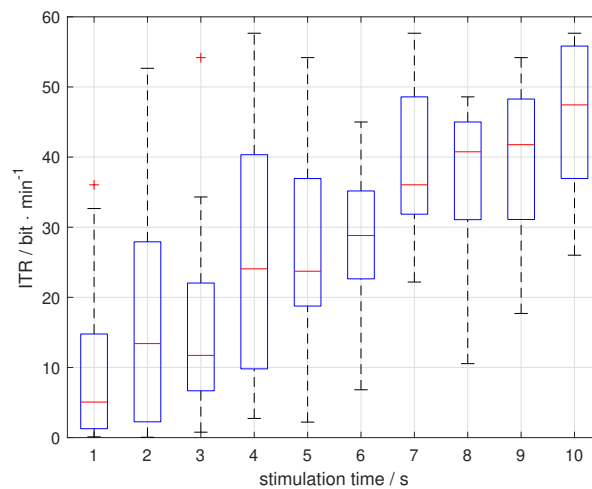


Fig. 3.8 Median classification versus SSVEP stimulation time (almost coincident with system latency). The interquartile range is also reported with a shaded area as a measure of dispersion around the median. The "1 stimulus" case is compared with the "2 stimuli" one.

With specific regard to the combination of BCI with AR glasses, researches on VEP-based paradigms were recently surveyed [99]. By focusing on SSVEP-based works, it was reported that video see-through technology is mostly exploited instead of optical see-through such as in our case. Moreover, the main applications are in the robotic field. A system integrating smart glasses and SSVEP-BCI is reported in [51]. The system was proposed for quadcopter control. However, in this system a total of 16 electrodes were employed, and the accuracy achieved while executing a flight task was 85 % (on only five subjects). The quite low accuracy points out that there are still many issues to face before the exploitation of such technology outside laboratories. Indeed, motion artifacts [101], which are probably caused by the flight task, affect the SSVEP detection. Furthermore, proper focusing on the flickering icon is important for eliciting SSVEP. In comparison with these literature works, our system optimizes wearability and low-cost while reaching compatible classification performance. However, it is to note that even our SSVEP system was tested in a laboratory environment: though the setup is optimized for real-life applications, issues like motion artifacts were avoided by asking the subject to limit movements.

Many improvements are thus possible for our SSVEP-based BCI. The ITR should be increased while continuing to exploit the user-friendliness of a single-channel setup. Moreover, the EEG electrodes placement must be stabilized in order to use the system even during movements (portability). Especially for the

present system, the EEG quality is essential for the system performance, while the processing algorithm can be based on a relatively simple approach. Finally, following an interesting suggestion from [87], the algorithm could exploit a dynamic stop to furtherly optimize the latency/accuracy trade-off: such an algorithm would classify the EEG in real-time and stop when a certain degree of confidence is reached on the assigned class; in doing so, the time window would be variable, and possibly it would be the shorter possible per each task. Indeed, a critical part of such an approach would be the stopping criterion, which must limit the possible misclassifications. Some applications for the SSVEP system at the current development state are reported in the paragraph 3.4.

3.4 Applications

Many possible applications for a SSVEP-based BCI have been already recalled in discussing inherent literature. In this paragraph, the applications tested with our wearable system are described in order to show its possibilities in fields such as industry 4.0 [107] and healthcare.

Industrial maintenance

The possibility of successfully employing the wearable SSVEP-BCI was first investigated for a hands-free inspection task in an industrial context [49]. This case study was exploited to test the system prototype on the field. The scenario consisted of a technician conducting inspection and maintenance of a complex industrial plant. In checking its parts, the technician can fix cables, electrical machines, or power drives while simultaneously visualizing useful information on smart glasses. Hands-free operation can thus provide an interesting feature: for instance, the user can scroll textual information without interrupting the task, or he/she can access sensor data if the industrial plant is equipped with transducers. Fig. 3.9 shows the SSVEP-BCI system communicating with a wireless sensor network for advanced diagnostics and real-time monitoring of an industrial plant. Bluetooth was exploited for communication between the smart glasses and the sensor network.

An Android application was purposely developed to scan available smart transducers and then connect to the one of interest. Therefore, the user was prompted to a

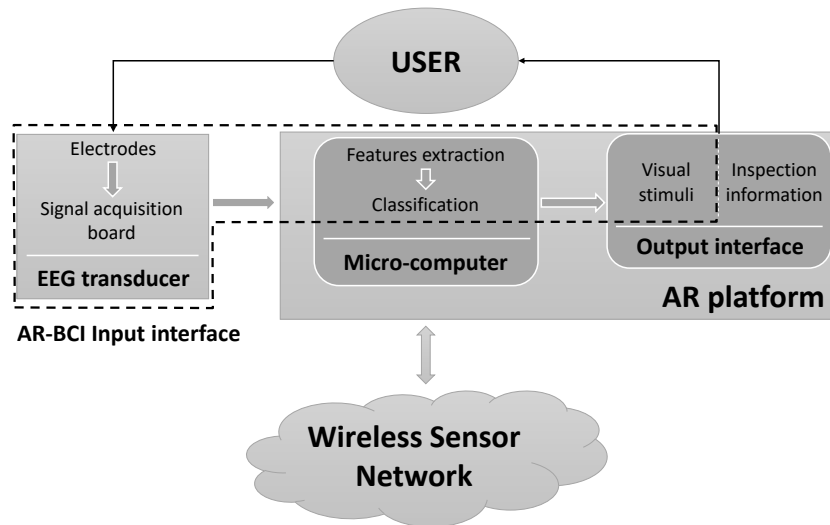


Fig. 3.9 AR-BCI system based on SSVEP proposed for accessing data from a wireless sensor network.

transducer selection window. Once connected, available data was made accessible and the user could ask for specific measures, such as temperature or hydraulic pressure. The Android application diagram is depicted in Fig. 3.10. The commands were sent to the transducer by merely staring at the corresponding icon, without the use of hands.

Fig. 3.11a shows a user wearing the SSVEP-BCI prototype during an emulated inspection task. As an example, temperature and humidity of an industrial oven could be selected by the icons appearing on the smart glasses display: the user stares at the desired flickering icon and, after a few seconds, the corresponding command is sent. Fig. 3.11b is a representation of the user's view through the smart glasses. Note that, while focusing on the icon to select, the background naturally appears blurred. This was even replicated in Fig. 3.11b, which was obtained by simulating a real situation. Nonetheless, the user can inspect the real environment while having superimposed textual information by means of the augmented reality glasses.

Civil engineering

A further noteworthy application for the wearable SSVEP-BCI is in inspecting bridges and viaducts. This application was developed during a university course on instrumentation and measurement for smart industry, and it clearly belongs to

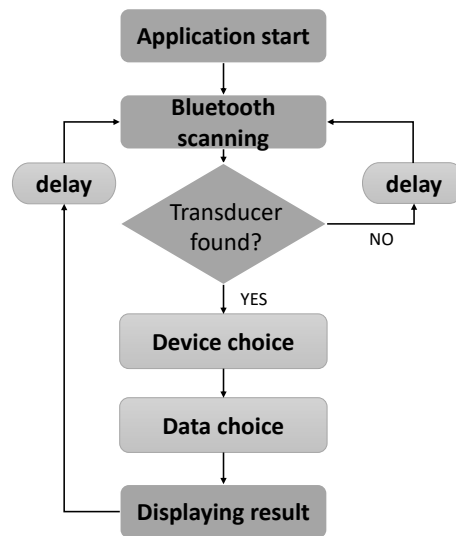
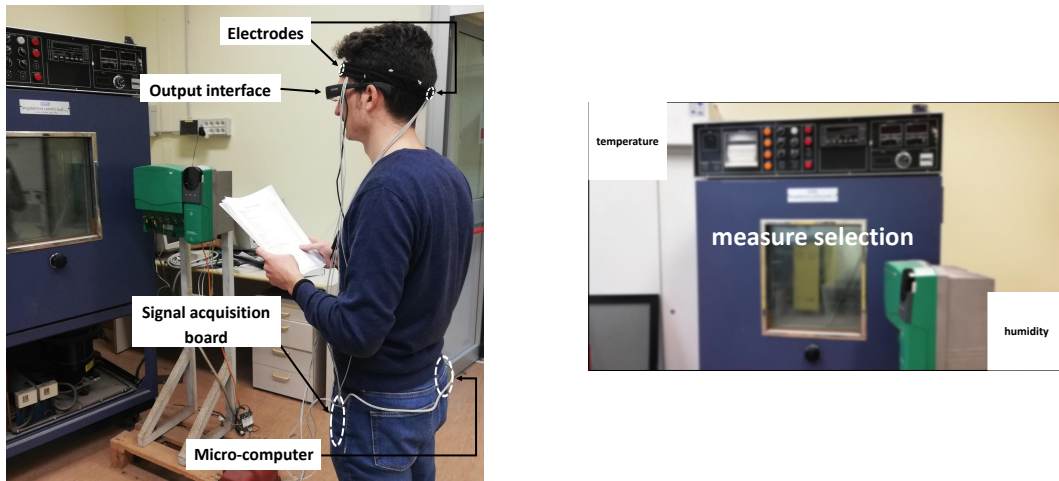


Fig. 3.10 Android application diagram for an inspection task in industrial framework: smart transducers and related measures are selected by staring at corresponding flickering icons.

the industry 4.0 framework. Nevertheless, despite the similarities with the previous case study, it seems useful to discuss the peculiar aspects associated with practical applications in civil engineering. In this field, optical-see-through devices appear useful for visual inspection, which is a crucial task when checking the integrity of a bridge or a viaduct. Hence, visualizing additional information about an infrastructure must not obstruct the visualization of the structure itself. The exploitation of AR technologies in civil engineering is still at an early stage, but it is indeed appealing. In addition, the hands-free feature, provided in the present case by the BCI, guarantees easier navigation into the available information. Indeed the need to check the state of architectural works has always been an important and challenging issue, and the efforts in this direction have increased in recent years. With the wearable SSVEP-BCI, the attempt was to aid in this task. For the civil engineering case study, the information consisted of static and dynamic measures. In detail, accelerometers, gyroscopes, magnetometers, and strain gauges, as well as temperature and humidity sensors were installed on a beam to emulate measurements on a bridge within a laboratory setup. The technician is interested in monitoring these quantities during a load test in which deformations and vibrations must be measured. Fig. 3.12 represents the basic idea for the bridge inspection: wireless transducers are installed on the bridge, smart glasses communicating with them to retrieve useful information, and the BCI aims to replace the default touch-pad interface of the glasses.



(a) a user wearing the SSVEP-BCI system during an emulated inspection task

(b) simulated measure selection window with two possible choices

Fig. 3.11 Example of inspection with the wearable SSVEP-BCI: measure selection menu, with flickering white squares for options (as usual in AR glasses, background image is blurred to focus on the selection).

A sketch of the SSVEP-based system communicating with a sensor stack is instead reported in Fig. 3.13. This clearly represents a novel possibility of interaction that also exploits the internet of things (IoT) for advanced monitoring systems. From a general point of view, the system followed the same implementation described throughout this Chapter. Nonetheless, the need to continuously acquire and process the EEG arose since, differently from the previous case study, the application required the possibility to asynchronously choose an icon/the measures to visualize. In doing that, the implementation of a variable acquisition window was attempted by considering the confidence associated with a class. Remarkably, this possibility was already mentioned at the end of paragraph 3.3.4 as a future development. Unfortunately, a proper study on the acquisition stopping criterion is still missing and a rigorous analysis of such an implementation is addressed to future developments. Nonetheless, despite being in a very early stage of development, this principle was exploited in developing an Android application through which the BCI user can access the measures of interest.

The Android application for inspection tasks was customized to the civil engineering case study. The different activities are synthetically reported in Fig. 3.14. In there, the smart glasses simultaneously connect to the installed transducers, and then the user visualizes environmental measures and has the possibility to choose other data to

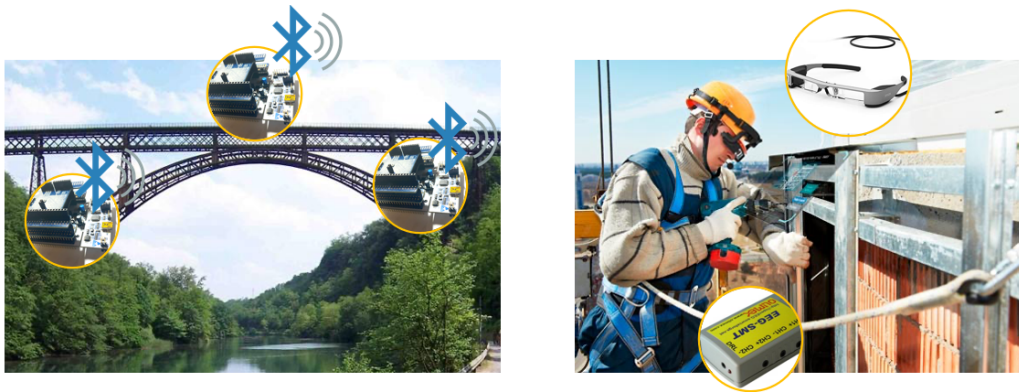


Fig. 3.12 Example of a bridge inspection with smart glasses and a distributed wireless sensor network for measuring static and dynamic mechanical quantities.

visualize, either static measured or dynamic ones. The choice is conducted by means of flickering icons. In the current example, the static data consist of a deformation curve derived by merging strain gauges' measures and angle measures. Meanwhile, the dynamic data consist of vibration measures derived with 3D accelerometers.

Healthcare

The proposed SSVEP-BCI has also found applications in healthcare with particular regards to the rehabilitation of children with attention-deficit/hyperactivity disorder (ADHD). Such an investigation was conducted in parallel to the present thesis work and the author of this thesis did not work directly on the topic. However, the main findings are briefly reported hereafter to give a comprehensive overview of the potential applications for the SSVEP-BCI. The experiments were conducted by our research group in collaboration with an accredited rehabilitation center (Villa delle Ginestre). The system guarantees the interaction with a robot through the wearable BCI to implement a behavioural therapy protocol. In this context, the smart glasses were still used to display the possible commands for the robot, while in future it is foreseen to also mix virtual objects with reality so as to achieve different levels of complexity in the interaction (mixed reality). At the current development state, the usefulness of the SSVEP-BCI relies on the fact that the children must focus on a flickering icon in order to interact with the robot. Therefore, the task cannot be conducted without paying attention, and this should enhance children's engagement in the therapy. Fig. 3.15a depicts the robot to control during the interaction and

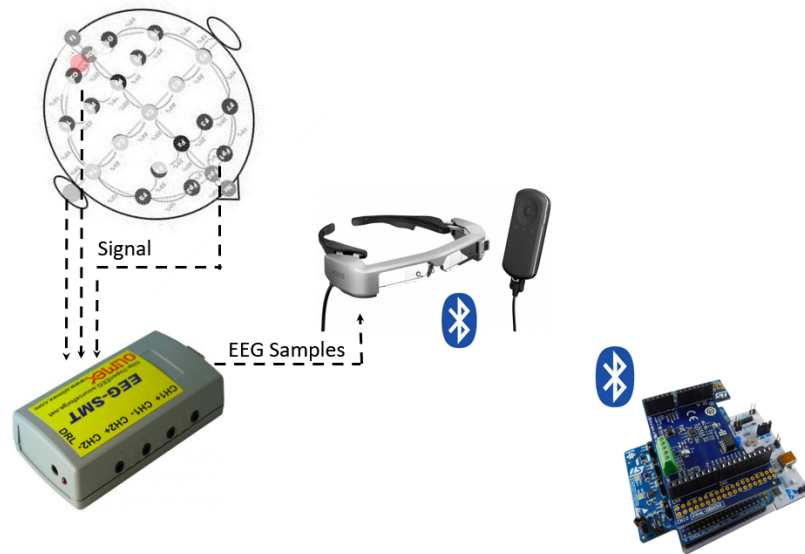


Fig. 3.13 AR-BCI system based on SSVEP communicating with a sensor stack through Bluetooth low-energy.

the possible choices appearing on the smart glasses display. Details about this application are described in [5].

An interesting feature was added to the system, i.e. the possibility to have a third control command through the detection of voluntary eye-blinks. Therefore, such a system can be defined as a hybrid BCI, since it integrates SSVEP with another type of control paradigm. Note that the eye-blink is typically an artifact from the point of view of EEG measurement, and involuntary eye-blinks were often present in measuring the brain signals with our low-cost acquisition system. Nonetheless, in this case the artifact is exploited by implementing a finite state machine as follows (see Fig. 3.15b):

- *idle state*: at the beginning of the interaction, no flickering icon is appearing and the robot is not moving; if a voluntary eye-blink is detected, the state is changed to select the direction;
- *selection direction*: through the SSVEP the user can choose left or right movement, and then confirm the choice with a voluntary eye-blink, which starts the movement;
- *move forward*: in this state the robot is moving as decided in the previous state and it can be stopped with a voluntary eye-blink to return to the idle state.

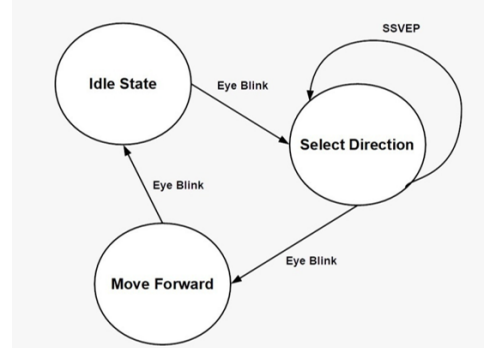


Fig. 3.14 User interface realized in Android for bridge inspection during a load test. In the first activity (up) the smart glasses automatically connect to multiple wireless transducers. In the second activity (middle) the user visualizes environmental data. The third and fourth activities (down left and down right) can be accessed by selecting the data to visualize. The black background is equivalent to transparency when the application is running on smart glasses.

The exploitation of the eye-related artifact is based on the possibility to distinguish voluntary eye-blinks from involuntary ones. This was actually done by choosing a proper threshold in analyzing the peaks related to eye-blinks in the time domain as shown in Fig. 3.16. The threshold was empirically determined. Clearly, errors are possible in the detection of the voluntary eye-blink and this further feature contributed to inaccuracy of the user's intention detection. However, such a feature allows to avoid continuous flickering of the icons, which can be activated with a purposely-designed command.



(a) possible control commands in interacting with the robot



(b) finite state machine implemented for robot control

Fig. 3.15 Application of the wearable SSVEP-BCI in the rehabilitation of children with ADHD through a behavioural therapy, as documented in [5].

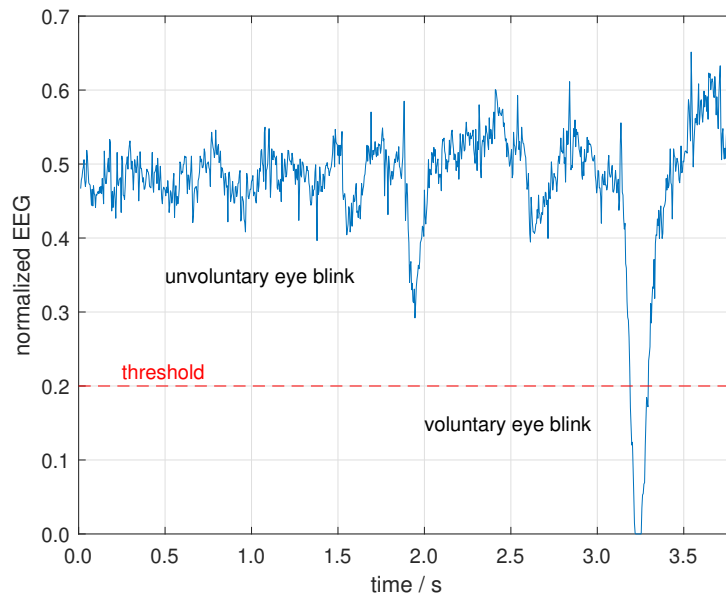


Fig. 3.16 Distinction between voluntary and involuntary eye-blinks in time domain with an empirically determined threshold.

Chapter 4

A wearable BCI based on spontaneous brain activity

Active brain-computer interfaces are attractive because they rely on spontaneous brain activity that is voluntarily modulated by the subject, without the need of any external stimulation. However, they typically require long training for both the user and the algorithm before brain patterns can be correctly recognized, especially when non-invasive techniques are adopted to record neural activity. Motor imagery (MI) is the most known paradigm for active BCIs. It relies on mental tasks in which the user envisions a movement without actually executing it. Understandably, this is largely studied in rehabilitation protocols, e.g. in presence of a post-stroke brain damage. On the other hand, MI can be used as an alternative way of communication and control. Therefore, the current chapter discussed the possibility to realize a wearable BCI relying on MI. In this case, setups with at least 8-10 electrodes are usually considered. Hence, first analyses were conducted regarding the possibility to reduce the number of acquisition channels and optimize system wearability and portability. Then, neurofeedback was investigated in order to improve the training of the user and hence the performance.

The current chapter is organized as follows. Section 4.1 briefly recalls the background knowledge on MI, while Section 4.2 presents a well-known and effective approach adopted for the classification of imagery tasks. Next, Section 4.3 deals with the number of channels required for the acquisition of MI-associated brain activity, and notably it reports the results of analyses conducted on benchmark datasets

to highlight the trade-off between number of channels and classification accuracy. Then, the possibility to exploit neurofeedback is discussed in Section 4.4 with the aim to improve the detectability of such phenomena. Particular attention has been paid to the analyses of MI-related EEG signals with the attempt to highlight the neurophysiological phenomena of interest and thus explain the classification results.

4.1 Motor imagery

Sensorimotor rhythms are brain signals associated with motor activities, e.g. limb movements. They consist of EEG oscillations measurable in the μ and β bands, typically corresponding to the 8 Hz to 13 Hz and 13 Hz to 30 Hz ranges, respectively. The brain area of concern is located near the central brain sulcus. Hence, these signals are naturally linked to movement-related brain areas, and the information contained in μ and β rhythms is suitable for communication and control in BCI applications. Interestingly, they are not merely generated in correspondence of an action, but they also subsist when the action is imagined [108]. This phenomenon implies that people with lost motor functions might use motor imagery (MI) as a surrogate for physical practice [109, 110]. Indeed, the aim of a MI-based BCI is to measure and classify brain signals related to movement imagination without requiring to actually perform a movement. Typical mental tasks are the imagery of left hand or right hand movement, but also imaging the movement of feet or tongue can be considered. In this sense, MI is an endogenous paradigm for EEG-based BCIs, namely it relies on spontaneous and voluntarily modulated brain activity. Application examples involve motor rehabilitation or the driving of robotic prostheses, but MI-BCIs are also addressed to able-bodied people for communication and control tasks in everyday life.

The cortex, the basal ganglia, and the lateral portion of the cerebellar hemisphere are generally involved in planning the movement, and the electrical activity in this region changes according to the motor intention. Without entering into neurological details, the operating principle of an MI-based BCI is to measure both the frequency content and the spatial distribution of the brain activity. Figure 4.1 illustrates how the different parts of the body are mapped to the primary motor cortex. This shows the disproportion among the different body parts, and it also gives hints on the most suitable movements to imagine. It is also worth mentioning that each side of the body

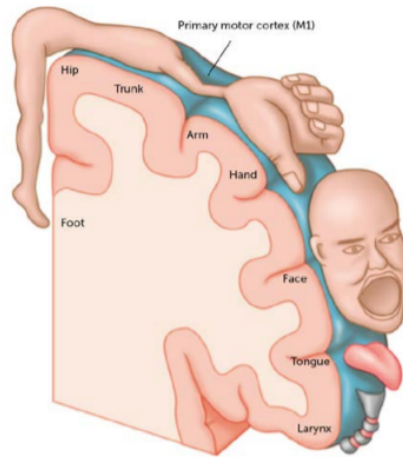


Fig. 4.1 Map of the primary motor cortex associated with different motor processes according to the anatomical divisions of the body.

is controlled by the contra-lateral hemisphere of the brain. As shown in Fig. 4.1, left hand, right hand, and feet movements should be relatively simple to discriminate through brain signals recording, because the associated body parts entail a large area of the sensory motor cortex and they are well-separated in space. Notably, right hand motor imagery produces relevant brain activity changes in the sensorimotor cortex around the electrode position C3 (see standard locations in Fig. 1.5), while the left hand is associated with the area around electrode C4. Foot movement, instead, produces signals on the medial surface of the cortex, around electrode location Cz. For a better understanding, the Fig. 4.2 recalled from [6] depicts patterns in time-frequency domain according to EEG signals acquisition during left hand, right hand, or feet motor imagery. In particular, the activity at the standard locations C3, Cz, and C4 are highlighted. As mentioned above, patterns for these imagined movements were expected to be spatially distinct.

The patterns shown in the Fig. 4.2 are examples of event-related desynchronization (ERD) and event-related synchronization (ERS), two linked phenomena that the literature has pointed out as responses of neuronal structures in the brain during movement execution or imagination [111, 112]. Such phenomena are typically evaluated in MI-BCI studies to better understand the informative content of the EEG signals under analysis. In this work, this has been done in association with classification results. Therefore, the next section introduces a well-known processing approach adopted for the classification of motor imagery tasks. This processing

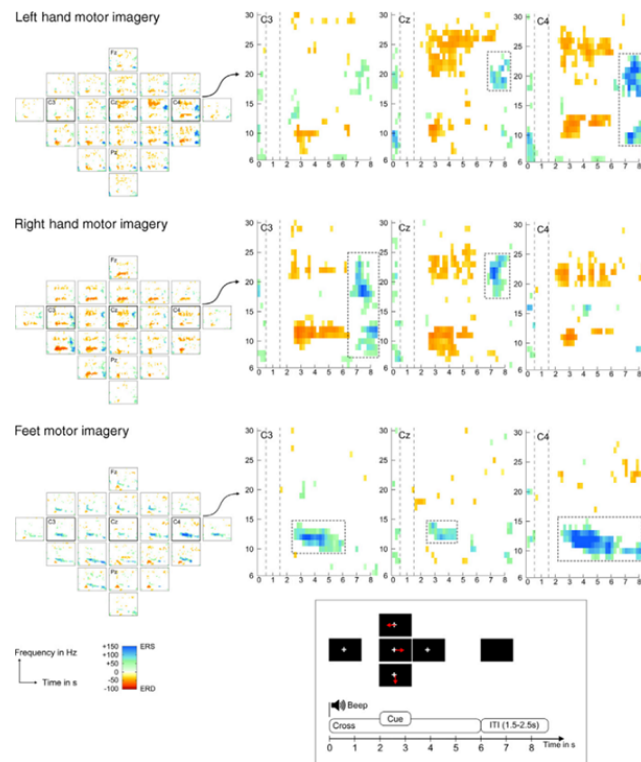


Fig. 4.2 Time-frequency representation of EEG patterns associated with three motor imagery tasks and their spatial distribution [6].

approach has been adapted and exploited throughout the MI-BCI development for both channel reduction and online feedback.

4.2 Filter bank common spatial pattern

In detecting MI, classification is broadly considered to distinguish among different mental tasks and associate each of them to a control action. The processing is conducted by means of artificial intelligence, and in particular machine learning dominates the field. In doing that, two general approaches can be distinguished: traditional machine learning based on the design of features extraction, or deep neural networks that are totally data-driven. The latter approach has recently attracted much investment by the BCI community. Nonetheless, it was already mentioned in the introduction that the amount of data required to identify a deep neural network model appears too big with respect to actually available data, and literature results are not yet well-defined. Given that, the approach considered for this work was

the former one, in which the choice of signal features to extract and classify was partially guided by neurophysiological knowledge, though the algorithm must still be trained by means of available measures. It is worth noticing that, in discussing a wearable MI-based BCI, signal processing is here introduced before the description of signal acquisition, in contrast with what was done in the previous chapter for the SSVEP-based BCI. This is justified by the fact that the choice of acquisition channels for MI detection is usually more data-driven than for the SSVEP case. Indeed, the processing introduced in this section has been exploited for a channel selection method proposed in the context of the present thesis.

A well-known machine learning approach proposed in literature for the classification of MI is the *filter bank common spatial pattern* (FBCSP) [62]. This approach was developed and it won two contests during the BCI competition IV (2008). Since then, many variants have been proposed due to its effectiveness. Therefore, the FBCSP approach has been taken into account during the current work, and possible variants have been explored. As represented in Fig. 4.3, the basic structure of the FBCSP can be divided into four blocks:

1. a filter bank, extracting the frequency content of EEG signals in different bands;
2. the common spatial pattern algorithm, a widely used features extractor considering EEG spatial information;
3. a mutual information-based best individual feature selector of features accounting for class-related information;
4. an optimal classifier.

Each block is here better discussed in describing the particular implementation of the FBCSP processing, along with the training and evaluation phases needed for identifying and testing the algorithm model.

4.2.1 Filter bank

The first step of FBCSP is the *filter bank*, which separates the frequency content of each EEG signal with multiple pass-band filters. Chebyshev filters were employed,

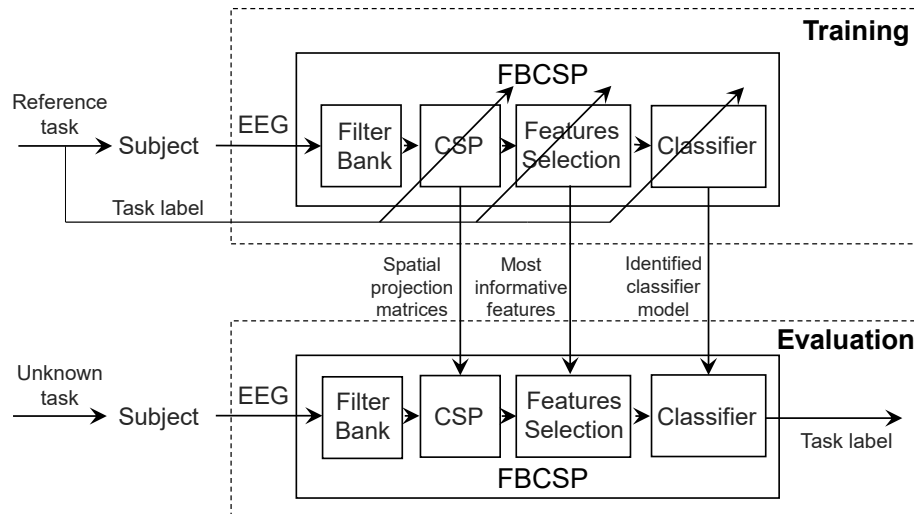


Fig. 4.3 Architecture of the filter bank common spatial pattern algorithm for both the train and evaluation phases [7]. The transverse arrows highlight the blocks needing training before their usage.

each one with 4 Hz-wide band and with 2 Hz overlap between consecutive filters. The overall band considered in this implementation was 4 Hz to 40 Hz, thus resulting in 17 bands (4 Hz to 8 Hz, 6 Hz to 10 Hz, 8 Hz to 12 Hz, . . . , 36 Hz to 40 Hz). Despite the original proposal [62], overlapping bands were chosen to avoid losing information in correspondence of band edges, as it may happen in the non-overlapping case. For instance, in the original FBCSP implementation, 8 Hz was the high cut-off frequency and the low cut-off frequency for two adjacent bands, 4 Hz to 8 Hz and 8 Hz to 12 Hz, respectively. To achieve a -200 dB/decade slope of the filter frequency response, the stop-band attenuation was set to -40 dB and the order was set to 10. The high slope here is needed to have a sharp cut between pass band and stop band, but this also implies a significant computational burden for filter application to many EEG data. Since the filter bank is applied to each EEG signal, different channels are treated separately. At the end of this step, the number of signals is 17 times the number of the original signals.

4.2.2 Spatial filtering

The *common spatial pattern* (CSP) extracts features relying on the covariance matrix of measured EEG signals. Within this procedure, the spatial content associated with EEG signals is projected in a new space, so that features are sorted according to

the class-related variance [113]. For instance, if data are available for left hand and right hand motor imagery, two matrices for spatial projection can be derived: the first leads to features with left-related variance in descending order, while the second leads to features with right-related variance in descending order. Note that, in this binary case, maximizing the variance associated with a class automatically minimizes the variance associated with the other class. Therefore, the two matrices are linked. After the spatial projection, only most relevant features are taken into account. In this sense, the CSP is a spatial filter.

Since the CSP computes projection matrices from available data, two phases must be distinguished: the matrices are calculated from data during the training phase, while they are applied to data in the evaluation phase. The projection matrix computation is as follows. Given a $n_{ch} \times n_{samp}$ matrix E_j of EEG signals per each experimental trial, where n_{ch} is the number of channels while n_{samp} is the number of samples, the covariance matrix associated to the class c is calculated as

$$K_c = \frac{1}{n_{tr,c}} \sum_{j=1}^{n_{tr,c}} \frac{E_{j,c} E_{j,c}'}{\text{trace}(E_{j,c} E_{j,c}')}, \quad (4.1)$$

where $n_{tr,c}$ is the number of trials available for class c and the apostrophe (') indicates the transposition of a matrix. Note that matrix K_c is actually obtained as a mean of the covariance matrix associated with the trials $j = 1, 2, \dots, n_{tr,c}$, each of which is normalized by the respective matrix trace. Summing the K_c matrices of the classes, the composite covariance matrix

$$K = \sum_c K_c \quad (4.2)$$

is then obtained. Note that $c = 1, 2$ in the simple binary case, but (4.1) and (4.2) still hold in the multi-class case.

A complete projection matrix W_c is computed per each class by solving the eigenvalue decomposition problem

$$K_c W_c = K W_c \Lambda_c, \quad (4.3)$$

where eigenvalues are the non-zero values of the diagonal matrix Λ_c , while W_c is made of eigenvectors. If eigenvalues are sorted in descending order, the eigenvectors are sorted accordingly. In the final step, the actual projection matrix W_c^r is retrieved

from W_c by considering only the first and last m columns. The former have maximum variance with respect to class c , while the latter have minimum variance with respect to class c . Ultimately, the CSP training phase consists of calculating the W_c^r for all the classes of interest.

In the evaluation phase, instead, the CSP projection is applied. The matrices W_c^r transform the $n_{ch} \times n_{samp}$ data associated to each trial following the equation

$$C_{j,c} = W_c^r E_j E_j^r W_c^r, \quad (4.4)$$

and then features are obtained as

$$\mathbf{f}_{j,c} = \log \left[\frac{\text{diag}(C_{j,c})}{\text{trace}(C_{j,c})} \right]. \quad (4.5)$$

In there, the $C_{j,c}$ matrix is diagonalized, and $2m$ features are obtained per trial. Spatial content of EEG data is thus filtered because $2m < n_{ch}$. Hence, the array $\mathbf{f}_{j,c}$ synthetically describes the j -th trial with respect to the class c . If the CSP is exploited after the filter bank, this reasoning must be repeated for each band. By merging the features of all bands, each trial is described with $2mf$ features (with regard to class c).

Literature works demonstrate that the CSP is effective in extracting discriminatory information from two populations of motor imagery data [114], but multi-class extensions are feasible as well [113]. With the CSP trained and applied according to (4.1)-(4.5), a possible approach is the one-versus-rest (OVR). In there, the binary discrimination is extended by considering each class against the remaining ones.

4.2.3 Features selection

Other than feature extraction, the CSP naturally encompasses feature selection. However, since multiple bands are derived from the filter bank, a further selection step is needed in choosing only the best features combining spatial and frequency content. The selection approach considered in this work is the *mutual information-based best individual feature* (MIBIF), which relies on class-related information associated with each feature. This reduces the $2mf$ features representing each trial to $n_{M,c}$ features. Note that the subset of selected features depends on the class c . Also in this algorithm step, data-driven training is needed before the actual selection.

Notably, the mutual information between a class and a feature is calculated in the binary case as

$$I_c(f_i) = H_c - H_{c|f_i} = - \sum_{c=1}^2 P(c) \log_2 P(c) - \sum_{c=1}^2 \sum_{j=1}^{n_{tr}} p(c|f_{j,i}) \log_2 p(c|f_{j,i}), \quad (4.6)$$

which is the information related to a feature $i = 1, 2, \dots, 2mf$ with respect to class c is obtained by subtracting from the class entropy H_c the feature-related entropy $H_{c|f_i}$. The latter is derived with the conditional probability between a feature and a class summed over trials, which must be estimated with the Bayes rule

$$p(c|f_{j,i}) = \frac{p(f_{j,i}|c)P(c)}{\sum_{c=1}^2 p(f_{j,i}|c)P(c)}. \quad (4.7)$$

In there, the a-priori probability $P(c)$ of a class is estimated with the frequentist approach as the ratio between the $n_{tr,c}$ trials available for the class and the total number of available trials n_{tr} . Meanwhile, the conditional probability $p(f_{j,i}|c)$ is estimated, in the present work, with the Parzen Window [62]:

$$\hat{p}(f_{j,i}|c) = \frac{1}{n_{tr,c}} \sum_{k=1}^{n_{tr,c}} \frac{1}{\sqrt{2\pi}} e^{-\frac{(f_{j,i}-f_{k,i})^2}{2h^2}} \quad (4.8)$$

Remarkably, in the sum, a feature $f_{j,i}$ associated with the j -th trial appears in the difference with each features $f_{k,i}$ from the same class, and it is weighted by the smoothing parameter

$$h = \left(\frac{4}{3n_{tr}} \right)^{1/5} \sigma, \quad (4.9)$$

with σ equal to the standard deviation of $f_{j,i} - f_{k,i}$.

By these calculations, the I_c values associated with each of the $2mf$ features are obtained. They are then sorted in descending order so as to select the first $k_{MIBIF} = 5$ ones, i.e. the most informative ones. The number of features was empirically chosen after some preliminary trials and then fixed for next elaborations. Actually, since the CSP features are paired (first m ones versus last m ones), when one feature is selected, one must also select the paired one. For this reason, the effectively selected features $n_{M,c}$ can be 6 to 10. Overall, the MIBIF chooses the best features according to the data-driven training, while in the evaluation phase these same features are selected. Incidentally, this implies that the band choice is subject-related

if a subject-by-subject training is carried out. Finally, the MIBIF algorithm here presented for two classes can be extended to more classes, for example with a pairwise approach (discrimination among pairs of classes) or with the already mentioned OVR approach.

4.2.4 Classification of mental tasks

In the last algorithm step, the features are classified. A supervised approach was exploited, hence training is needed before the evaluation phase. Again, the classifiers are introduced for a binary case but they can be extended to more classes. The first FBCSP implementation [62] proposed a *naive bayesian parzen window* (NBPW) classifier, but also the support vector machine (SVM) was investigated. Broadly speaking, the classifiers led to compatible performance. While the SVM is extensively described in specialized texts [3], it is useful to discuss the NBPW implementation.

The idea behind the Bayesian classifier consists of calculating, for a trial, the probability of a class given the features $\bar{\mathbf{f}}$ describing that trial. The Bayes rule

$$p(c|\bar{\mathbf{f}}) = \frac{p(\bar{\mathbf{f}}|c)P(c)}{\sum_{c=1}^2 p(\bar{\mathbf{f}}|c)P(c)} \quad (4.10)$$

is applied. While the $P(c)$ is obtained with the frequentist approach on training data, the conditional probability is computed with a "naive assumption", according to which all features are conditionally independent, so that

$$p(\bar{\mathbf{f}}|c) = \prod_{i=1}^{n_{M,c}} p(f_i|c). \quad (4.11)$$

Each of these conditional probabilities are estimated with the Parzen window of (4.8) and (4.9) already introduced for the MIBIF selector. Note that the training of the NBPW consists of using features associated with training trials in the Parzen window expression, as well as in the frequentist estimation of $P(c)$. After the probability $p(c|\bar{\mathbf{f}})$ is calculated per each class, the most probable class is assigned to the trial during the evaluation phase.

The FBCSP approach with NBPW or SVM classifiers were implemented in Matlab and tested on benchmark datasets from BCI competitions. Such data were

created in different European institutes to let BCI researchers compete in developing the best processing approach. After the competitions (the last one was in 2008), these data were published and they have been largely used in research activities. Thanks to that, different research groups can compare their results, though the lack of standardization in this community still prevents their full interpretation and replication. The benchmark datasets used in this thesis are presented hereafter, and inherent results are then presented. However, it is worth noting that few expert subjects were usually involved in acquiring those data. This implies that the real usability of a motor imagery BCI in daily life could not be simply evaluated by this data, and statistical significance of eventual improvements could not be proven due to the small subjects sample. For these reasons, in the following sections more data will be considered to better evaluate the proposed FBCSP variants.

Benchmark datasets

The first dataset used for testing the FBCSP implementation is the *dataset 2a from BCI competition IV* (2008) [115]. It includes EEG data from 9 subjects recorded through 22 channels in two different days (sessions). Data were sampled at 250 Sa/s. Each session is composed of 6 runs separated by short breaks. A run consists of 48 trials balanced between motor imagery classes, which are "left hand", "right hand", "feet", and "tongue". Hence, 12 per class are available. In processing these data, cross-validation was applied to data from the first session (referred to as A0xT for subject "x") in order to predict the classification accuracy expected on further data. In a second step, these data were used for training the algorithm, while the second session (A0xE) was used for the evaluation. The second dataset used in this work was the *dataset 3a from BCI competition III* (2006) [116], including 60-channels data from only 3 subjects. Data were sampled at 250 Sa/s. Per each class 60 trials were available, and the classes were "left hand", "right hand", "single foot", and "tongue".

Two more datasets from BCI competitions were then considered, namely the *dataset 2b of BCI competition IV* [117], and the *dataset 3b of BCI competition III*. These include 9 and 3 subjects, respectively, but the peculiarity is that data were recorded from 3 bipolar EEG channels and that neurofeedback was provided during the trials. Again, data were sampled at 250 Sa/s. Details about the number of available trials are not recalled here, but they will be recalled later when relevant.

However, it is to remark that these data were split in half for training and test, as already explained for the first dataset. For all the four datasets, a cue-based paradigm was adopted. This meant that in each trial the user is relaxed until an indication appears on the screen. After about 1 s from the indication, the user has to carry out the specific mental task until a stop indication was provided. In this sense, this was a synchronous BCI paradigm. The feedback, when present, was provided on the same screen. Finally, electrooculographic signals were also recorded for easing artifact removal, but they were not exploited in achieving the following results.

Testing the FBCSP

The first evaluation of the FBCSP performance was done on dataset 2a with a 6-folds cross-validation on training data. The six possible class pairs were considered as well as the four classes altogether. Results are reported in Tab. 4.1 for the NBPW classifier case. In particular, the mean classification accuracy among subjects is reported along with the associated standard deviation to also have an estimate of the mean dispersion. Notably, the results are compatible with the ones obtained by an SVM with linear kernel, which are not reported in the table. In the binary cases the accuracy goes from 74 % to 84 % depending on the considered pair, while in the four classes case it is 63 %. Note that directly comparing results achieved for different numbers of classes is unfair because the more the classes and the easier the misclassification. Hence, other metrics exist for normalizing the classification accuracy to the number of classes (e.g. see the Cohen's kappa [118]). Despite that, the classification accuracy will be still considered in the following as it is the most diffused one.

TASKS	ACC \pm STD / %
left hand vs right hand	74 \pm 20
left hand vs feet	81 \pm 13
left hand vs tongue	82 \pm 13
right hand vs feet	81 \pm 15
right hand vs tongue	84 \pm 13
feet vs tongue	75 \pm 13
four classes	63 \pm 19

Table 4.1 Mean and standard deviation of the cross-validation accuracy obtained on dataset 2a with a Bayesian classifier.

The relatively high values for the standard deviations indicate that there is much performance difference among subjects. To better highlight that, Fig. 4.4a shows box-plots related to the cross-validation accuracies of the 9 subjects from dataset 2a with the addition of the 3 subjects from dataset 3a. These results are shown for the same classes set as before, and again only the NBPW-related results are shown. In addition, Fig. 4.4b reports classification accuracies obtained by training on the first half on data and evaluating on the other half (i.e. the hold-out method). In both figures, the dashed line represents the random accuracy level, i.e. the theoretical accuracy that would be obtained if one guesses at random the classes. By assuming balanced classes, this level equals 50 % in the two-classes cases and 25 % in the four-classes case.

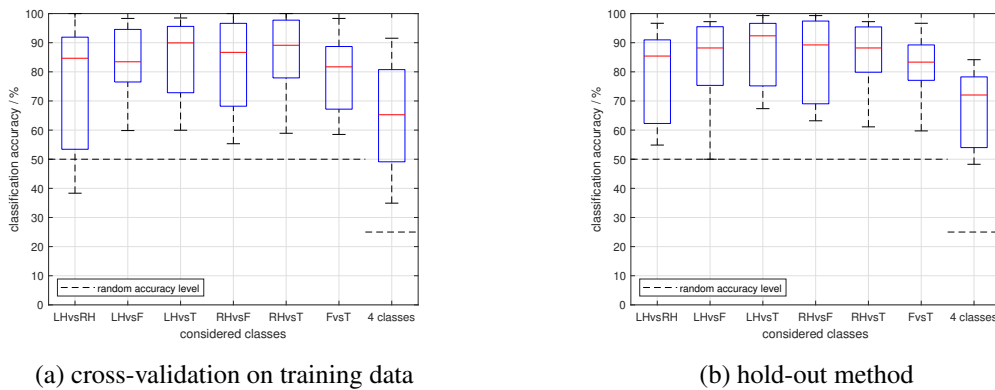


Fig. 4.4 Classification accuracies for the 12 subjects from dataset 2a and dataset 3a. The six possible classes pairs are considered as well as the four classes case.

The above results show how the median accuracies (red lines) are well above the random accuracy level, and that only in few cases the accuracy distribution goes below that level. Overall, classification accuracy is relatively high if compared to other datasets or more real applications, as it will be seen later in this thesis.

To conclude, results are also reported for the 12 subjects from dataset 2b and dataset 3b. Only two classes are available, thus Tab. 4.2 reports the accuracy of all subjects by comparing cross-validation results (CV) with hold-out ones (HO). Only two bipolar channels out of three were considered in these tests. Despite the low channel number, the results are compatible with the previous ones, namely the performance is unexpectedly high. Indeed, later results will show that reducing the number of channels is typically associated with accuracy decrease. On the one hand, the results of Tab. 4.2 may point out that datasets from BCI competitions are not

always representative for real application scenarios. On the other hand, these data were acquired while providing neurofeedback during MI.

Subjects	ACCURACY / %	
	CV	HO
B01	72	67
B02	61	59
B03	54	57
B04	92	96
B05	84	88
B06	80	82
B07	72	74
B08	78	89
B09	80	85
S4b	80	79
X11b	75	74
O3VR	65	64
mean	74 ± 10	76 ± 12

Table 4.2 Classification accuracies for the 12 subjects from dataset 2b and dataset3b. Subject-by-subject accuracies are reported for cross-validation (CV) and hold-out (HO).

4.3 Acquisition channels

In satisfying the requirements of daily-life brain-computer interfaces, wearability and portability are strictly linked to the number of channels employed in measuring the EEG. Selecting a minimum number of channels not only enhances system wearability and portability, but also optimizes the performance by reducing overfitting and excluding noisy channels [119]. Differently from the SSVEP case, many channels are usually needed to map the spatial information associated with motor imagery. Moreover, it is not trivial to choose electrodes locations a-priori. For these reasons, the number and location of the acquisition channels were firstly investigated with a data-driven approach. In doing that, the FBCSP algorithm introduced above was mainly exploited. Then, also a knowledge-based approach was investigated, in which the aim was to choose a small number of subject independent channels.

4.3.1 An attempt with a single channel

In pursuing utmost wearability and portability for the MI-BCI, the possibility to exploit a single-channel EEG was firstly attempted. This investigation was inspired by a research of 2014 [120] proposing the classification of four motor imagery tasks with single-channel EEG data. In their work, the authors proposed the usage of a short-time Fourier transform to obtain spectrograms from single-channel EEG signals, and then the application of the CSP for features extraction. Since the CSP would require multi-channel data, the idea behind that work was to exploit the different frequency bands of the spectrogram in spite of channels. A single channel was selected in post-processing among the available ones, and 3 s-long time windows were processed in order to classify the MI tasks. In replicating the proposed approach, the short-time Fourier transform was calculated in Matlab with the "spectrogram" function, by considering 100 samples-long windows with 50 % overlap between consecutive windows. Each one was zero-padded to 128 samples and a Hamming window was used. Considering the module of the spectrogram, a real matrix is associated to each single-channel signal. From the spectrogram, if frequency bands are considered in place of channels, the CSP can be applied for extracting features. Finally, these features are classified with an SVM. Note that data-driven training is needed for both the CSP and SVM.

The authors of [120] reported a mean classification accuracy equal to 65 % when classifying four motor imagery tasks from the dataset 3a of BCI competition III. The maximum accuracy, obtained in a very specific condition, was about 88 %, and 4 s of the input EEG signals were analysed. One attempt of the present work was thus to replicate such results even on a further benchmark dataset, i.e. the dataset 2a of BCI competition IV. The analyses were conducted first by fixing the number of CSP components to $m = 2$ in accordance with the FBCSP approach introduced earlier, and then by also varying the number of CSP components, as the authors of [120] proposed. Classification results suggest that in classifying two motor imagery tasks with data from the dataset 3a, the maximum accuracy that can be obtained is about 85 % (subject k6b, right hand vs tongue). However, all the accuracies associated with subjects from dataset 2a are compatible with the random accuracy, i.e. 50 %. Fig. 4.5 shows the results with respect to the 9 subjects of the dataset 2a when considering two motor imagery tasks to classify. The random accuracy level is also reported as a red dashed line which is practically superimposed to the lines

indicating classification results. Then, if considering four classes, accuracy was even lower. This evidence, together with the fact that no other relevant literature work attempts the usage of a single channel for MI, discouraged further investigation in this direction. Instead, such results triggered the need to study the trade-off between the number of channels and the achievable classification accuracy, as it is reported in the following paragraph.

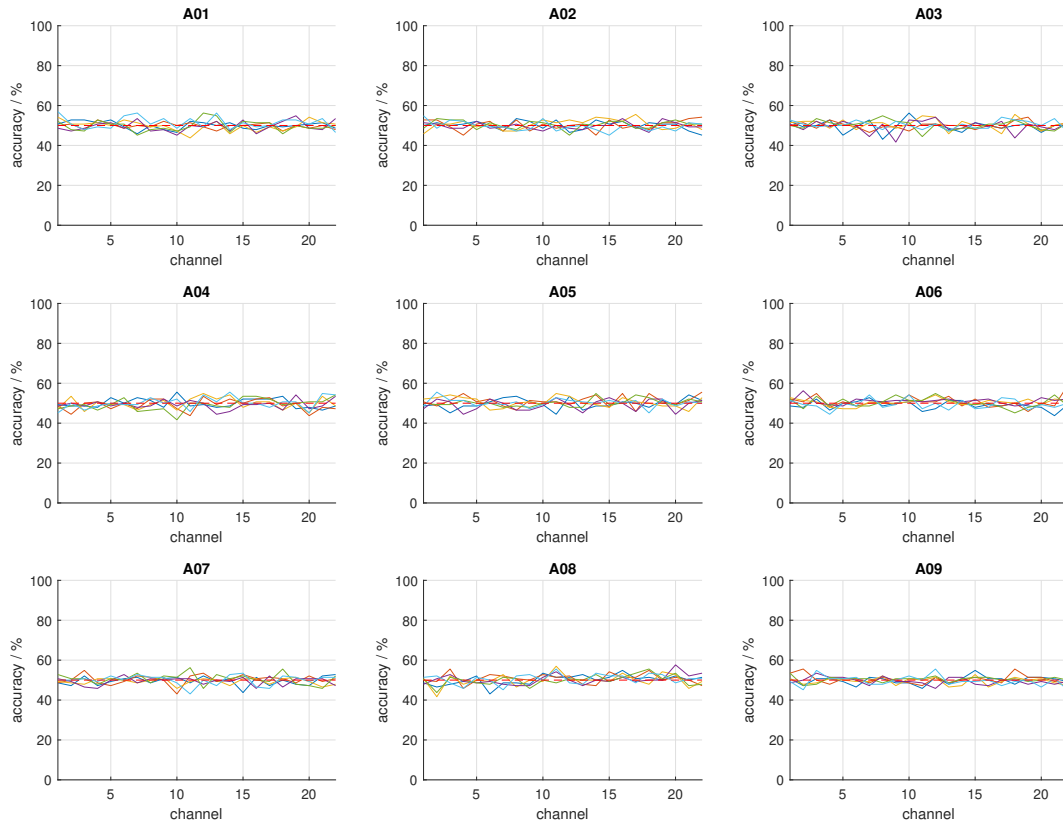


Fig. 4.5 Results of motor imagery classification with single channel data from dataset 2a of BCI competition IV. The six possible pairs of classes are considered for the 9 subjects: left hand vs right hand (blue), left hand vs feet (red), left hand vs tongue (yellow), right hand vs feet (magenta), right hand vs tongue (green), feet vs tongue (cyan).

4.3.2 EEG channels selection

In selecting channels with a data-driven approach, the contribution of each of them to motor imagery classification had to be estimated. Therefore, during the work of this thesis, a method was proposed for selecting and then validating the selection of EEG channels. The method exploited the FBCSP classification approach

[62] and, to evaluate the contribution to the final performance per each channel, a non-uniform embedding strategy [121] was added. According to [119], which distinguishes between different selection approaches, the proposed method is a wrapper technique, because, in contrast with filtering approaches, classification is involved in the selection process. Overall, the method consists of a progressive channel selection, thus allowing to retrieve the trade-off between the number of channels and the classification performance.

In more details, the selection step involves an iterative process known as *sequential forward selection strategy* [3], so to choose the best-performing channels: firstly, motor imagery classification is attempted with every single channel in order to select the best one, and then the other available channels are added one-by-one again according to classification performance. Therefore, n channels are used in the n -th iteration: the first $n - 1$ are the best from previous iterations, while the last one is found from the remaining channels by assessing the classification accuracy resulting from an n -channel set. Clearly the iterations are stopped when reaching the maximum number of available channels. Moreover, the classification performance at each iteration was assessed as the mean among all available subjects. By doing that, the method attempts to find subject-independent best channels. To decide for the best performance, the difference between mean classification accuracy and associated standard deviation among the subjects ($\mu - \sigma$) was maximized. Note that this kind of objective function tries to also minimize the performance variation (σ). To ease the comprehension of the selection algorithm, this is represented in Fig. 4.6

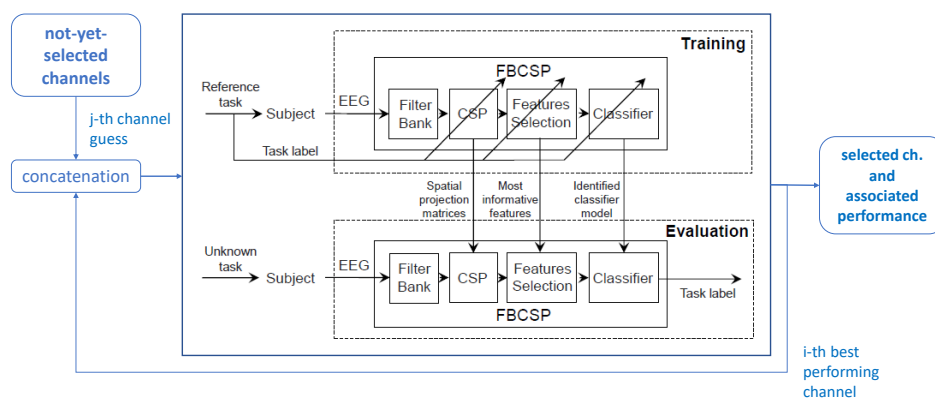


Fig. 4.6 Representation of the channel selection algorithm exploiting the FBCSP approach for the classification of EEG signals.

The channel selection step corresponds to the training of the system, and clearly it should only exploit training data. Therefore, a 6-fold cross-validation was used for the performance assessment. The training data are thus split 6 times in 6 folds, of which 5 folds are used for training the FBCSP and the remaining one for calculating the accuracy. Per each subject, cross-validation accuracy is hence obtained as the mean across 6 folds, and then mean and standard deviation across the subjects can be obtained. Thanks to the cross-validation, the method aims to determine the most significant channels in terms of predictive information. In using the FBCSP approach, a suitable classifier was also found by comparing state-of-the-art solutions, such as the NBPW [62], the SVM, and a k-nearest neighbors (kNN) classifier [3]. The classifier choice was again data driven. Note that these binary classifiers were extended to multi-class with the "one-versus-rest" approach. Hence, each class was discriminated against the remaining ones, and the class assigned to each trial was the one with the highest classification score.

At the end of the channel selection step, a sequence of sorted channels is available. Clearly channels are sorted according to the predictive information evaluated with cross-validation, and these results are useful in designing a BCI system because the expected classification performance (μ, σ) is given as a function of the channels subset. However, the channel sequence should be validated on new (independent) data. Hence, a testing phase is needed to validate the BCI design by also taking into account the trained FBCSP with the classifier. Such a validation was conducted by simply considering possible channel subsets according to the found sequence. In the first test step a single channel was considered, while for the following steps a channel was added each time according to the channels order. Note that, instead, it would be unfair to select channels by relying on test data. The results for the channel selection and validation are reported in the following.

Results

The proposed channel selection method was applied to the benchmark datasets of BCI competitions 2a (9 subjects) and 3a (3 subjects) introduced earlier. The method was implemented in MATLAB. First, the optimal classifier was chosen by considering both binary and multi-class (four classes) classification. Tab. 4.3 reports the comparison results for the NBPW, SVM, and kNN classifiers in terms of μ and σ for the 9 subjects of the dataset 2a. The six possible pairs of classes were considered

for the binary cases (combination of "left hand", "right hand", "feet", "tongue"). The cross-validation accuracy was calculated on data from the *sessions T*, thus choosing the classifier regardless of evaluation data data (sessions E) to be employed later. All channels (22 for dataset 2a) were taken into account in this step. Performances appear compatible for the different classifiers if looking at the intervals defined by mean and standard deviation. Nonetheless, paired t-tests [122] were performed to have an objective criterion for the choice. Tests were conducted by considering two classifiers per time for a binary classification problem or for the multi-class case. The null hypothesis for each paired test was that the mean accuracy μ associated with a classifier was equal to the one associated with the other. Therefore, rejecting the null hypothesis would suggest a difference in the performance in terms of mean accuracy. Then, in calculating the t-statistic, also the standard deviation is taken into account. The level of significance α for the test was fixed at 5 %.

TASKS	ACC \pm STD / %		
	NBPW	SVM	kNN
left hand vs right hand	74 \pm 20	74 \pm 20	73 \pm 19
left hand vs feet	81 \pm 13	82 \pm 12	82 \pm 13
left hand vs tongue	82 \pm 13	81 \pm 13	82 \pm 13
right hand vs feet	81 \pm 15	81 \pm 15	81 \pm 15
right hand vs tongue	84 \pm 13	83 \pm 14	83 \pm 13
feet vs tongue	75 \pm 13	76 \pm 13	75 \pm 14
four classes	63 \pm 19	63 \pm 19	63 \pm 20

Table 4.3 Comparison between NBPW, SVM, and kNN classifiers for different classification problems. Mean cross-validation accuracy and associated standard deviation were calculated among 9 subjects (dataset 2a) by taking into account all channels.

In these conditions, the null hypothesis was only rejected when comparing the NBPW with the kNN in "left hand vs tongue". This suggested that the NBPW should be slightly better (p-value = 0.0145), but there was no evidence for the other cases. However, hyperparameters were tuned for the SVM and the kNN, while this was not needed in the NBPW case. This implied a small preference for the NBPW, and in addition the Bayesian approach was preferred in our work since it naturally gives back a probability as classification score, which could indicate class uncertainty.

After the classifier selection, the channel selection procedure was carried out. The results are reported in Fig. 4.7 and Fig. 4.8, in terms of mean cross-validation accuracy (blue line) and standard deviation of the mean $\sigma_{\mu} = \sigma/\sqrt{9}$ (blue shaded

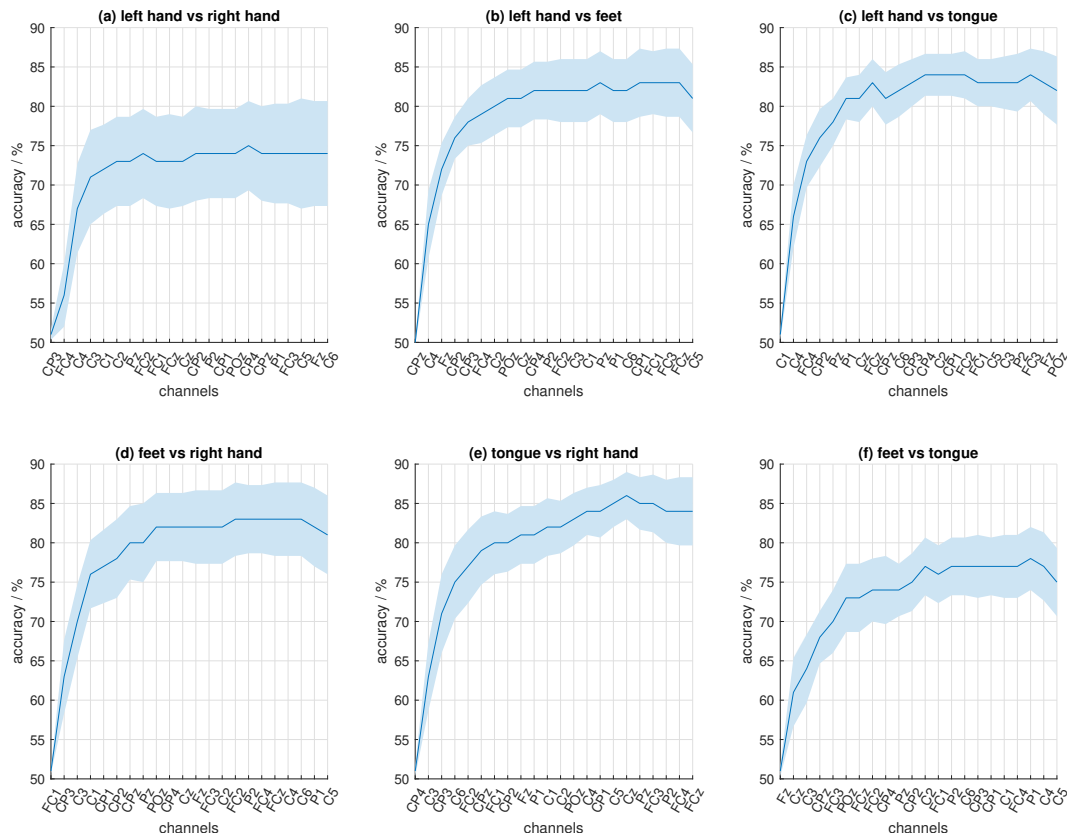


Fig. 4.7 Classification performance (cross-validation) for progressively selected channels and for each pair of classes.

area). On the x-axis, the channels that are progressively selected within the proposed procedure are reported, while the y-axis reports the classification accuracy. Note that a direct comparison between Fig. 4.7 and Fig. 4.8 would not be possible because the y-axis should report a performance normalized by the number of classes. Such a metric could be the kappa coefficient [118], but classification accuracy was still chosen since it is more common in literature. In trying to overcome this issue, the y-axis values reported in the figures are such that there is a one-by-one correspondence between Fig. 4.7 and Fig. 4.8, namely they correspond to the same Cohen's kappa coefficients.

The plots show the trade-off between channels and classification performance. In some cases, an acceptable performance can also be achieved with 4 channels, especially in the binary classification problems. Meanwhile, more channels are typically required in the four-task case. Hence, the figures highlight the possibility of suitable minimization for the number of channels while preserving the desired

classification performance. Focusing on the four classes, for instance, the same accuracy of the 22 channels case can be achieved with 18 channels, but the accuracy corresponding to 10-12 channels could be still acceptable while gaining in wearability and portability. It should be also noted that, in some other cases, the maximum accuracy seems to be reached with less than 22 channels. Although this could indicate that some noisy channels had been removed, in our case those values were a random occurrence since they did not result (from the statistical point of view) significantly different from the accuracy with the whole number of available channels.

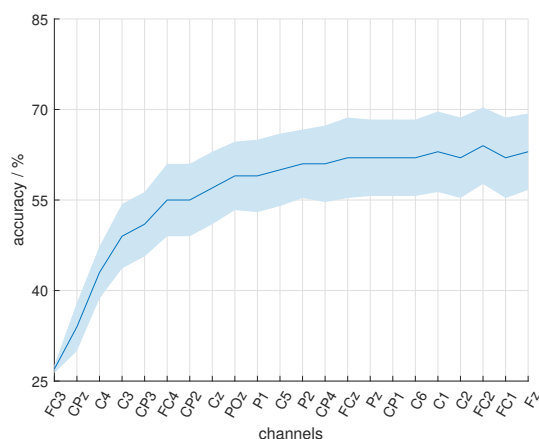


Fig. 4.8 Classification performance (cross-validation) for progressively selected channels in the four-class problem.

The results of the channel selection step are resumed in Tab. 4.4, where the classification performance at the maximum number of channels (22 in this case) is compared to the performance obtainable with a reduced number of channels, which was here chosen as 8 channels as a reasonable trade-off between performance and user-friendliness for the final system.

The sequences of channels were validated in a further step by employing the independent data from *sessions E*. As anticipated, for each pair of classes and for the multi-class problem, the algorithm was trained on data from the first session before the second session data could be classified. The results are plotted in Fig. 4.9 and Fig. 4.10. The channels on the x-axes correspond to the respective sequence, which were found during the selection, while on the y-axes the accuracy values were chosen as before. As a whole, validation results are compatible with the results obtained during channel selection, but more fluctuations are present with respect to the almost

TASKS	ACC \pm STD / %	
	8 channels	22 channels
left hand vs right hand	74 \pm 17	74 \pm 20
left hand vs feet	81 \pm 11	81 \pm 13
left hand vs tongue	83 \pm 9	82 \pm 13
right hand vs feet	80 \pm 15	81 \pm 15
right hand vs tongue (12)	80 \pm 11	84 \pm 13
feet vs tongue (11)	74 \pm 12	75 \pm 13
four classes (18)	57 \pm 18	63 \pm 19

Table 4.4 Mean and standard deviation of the classification accuracy obtained during channel selection, for both 8 and 22 channels.

monotonic behavior of the channel selection. Therefore, the results of Fig. 4.9 and Fig. 4.10 were analyzed with paired t-tests. The null hypothesis was that the accuracy at the maximum number of channels equals the accuracy at a reduced number of channels, so rejecting the null hypothesis would mean that the performances are different, either better or worse at the maximum number of channels. The level of significance was again set to $\alpha = 5\%$. In this case one must also note that failing to reject would not mean that the null hypothesis is necessarily true. Therefore, when rejection was not possible, the probability β of a false positive was also taken into account, so that $\beta \leq 5\%$ was considered as a reasonable risk of accepting the null hypothesis. These tests highlighted that performances are significantly worse than 22 channels ones when 3 to 5 channels are considered. Meanwhile, performances become acceptable with 6 to 13 channels, depending on the considered classification problems.

Validation results are resumed in Tab. 4.5 by reporting the classification performances for both the reduced number of channels (highlighted in the table) and the maximum number of available channels. In accordance with previous tables, also this table reports the standard deviation σ in spite of the standard deviation of the mean $\sigma/\sqrt{9}$ plotted in the figures. As a further validation of the proposed method, data from session T and E were flipped in order to repeat the channel selection and channel selection steps. Apart from an accuracy diminishing of about 1%-5%, the channel selection proved still effective in selecting a smaller number of channels while accepting a known accuracy diminishing. Hence, flipping data from the two sessions suggest that the results shown above are not restricted to the particularly chosen data. In going further, however, also the dataset 3a was used. With the

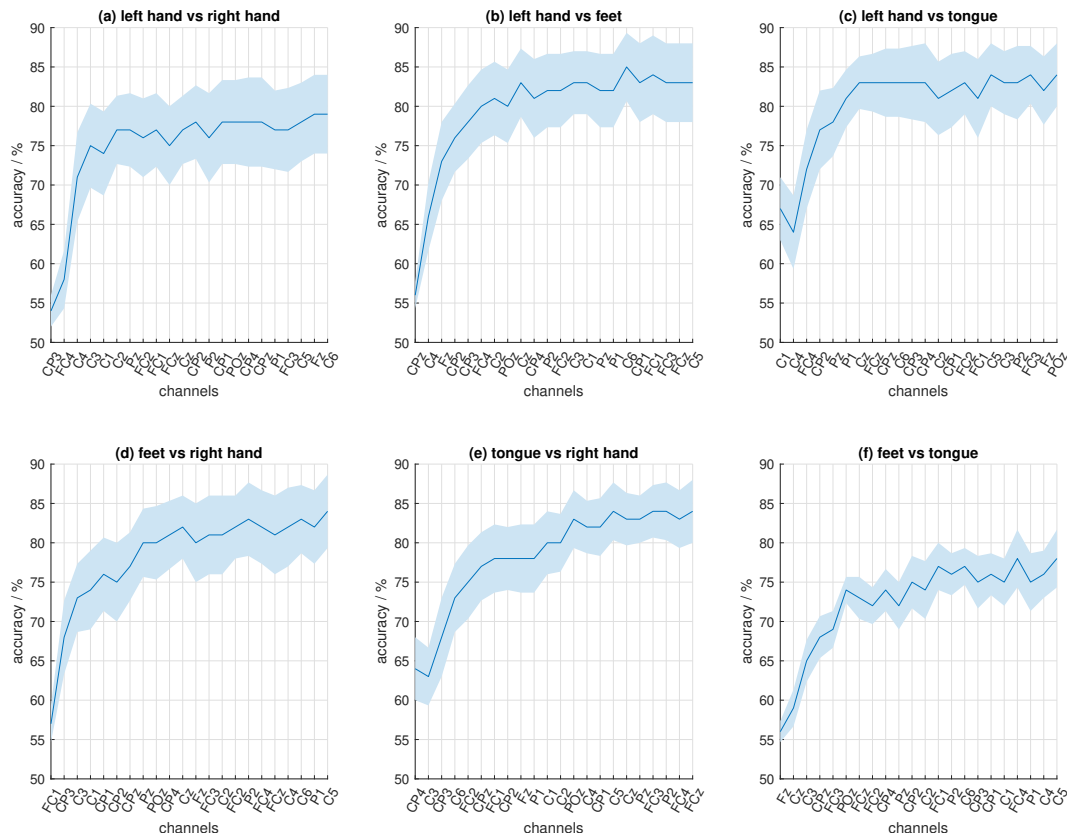


Fig. 4.9 Mean classification performance obtained to validate the respective sequence of the channel selection procedure in the binary classification cases.

FBCSP approach plus NBPW, classification accuracy for all the available channels (60) resulted above 80% for 2 tasks, and above 70% for 4 tasks, while the accuracies for reduced sets of channels resulted between 78% and 92% for in the binary cases, and about 72% with 10 channels in the four tasks case. These results are also plot in Fig. 4.11 by considering a representative example of the binary cases ('right hand vs tongue').

In general, the presented results are compatible or better than the findings in the recent literature [123, 124]. However, results can be criticised under some aspects. Firstly, although considering datasets from BCI competitions guarantees reproducibility of the results, classification accuracies in real applications are usually lower because only the best subjects were selected for acquiring these datasets. Moreover, the results also point out the need for further improvements. For instance, the fluctuations of the mean accuracy in validating the channel sequences is probably addressable to the non-stationarity of EEG signals. Indeed, thanks to the modular

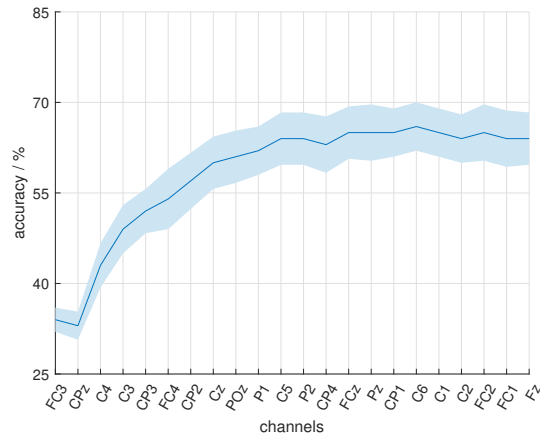


Fig. 4.10 Mean classification performance obtained to validate the respective sequence of the channel selection procedure in the four-classes case.

TASKS	ACC \pm STD / %	
	reduced ch.	22 channels
left hand vs right hand (6)	77 \pm 12	79 \pm 15
left hand vs feet (6)	80 \pm 15	83 \pm 15
left hand vs tongue (6)	81 \pm 12	84 \pm 12
right hand vs feet (10)	81 \pm 12	84 \pm 15
right hand vs tongue (13)	83 \pm 12	84 \pm 12
feet vs tongue (13)	77 \pm 9	78 \pm 12
four classes (10)	62 \pm 12	64 \pm 12

Table 4.5 Mean and standard deviation of the classification accuracy obtained during channel sequences validation.

channel selection involving FBCSP, the algorithm can be refined, especially for managing the non-stationarity. In addition to that, the iterative selection itself could be also enhanced. In particular, figures report an accuracy diminishing for some selection steps, and then an increase if one or more other channels are added. This should suggest that channels are correlated. Therefore, correlation-based selection could improve the results [125].

To conclude, the location on the scalp of predictive information was analysed. According to literature, the right hand is related to contralateral activation, the left hand generally shows a bilateral activation, the tongue is related to the interhemispheric fissure of the sensorimotor cortex, while feet are related to a strong bilateral activation [126, 127]. Hence, Fig. 4.12 shows contour plots for the binary classifications in which a weight is assigned to each channel of a sequence: maximum weight

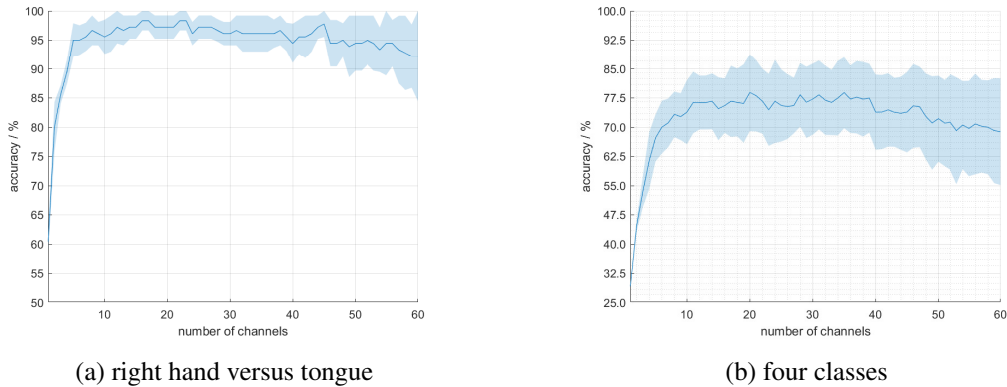


Fig. 4.11 Classification performance in validating the channel sequences found on dataset 3a.

is assigned to the firstly selected channel, while the weight progressively diminishes as the channels are selected later. With this reasonable assignment of weights, the areas highlighted by a concentration of most predictive channels are effectively in agreement with the above-mentioned literature.

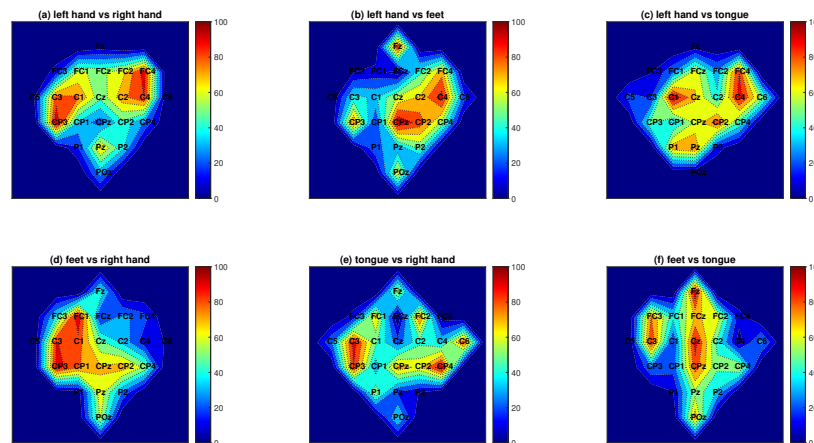


Fig. 4.12 Most predictive information on the scalp for each pair of classes.

4.4 Neurofeedback in MI-BCI

Neurofeedback consists of measuring brain activity and giving back to the user an activity-related information. Such information is usually presented with a visual, auditory, or haptic feedback [128]. In implementing a BCI, the feedback can be part of the system functionality or it can be only exploited during the training

process [129, 130]. Studies have shown that self-regulating brain activity through neurofeedback can be beneficial for the BCI performance [131, 132]. Notably, large ERDs can be observed during the online feedback sessions [133]. Indeed, neurofeedback training determines performance in the successive sessions, but it is still not clear the influence of factors such as given instructions, importance of the mental strategy, aptitude of the user in performing the task, attention to the feedback, and how the feedback is provided. In the following, neurofeedback is investigated in the operation of a wearable BCI relying on motor imagery classification. Notably, visual and vibrotactile feedback have been taken into account.

Many BCI technologies rely on vision for their functionality, and, in particular for MI-BCI, visual feedback has been employed to enhance the engagement in movement imagination [134]. The advent of virtual and augmented reality (VR/AR) technologies has given great contribution to that, thanks to the immersive experience offered by a computer-generated scenario [135]. Indeed, it is possible to create virtual objects to interact with, in order to enhance the user engagement in employing an MI-BCI, and hence receive feedback based on the measurement and interpretation of the sensorimotor rhythms. More recently, auditory feedback has been proposed as an alternative for people with deteriorated vision [136] or in conjunction with visual feedback in trying to improve the performance of motor imagery training [137]. These studies investigated different audio settings, from mono, to stereo, and even 3-D vector base amplitude panning. They demonstrated that auditory feedback can be a valid equivalent of the visual one. The need to investigate further feedback paradigms arises in aiming to create a more immersive experience, which would lead to a stronger engagement of the user. In particular, haptic feedback is of great interest for the AR (and VR) community because it enhances the simulation of a real situation [138, 139]. The sensation given by haptic feedback allows the user to better interact with virtual objects by feeling like touching a real object. Starting from that, in a BCI experimental protocol, the haptic feedback can help in user training for motor imagery. This could even be an alternative for people with both visual and auditory impairments, or it could be combined for a multi-modal feedback.

Visual and auditory feedback were already compared [136] showing that there is no statistical difference in their performance. Instead, there is little evidence on vibrotactile feedback, especially if exploiting wearable and portable actuators. Therefore, it was worth investigating this feedback modality as well as a feedback combination to enhance the BCI user engagement. The combination between visual

and vibrotactile feedback will be thus considered. The proposed system could find applications in rehabilitation, gaming, and even in robotics. It can enhance user experience both for helping in motor imagery training in rehabilitation protocols or for the usage of the system itself. In the case of users with disabilities, the kind of feedback to provide can be chosen according to the functional possibilities. For instance, vibrotactile feedback could be the only solution for deaf-blind people. In general, the optimal combination of feedbacks should be used to achieve an enhanced engagement by multi-modal feedback and hence increase the performance of MI-BCI.

4.4.1 Measuring MI-related phenomena

As discussed above, the same brain areas involved in motor execution are also activated during MI. Both sensory stimuli and motor activity induce changes in the activity of neuronal populations [111]. To measure such phenomena, averaging over multiple trials is required, and in particular it is assumed that (i) the measurand activity is time-locked with respect to the event, and (ii) the ongoing EEG activity is uncorrelated additive noise. Literature reports that some events may be time-locked but not phase-locked, thus averaging can either highlight a decreased or increased synchronization of neuronal populations. Therefore, event-related desynchronization and event-related synchronization (ERD/ERS or ERDS) reflect changes in the activity of local interactions between principal neurons and inter-neurons due to voluntarily modulated spontaneous activity, i.e. without any external stimulus. Such phenomena are associated with MI indeed. They are investigated in the time domain, frequency domain, and also spatial domain. By focusing on the discrimination of left hand imagery versus right hand imagery, the analysis of EEG signals associated with motor execution and motor imagery pointed out that the following phenomena can be detected:

- *alpha band ERD*: a decrease in alpha rhythms amplitude is expected at the contralateral area when starting movement (e.g. ERD at electrode C3 when executing or imagining right hand movement);
- *alpha band ERS*: an increase in alpha rhythms amplitude could be expected at the ipsilateral area, almost simultaneously to alpha ERD (e.g. ERS at electrode C4 when executing or imagining right hand movement);

- *beta band ERS*: an increase in beta rhythms amplitude is expected at the contralateral electrode at the end of the motor task (e.g. ERS at electrode C3 when stopping the execution or imagination of right hand movement).

Studies argue that the more evident these phenomena are, the higher the classification accuracy of MI-related EEG is [140]. It was thus interesting to assess the presence of ERDS in the brain signals under analysis and associate it with classification accuracy. This could be done either without or with the introduction of neurofeedback in aiming to investigate MI-related phenomena and their sought improvement.

In assessing the ERDS, a standard framework was used, notably the python MNE (MEG + EEG analysis & visualization) package [141]. An ERDS map was obtained, namely a time/frequency representation of the phenomenon [142]. To this aim, epochs were extracted from the initial relax period to the break after motor imagery, time-frequency decomposition was applied to all epochs by means of a multi-taper transform, then a cluster test was conducted so that only epochs with p-value less than 5 % would be considered for averaging, and finally time-frequency maps were obtained per each electrode by averaging over considered epochs. As a second step, the time course of ERDS could be derived from the time-frequency map by considering alpha and beta bands. In the present case, this was done for channels C3 and C4, on the left and right side of the somatosensory area, respectively.

In addition to the ERDS, also the time course of classification accuracy can be investigated. As already discussed, the FBCSP implemented in Matlab was taken into account for the classification of MI-related signals. In doing that, trials are segmented according to the timing of the experiment. The classification should be random in the relax periods and non-random in the motor imagery periods. Hence, if trials are analysed with a sliding window, one should expect a random level for the classification accuracy at the beginning, an increase in the motor imagery period, and again a random classification in the final break. In addition to that, in the adopted FBCSP implementation, selected features could be analysed. This was done to highlight regularities in their choice. In that, cross-validation was considered, and histograms were built with the features selected across all iterations.

These analyses were first applied to data from a benchmark datasets, the BCI competition IV dataset 2a. If analysing EEG data associated with subject A03, the ERDS time course of Fig. 4.13 is obtained. An ERD in the alpha band is clearly visible for the right hand imagery at the contralateral electrode (C3). This ERD is

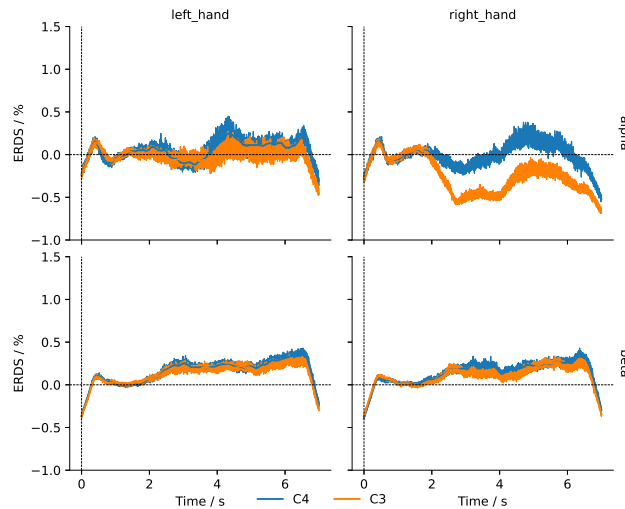


Fig. 4.13 Time course of ERDS for subject A03 (session T) from BCI competition IV dataset 2a.

localized at about $t = 2$ s, which corresponds to the cue indicating the task to perform. Then, an ERS seems present before $t = 6$ s, where the imagination should be stopped, though this is still in alpha band (not beta band). No other phenomenon among the abovementioned one appears evident. Moreover, these phenomena are not even clear for the left hand imagery. Next, the time course of classification accuracy for the subject A03 (Fig. 4.14a) shows that the discrimination between left and right hand imagery is random in correspondence of the starting relax period and then it increases up to almost 100 % during the motor imagery period. Hence, A03 can be considered a "good" subject in the sense of classification. In the final part, the accuracy also decreases as it should (ending relax period). In addition to that, the analysis of features is proposed in Fig. 4.14b. The histogram highlights that, across the several iterations, selected features are mostly concentrated in the alpha band. This is in accordance with the ERD phenomenon appearing in the alpha band for the present subject and it also points out a regularity in the features selected for classification.

The same analyses could be repeated for the subject A05. Fig. 4.15 shows that no clear ERD nor ERS phenomenon is visible. However, the time course of classification accuracy (Fig. 4.16a) points out that a classification accuracy up to 90 % is obtained during the motor imagery period. Hence, also A05 is associated with a good classification performance. Finally, the histogram of selected features

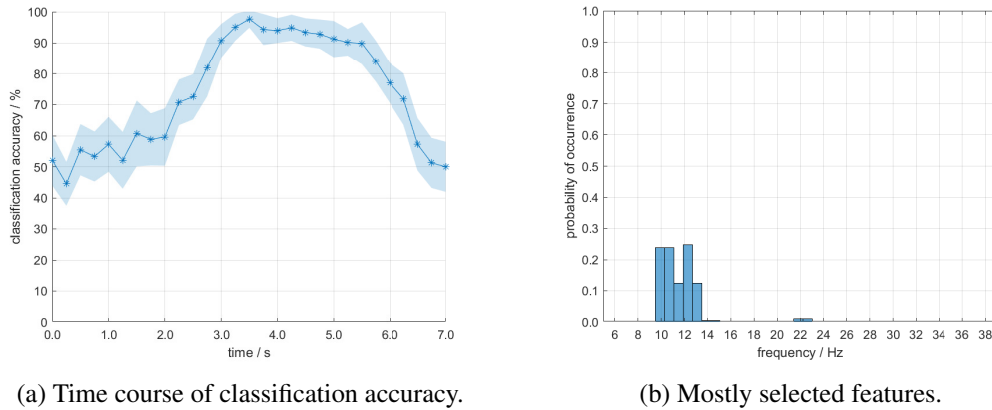


Fig. 4.14 Analysis of MI-related phenomena for subject A03 (session T) from BCI competition IV dataset 2a.

reported in Fig. 4.16b still shows concentrated features in the beta band, though they are more diffused than the previous case.

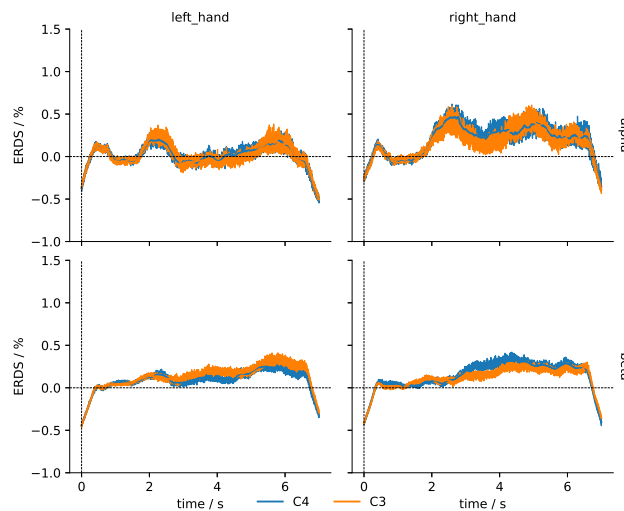


Fig. 4.15 Time course of ERDS for subject A05 (session T) from BCI competition IV dataset 2a.

As a last case, the ERDS associated with subject A02 is reported in Fig. 4.17. Here, an anomalous behavior appears in the alpha band for both left and right hand imagery. ERS seems present at the cue time instant, while ERD could be identified about in correspondence of the motor imagery stop. The analysis of classification accuracy in time reveals that there is random classification over the whole period

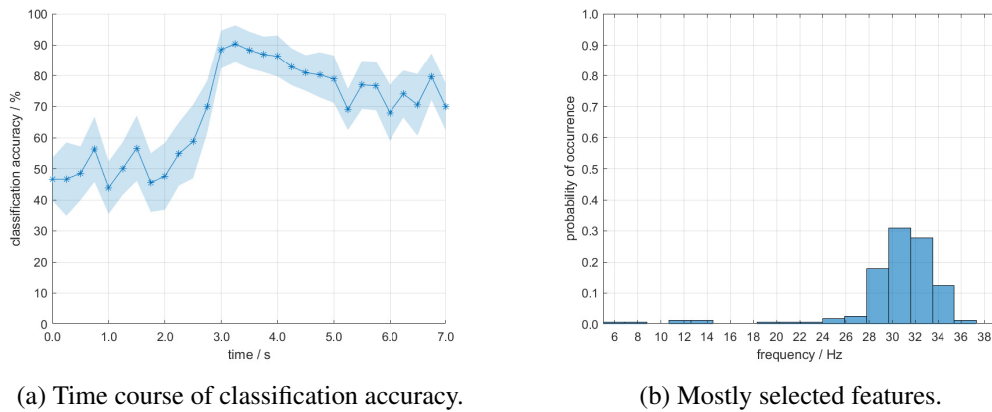


Fig. 4.16 Analysis of MI-related phenomena for subject A05 (session T) from BCI competition IV dataset 2a.

(Fig. 4.18a), and even the histogram does not show any regularity, but selected features are spread over the whole possible frequencies (Fig. 4.18b).

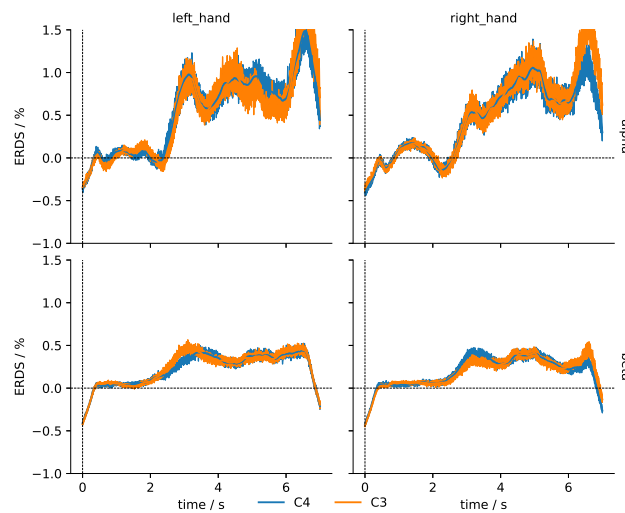


Fig. 4.17 Time course of ERDS for subject A02 (session T) from BCI competition IV dataset 2a.

Given the analyses on the benchmark dataset, further analyses were conducted on data from own experiments. Notably, the FlexEEG system was employed to build the MI-BCI with neurofeedback. The Olimex EEG-SMT was discarded because of the poor data quality that could be obtained when electrodes are placed over the sensorimotor area. In particular, a preliminary feasibility study demonstrated that the dry electrodes from Olimex have a poor contact impedance when placed at C3 and

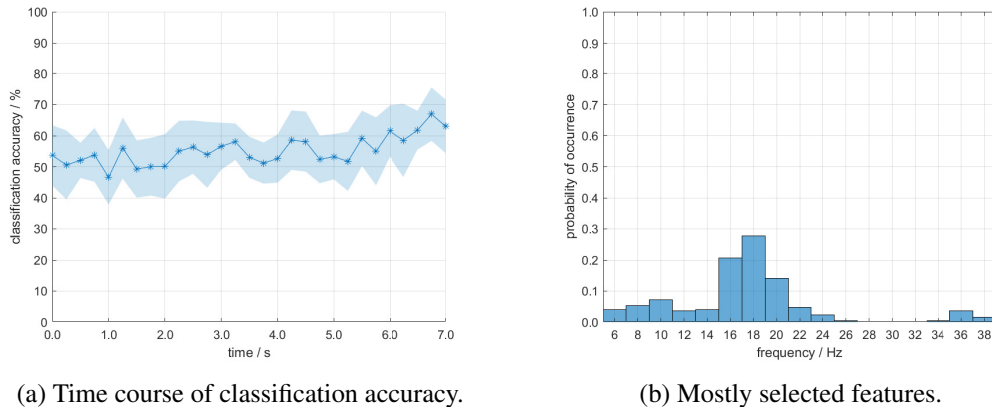


Fig. 4.18 Analysis of MI-related phenomena for subject A02 (session T) from BCI competition IV dataset 2a.

C4 because they are highly sensitive to head movements. The Helmate, instead, had to be discarded because the online data stream was not yet available, though offline analysis demonstrated that the EEG signals quality was good enough even with dry electrodes. In conclusion, the FlexEEG was used by exploiting the three bipolar channels CP3-FC3, CPz-FCz, and CP4-FC4 by applying conducting gel to ensure proper electrode-skin contact. As a representative example, a subject from the own experimental campaign is here considered. By referring to first trials without any feedback, the time course of ERDS is reported in Fig. 4.19. An ERD could be caught in the alpha band for right hand imagery, though it appears on both the contralateral and the ipsilateral channel. Instead, for left hand imagery, the ERD at imagination start could be present in the beta band. No other phenomenon is clearly present. The time course of classification accuracy (Fig. 4.20a) suggests that the result could be not random in the imagery period, but mean accuracy does not overcome 70 %, which is often considered an empirical threshold for good performance. Finally, the histogram of features in Fig. 4.20b points out that selected features are relatively concentrated in alpha band and at the limit between alpha and beta band. As a whole, these results could be considered a halfway between the A03/A05 case and the A02 one. However, in the following, results on neurofeedback experiments conducted with the same subject will show how these MI-related phenomena can be improved.

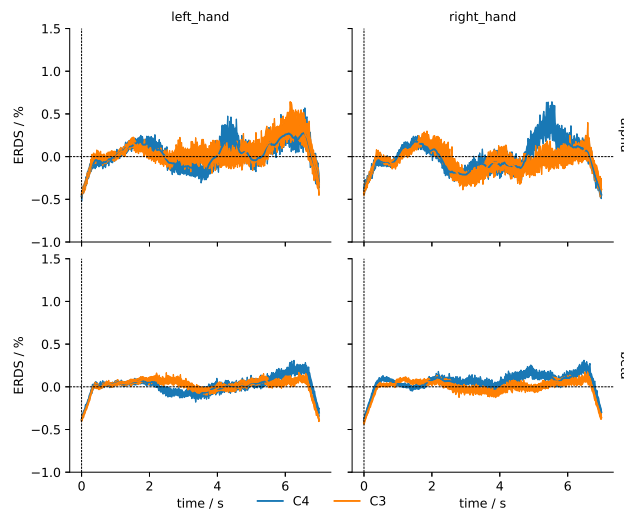


Fig. 4.19 Time course of ERDS for subject AE data acquired with FlexEEG while no neurofeedback was provided.

4.4.2 Measurement system

Building a system ready for daily life is indeed very challenging. Therefore, some assumptions had to be made to simplify the problem. In a daily-life application, the BCI should continuously measure brain activity and distinguish between mental resting and motor imagery. This system would be an asynchronous BCI, in which the user can freely decide when to execute a mental task. However, the discrimination between rest and motor imagery is still inaccurate. For that reason, motor imagery is often conducted according to an externally-paced cue, which exactly defines the instants for the mental tasks. The focus of this work is hence on cue-based discrete trials, namely a synchronous BCI is considered.

Another obvious request for the BCI system would be to have many possible control commands. This would mean that the system should correctly discriminate between many motor imagery tasks. On the other hand, the more the control commands, the less accurate the task classification. At least four classes would be needed for a 2D control capability, but in this first system implementation only two motor imagery tasks were taken into account, i.e. left versus right motor imagery. Then, as a further development, it is foreseen to also consider imagining both hands, or both feet, or tongue movements.

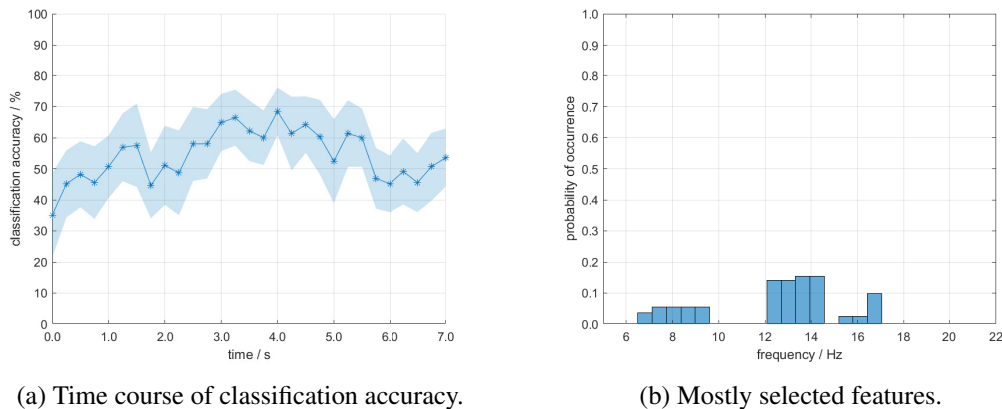


Fig. 4.20 Analysis of MI-related phenomena for subject subject AE data acquired with FlexEEG while no neurofeedback was provided.

Finally, exploiting portable instrumentation is indeed useful for applications outside the laboratory. This would certainly mean that the user's movements and the environment are harder to control. According to literature studies and to previous experiments conducted in our group, there are still many challenges to face before real portability can be achieved. Because of that, in validating the system implementation, the user was seated on a comfortable chair and was asked to limit unnecessary movements. This had to be done to first test the system in a controlled situation, but the characteristics of the system indeed foresee daily-life usability.

Neurofeedback protocol

In exploiting neurofeedback for improving motor imagery classification, the longer the experiment, the higher the performance should be due to more available data (for algorithm training) and long training for the user. However, stress must be avoided for the user, since this would be deleterious for the performance. Therefore, the proposed protocol tries to minimize experiment duration. In addition, three feedback modalities had to be compared: only visual, only vibrotactile, and visual plus vibrotactile (multimodal).

Different experimental sessions were carried out on different days. Each session was organized in two blocks. In the first block, EEG data were acquired while the user executed motor imagery tasks without any feedback. These data were then used to identify a model for online classification of EEG during the next block. Therefore,

in the second block, the user executed motor imagery tasks while receiving feedback about the adherence of his/her EEG activity to the identified model. The EEG data stream was processed with a sliding window approach. The width of the window and the overlap between adjacent windows was also decided during the model identification. The output of online classification consisted of a class and a score. In each trial, the feedback was actually provided only if the retrieved class was equal to the assigned task, while the score was used to modulate feedback intensity. The neurofeedback block was actually divided into three sub-blocks where the three feedback modalities were provided in a randomly different order per each subject. Moreover, left and right motor imagery was also randomly assigned during trial execution to avoid any bias. The described neurofeedback protocol is resumed in Fig. 4.21. The timing of a single trial is recalled from the common paradigm of BCI

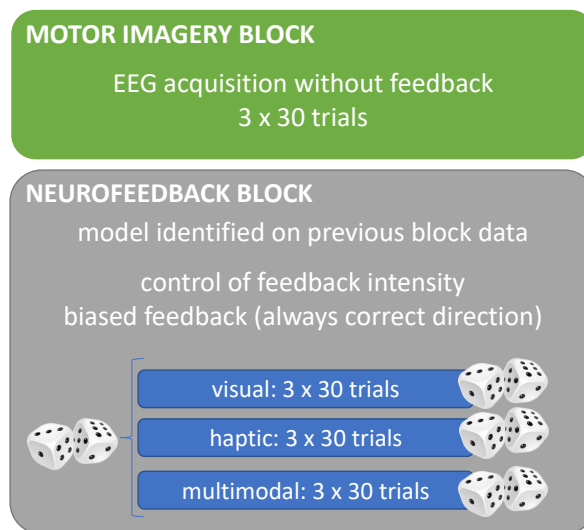


Fig. 4.21 Blocks and sub-blocks of the proposed neurofeedback protocol employed in the closed-loop motor-imagery-BCI.

competitions [115]. It consists of an initial relax (2 s), a cue indicating the task to carry on, the motor imagery starting at $t = 3$ s, and then its ending after 6 s. A final break/relax is also present and its duration is randomized between 1 s to 2 s.

System implementation

The block diagram of the system for neurofeedback experiments is shown in Fig. 4.22. It consists of EEG acquisition, EEG (online) processing, and feedback actuation.

The EEG signals are received by a custom Simulink model, where online signal processing is also implemented. The EEG classification output consists of a class label and a class score sent to a purposely designed Unity application. With such input commands, the Unity application drives the visual and haptic feedback. The user datagram protocol (UDP) was used in the Simulink-Unity communication. Details about each block are discussed in the following.

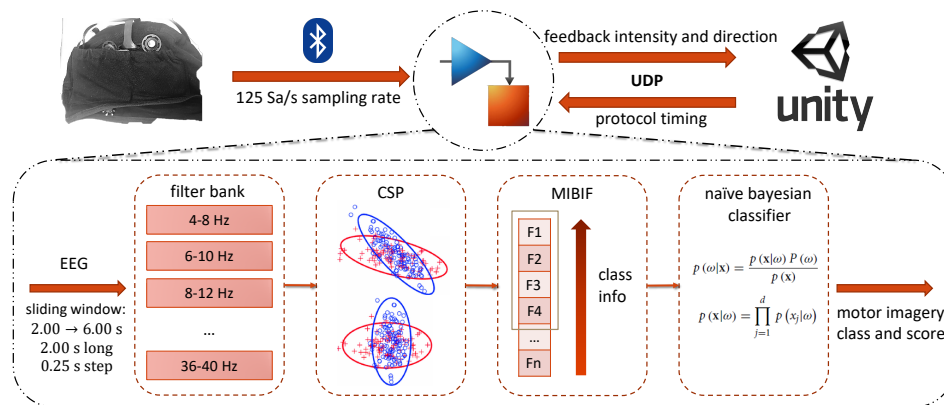


Fig. 4.22 Block diagram of the closed-loop BCI system based on motor imagery and neuro-feedback.

EEG acquisition was carried out with the FlexEEG headset by NeuroCONCISE Ltd with wet electrodes already introduced in Chapter 2 and recalled in Fig. 4.23. The headset was used with the FlexMI electrodes configuration, consisting of three bipolar channels over the sensorimotor area. Recording channels have electrodes placed at FC3-CP3, FCZ-CPZ, and FC4-CP4, according to the international 10/20 EEG standard [2], while the ground electrode is positioned at AFz. Electrodes position is shown in Fig. 4.23a Conductive gel was used to ensure low contact impedance and high stability at the scalp interface, though these electrodes could be also used without any gel. The EEG signals from the electrodes are filtered and amplified by the electronic board. Then, these signals are digitized by sampling at 125 Sa/s with 16-bit resolution. Finally, the data are transmitted via Bluetooth 2.0.

To translate the acquired brain activity into control commands, the acquired and digitized EEG signals were processed with the FBCSP approach, which was properly adjusted for real-time operation. Notably, a training was first executed with data from the motor imagery block to identify the classification model. Then, the EEG had to be classified during the motor imagery execution in order to provide a concomitant feedback. Therefore, the FBCSP approach with the naive Bayesian classifier was

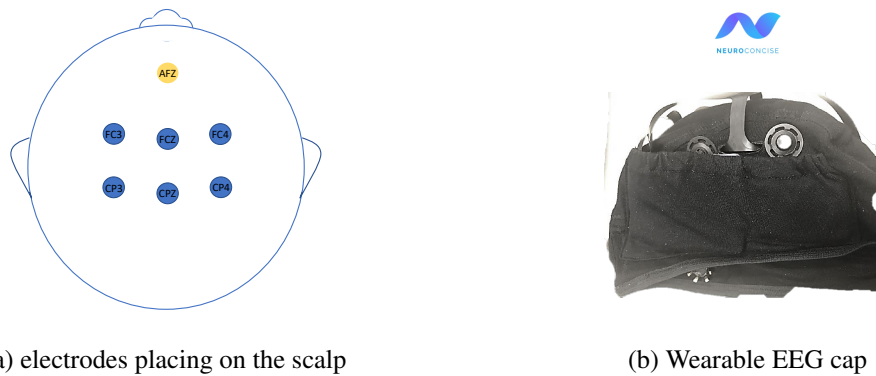


Fig. 4.23 Wearable and portable EEG acquisition system employed in experiments with neurofeedback during motor imagery.

applied to a sliding window. The width of the window could range from 1 s to 3 s and it was chosen on training data so as to maximize the classification accuracy. Then, the shift of the window was fixed so as to have a feedback of 250 ms. It is to note that the training of the algorithm considered the optimal motor imagery time window. The model performance after training was validated with a cross-validation. The timing of a trial is shown in Fig. 4.24. Though the EEG stream was continuously processed, during the experiments the feedback could be actually provided starting from the cue. Thanks to the Bayesian classifier, a class score could be naturally associated with the class assigned to the processed EEG data because it assigns a probability to each EEG data epoch.

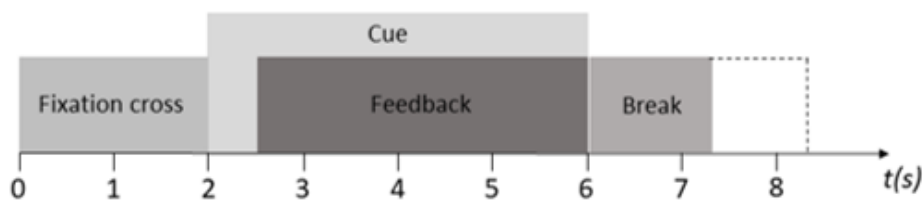


Fig. 4.24 Timing diagram of a single trial in the BCI experiment with neurofeedback.

The designed feedback consisted of controlling both intensity and direction of a moving virtual object. Multimodal feedback was obtained by merging visual and vibrotactile modalities. In detail, the visual feedback was provided by the rolling of a virtual ball on a PC screen, while the vibrotactile one was given by a wearable suit with vibrating motors. Intensity and direction of the feedback were determined by means of the user's brain activity, measured through EEG. In this prototype, a

generic PC monitor was used to provide the visual feedback. However, this will be replaced by smart glasses to provide a more immersive experience and hence furtherly increase user engagement. A Unity application was purposely developed to have a virtual environment with a rolling ball, as well as to control the haptic suit. Note that the applications also indicated the task to carry out (Fig. 4.25). The

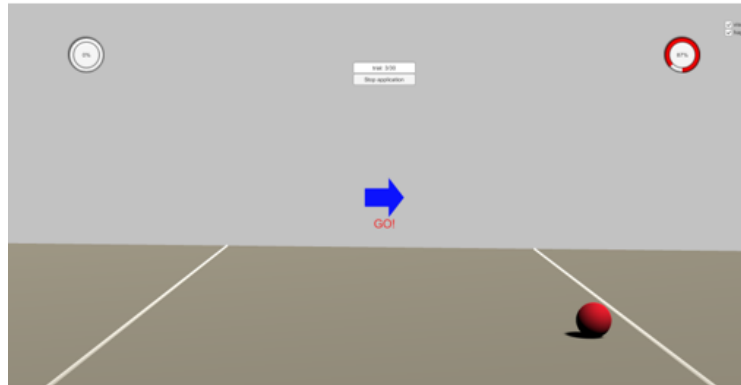


Fig. 4.25 Visual feedback consisting of a mentally-controlled virtual ball.

hardware for the haptic feedback consists of a vibrotactile suit from bHaptics Inc. This suit is indeed wearable and portable and it is commercially available for gaming [143]. It provides a double 5×4 matrix with vibration motors installed on the front and back of the torso. Vibration can be adjusted in terms of intensity per each single motor, so that patterns can be created to give a specific haptic sensation to the user. The suit can communicate through Bluetooth with a computing unit. In our application, it is controlled from a PC that receives the EEG data through UART and then sends control commands to the suit according to the EEG classification. The suit and the motors locations (vibration matrix) are shown in Fig. 4.26.

4.4.3 Experimental results

Experimental setup

Eight right-handed volunteers (SB1-SB8, three males, mean age 26 years) participated in the experiment. They were conducted at the Augmented Reality for Health Monitoring Laboratory (ARHeMLab), University of Naples Federico II, Italy. No subject reported medical or psychological illness and/or medication and they had normal or corrected to normal vision. Subject SB1 was experienced in active, passive



Fig. 4.26 Wearable and portable haptic suit with 40 vibration motors.

and reactive BCI paradigms, subject SB2 was experienced in active BCI, subjects SB3 and SB4 were experienced in reactive BCI, while the other four subjects had no BCI experience. Subjects were instructed with information about the experimental protocol before beginning the experiments. Regarding the visual feedback, the goal was to overcome the white line (Fig. 4.25). Instead, for the haptic feedback, the vibration patterns were provided on the front side of the torso starting from the center. They could move the ball or the vibration to the left or to the right according to the indicated motor imagery task, and the goal for the user was to reach the respective side. Finally, in the multimodal feedback case, the aforementioned feedbacks were jointly provided.

Experiments were conducted according to the neurofeedback protocol proposed above. This protocol attempted to balance the need of much EEG data with limited experiment duration to avoid stress to the user. Two or three sessions were recorded for each subject. Each session lasted about 2 hours. In order to monitor the mental and physical state, a questionnaire was administered to the participants at the beginning of the session, after the first block, and at the end of the session. By relying on the questionnaire proposed by [144], the questionnaire of Tab. 4.6) was proposed in the current experiments.

At the beginning of the first session, the participants were also instructed on the movement imagination itself. They were asked to try different ways of imagining hands movement (such as kinesthetic sensation, squeezing a ball, grasping an object, snapping their fingers, imagining themselves or another person performing the

movement) to identify the one they were most confident with. Once chosen, they were asked to keep it constant throughout the session. Finally, they were instructed to avoid muscle and eye movements during the motor imagery task. As already mentioned, the first block consisted of acquiring EEG data with no feedback provided in order to identify the classification model. Then, three runs with 30 trials each and two classes of imagery were recorded while providing feedback. Participants were asked to imagine the movement of the right or left hand. The order of the cue-based tasks was randomized to avoid any bias. A maximum of ten minutes break was given between the two blocks. In the meanwhile, the selection of the best time window to train the algorithm for the online experiment was carried out. For this purpose, the FBCSP was exploited in a 10-repeated 5-folds cross validation technique. Its performance is tested from 0 s to 7 s with an overlap of 0.25 s. A time window 2 s wide was used to extract the EEG signal. The time-varying classification accuracy and associated standard deviation was calculated from the time-varying classification accuracies obtained using the cross-validation setup. For each subject, the best time window was chosen in terms of maximum classification accuracy during the motor imagery task together with the minimum difference between accuracies per class. Therefore, the algorithm was trained by using such an optimal window. Notably, another run could be recorded if the results were not satisfactory. Finally, between feedback sub-blocks, a break of about 2 minutes was given. With 30 trials per run, the total number of available trails per each subject was 360 acquired under different conditions.

Data analysis

In analysing data offline, the scope was to highlight the effectiveness of a feedback modality in improving the detection of motor imagery. Hence, the classification accuracy associated with each experimental condition was calculated and compared to other conditions. In data processing, baseline removal was firstly carried out. Specifically, a period of 100 ms before the cue was used. Then, the time-varying analysis was performed for all subjects, blocks and sessions by means of the cross-validation technique.

Subsequently, a permutation test was performed per each session, subject and block. The purpose was to validate the results obtained in the time-varying analysis evaluating how far these differed from the random classification. Hence, the labels

associated with the left and right motor imagery tasks were randomly permuted and the time-varying analysis was repeated. The time-varying accuracy was calculated using true labels with the 2.00 s-wide time window and 0.25 s shift, and the mean of accuracies in cross-validation was taken into account for each window. The same time-varying accuracy was also calculated with the permuted labels. Finally, the comparison between the first results obtained and those from the permutation analysis was carried out using the non-parametric Wilcoxon test with the null hypothesis that the means of the two distributions were equal. Thus, rejecting the null hypothesis imply that the accuracy achieved with the true label is non-random. The significance level for the test was fixed at $\alpha = 5\%$.

Furthermore, based on the best 2 s time window in terms of classification accuracy, the one-way analysis of variance (ANOVA) was performed to compare the accuracy between blocks and sessions. The ANOVA was firstly conducted to analyse the difference between sessions per each subject and block and the difference between blocks per each subject and session. Then, by considering all subjects together, this analysis was done for each block to highlight differences between sessions and for each session to analyse differences between blocks. Before applying the ANOVA, inherent data assumptions were verified, i.e. data must be normally distributed and with equal variance (homoscedasticity). In case of normally distributed data samples with different variances, the Welch's correction was applied before using ANOVA. Instead, ANOVA could not be used when data were not normal, and a non-parametric test, namely the Kruskal-Wallis testm was set in those cases.

Results

A representative example of the time-varying analysis plots generated from the original and randomly permuted data is reported in Fig. 4.27 for subject SB1. The mean classification accuracy and the associated standard deviation are calculated with a cross-validation across trials and by considering the shifting time window. The three different sessions are reported on rows, while the four different feedback conditions are reported on columns. Each plot has time in seconds on the x-axis and mean classification accuracy expressed in percentage on the y-axis. The red curves indicate the accuracy corresponding to the permuted labels, while the blue line corresponds to the results reached using the true labels. As it would be expected, the two lines are indistinguishable up to the cue (at 2 s) in most cases. Then, it is

noticeable that the two lines separate during the motor imagery. At a first glance, it can be seen that the classification is more distant from random when neurofeedback is exploited. Moreover, better performance is also obtained in the last session, thus pointing out a training effect for the user. Similar results could be obtained with

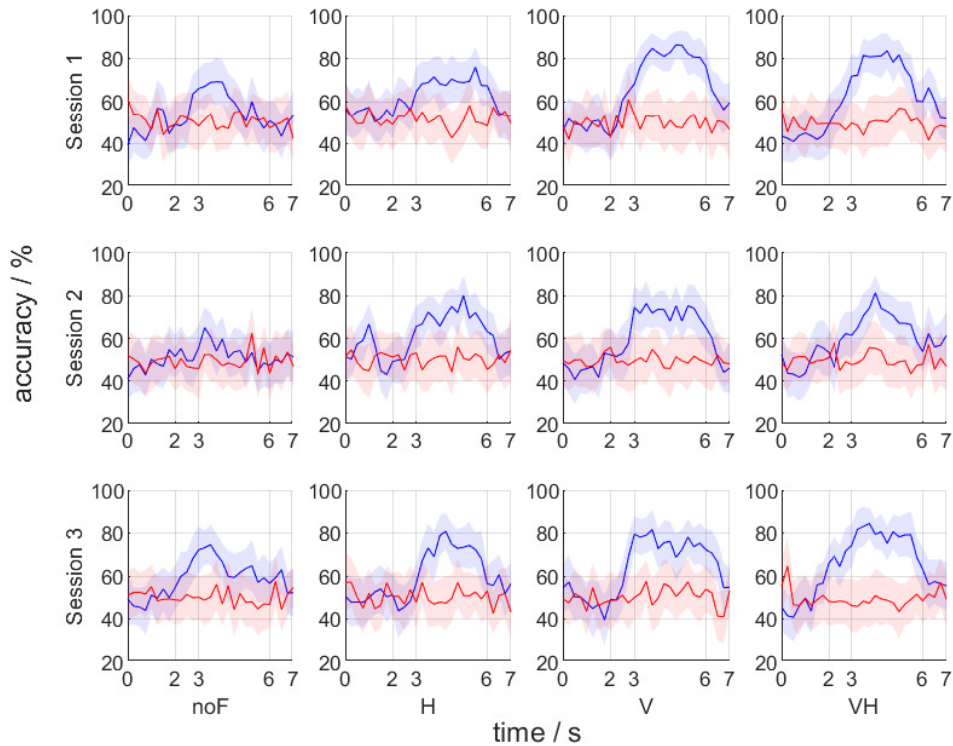


Fig. 4.27 An example of the permutation test for the subject SB1 executed on the time course of classification accuracy in different experimental conditions. The blue curves correspond to the accuracy calculated with true labels, the red curves correspond to the accuracy obtained with permuted labels.

other subjects, though in some cases the classification was compatible with the chance level. The results of the Wilcoxon test associated with the permutation test demonstrated that, as a whole, four subjects in the first session and six in the second session achieved non-random accuracy when no feedback was provided. Then, five to seven subjects, out of eight, achieved non-random accuracy in the first session with feedback, with no dominant feedback modality. In the second session, instead, at least six subjects achieved non-random accuracy. The results are compatible with literature, since they highlight that a training effect subsists between sessions and that feedback is useful for increasing the performance. Notably, such results have

been obtained with a wearable and portable system implemented with commercial hardware, which is a relatively novel trend for the BCI field. Also the results from the third session (with only four subjects out of eight) point out an increase in overall performance. Nonetheless, mean classification accuracies appear compatible across the sessions and further experiments will be needed to properly reveal an improved detection across sessions. On the other hand, the improvement due to the neurofeedback is already evident. This is also resumed in Fig. 4.28. There, the time-varying classification accuracy associated with subject SB1 is compared to the one associated with the subject A03 from BCI competition IV. The Fig. 4.28a highlights that the trained subject A03 has substantially higher classification accuracy in the motor imagery period if compared to the performance of subject SB1. Then, Fig. 4.28b shows that the accuracies obtained with the neurofeedback become closer to the one of a trained subject.

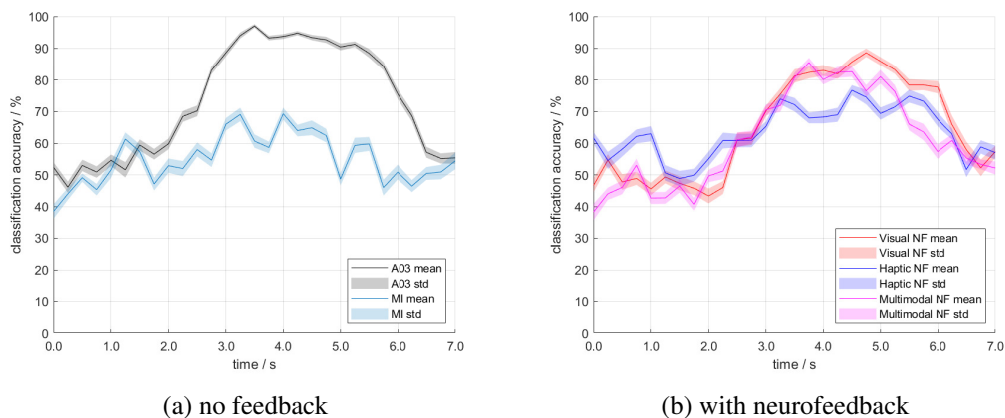


Fig. 4.28 Time varying decoding accuracy associated with motor imagery. The classification accuracy of subject SB1 is compared to the one of a trained subject (A03 from BCI competition IV).

Finally, the ANOVA executed as discussed above allowed to rigorously compare the classification accuracies in different conditions. As already mentioned, no statistically significant difference is revealed when considering the performance across sessions for all subjects. Moreover, the performance improvement with feedback is still not significant when all subjects are taken altogether. On the contrary, with the ANOVA executed subject-by-subject, the accuracy improvement is statistically significant for about half of the subjects between sessions, and the feedback results effective for six subjects out of eight. In conclusion, neurofeedback

resulted useful for most subjects in a daily-life BCI for improving motor imagery detection despite few channels being used, though future experiments are needed to furtherly assess the system performance and better evaluate its limitations.

Experimental Information at start	
Date	yyyy:mm:dd
Session	
Starting time	hh:mm
Handedness	1: left / 2: right / 3: both
Age	
Sex	1: male / 2: female
Do you practice any sport?	0: no / 1: yes / 2: professional
BCI experience	0: no / 1: active / 2: passive / 3: reactive / 4: multiple types
Biofeedback experience	0: no / number: how many times
How long did you sleep?	number: hours
Did you drink coffee within the past 24 h?	0: no / number: hours before
Did you drink alcohol within the past 24 h?	0: no / number: hours before
Did you smoke within the past 24 h?	0: no / number: hours before
How do you feel?	Anxious 1 2 3 4 5 Relaxed Bored 1 2 3 4 5 Excited (Physical state) Tired 1 2 3 4 5 Very good (Mental state) Tired 1 2 3 4 5 Very good
Which motor imagery are you confident with?	1: grasp / 2: squeeze / 3: kinesthetic
After training block	
How do you feel?	(Attention level) Low 1 2 3 4 5 High (Physical state) Tired 1 2 3 4 5 Very good (Mental state) Tired 1 2 3 4 5 Very good
Have you nodded off/slept a while?	No 1 2 3 4 5 Yes
How easy was motor imagery?	Hard 1 2 3 4 5 Easy
How do you feel?	(Attention level) Low 1 2 3 4 5 High (Physical state) Tired 1 2 3 4 5 Very good (Mental state) Tired 1 2 3 4 5 Very good
Have you nodded off/slept a while?	No 1 2 3 4 5 Yes
Did you feel to control the feedback?	(Visual) No 1 2 3 4 5 Yes (Haptic) No 1 2 3 4 5 Yes (Multimodal) No 1 2 3 4 5 Yes
How easy was motor imagery?	Hard 1 2 3 4 5 Easy
After the motor imagery experiment	
Which type of feedback did you prefer?	0: v / 1: h / 2: v-h
How do you feel?	Anxious 1 2 3 4 5 Relaxed Bored 1 2 3 4 5 Excited
How was this experiment?	(Duration) Too long 1 2 3 4 5 Good (Timing) Too fast 1 2 3 4 5 Good (Environment) Poor 1 2 3 4 5 Good (System) Uncomfortable 1 2 3 4 5 Comfortable

Table 4.6 Questionnaire provided to the participants at each experimental session

Conclusions

The present doctoral thesis has treated the development of daily-life brain-computer interfaces from a metrological perspective. The rigorous tools provided by metrology can be effectively employed in such systems because of two main reasons. First, these systems rely on the measurement of brain activity and their design must be carefully carried out, particularly when aiming to detect neurophysiological phenomena with a minimal hardware. Secondly, the instruments adopted in building brain-computer interfaces should be characterized in order to fully understand the system operation, especially when consumer-grade equipment is considered. Hence, the aim of this work was to contribute to bringing such a technology from a laboratory environment to everyday life, so as to address applications either for able-bodied people and impaired ones.

In Chapter 1, some background knowledge has been recalled concerning brain-computer interface technology, and measurement aspects have been underlined with specific regards to brain signals acquisition and processing. Then, key requirements for daily-life neural interfaces have been outlined. Indeed, a non-invasive neuroimaging technique had to be considered in acquiring brain activity. Hence, electroencephalography was exploited, for it is also suitable for developing wearable, portable, and relatively low-cost systems. However, this also implies some drawbacks: poor spatial resolution and lower signal-to-noise ratio if compared to more invasive neuroimaging techniques. The last aspect is even more relevant if few electrodes are employed. This was actually the case for the present discussion because of aiming at utmost wearability and portability. Finally, portability of the system also demands to deal with motion artifacts affecting brain signals measurement. This issue is particularly relevant when dry electrodes are employed, where no conductive gel is employed at the electrode-skin interface. Though artifacts were

already considered in the current work, this aspect surely deserves more investigation in the near future.

On this basis, Chapter 2 has dealt with the design of brain-computer interfaces. Consumer-grade devices with few electrodes have been first introduced as acquisition hardware for electroencephalographic signals. Then, signal processing was also considered for daily-life applications sought for minimal calibration time and real-time performance. Next, metrological aspects were stressed with specific regards to the measurands taken into account, namely evoked activity or spontaneous brain potentials. Thereafter, methods for a metrological characterization of brain-computer interface components have been proposed. Electroencephalograph calibration was carried out by means of laboratory instrumentation that is commonly used in metrological institutes. Meanwhile, a photo-transducer was designed and implemented for characterizing the flickering icons of smart glasses specifically addressed to evoked potential elicitation. Characterization results show that consumer-grade electroencephalographs can be successfully employed in brain-computer interface applications thanks to their linearity and limited gain error, which could be eventually calibrated. A low-cost device was notably used as the device under test. On the other hand, the characterization of flickering icons demonstrated that the harmonic content of such stimuli can be meaningfully different from the nominal optical response. The considerations reported here for three representative smart glasses should be also extended to further stimuli generators, as these are crucial in studying how the human brain transduces sensory stimuli. As a whole, the characterization of the visual stimuli justified the exploitation of commercial smart glasses in the operation of a reactive brain-computer interface, but it also pointed out that their harmonic content should be carefully measured before addressing the brain response to flickering lights.

After these general chapters, Chapter 3 has proposed a wearable system based on steady-state visually evoked potentials. Such a reactive interface was built with a low-cost electroencephalograph employing a single differential channel and dry electrodes, integrated with commercial augmented reality glasses. Evoked potentials were detected by means of a processing algorithm based on power spectral density. An experimental campaign conducted with 20 subjects pointed out the trade-off between classification accuracy and stimulation time. The former quantifies the success rate in understanding which icon the user is staring at. The latter is directly related to the latency of the system in choosing an icon. The performance results

demonstrate that mean classification accuracy among subjects can be as high as 95 % at 10 s stimulation time. Though this accuracy value is compatible with current literature, such a value drops to about 75 % when a 2 s stimulation is considered, and it is unacceptably low at 1 s stimulation. Thus, further studies should involve the enhancement of classification accuracy at low stimulation times because the currently required times limit the applicability of the system. Despite that, some applications were considered as case studies, either in the industrial and healthcare fields.

As a last chapter, Chapter 4 has proposed a wearable system based on motor imagery, i.e. a voluntarily modulated spontaneous brain activity. In this regard, the selection of a minimum number of acquisition channels was first considered. The reduction approach relied on the well-known filter bank common spatial pattern algorithm for the classification of motor imagery-related activity. However, such an approach is typically adopted when more than eight electrodes are employed in acquiring sensorimotor brain activity. The results of the present study have firstly demonstrated that a single channel is not suitable for the detection of motor imagery, but the number of channels can be as low as three while keeping a classification performance compatible with the one associated with more electrodes. The exact channels to exploit do depend on the involved tasks and subjects and they can vary from session to session. Nonetheless, the locations of selected channels were compatible with the sensorimotor area reported in the scientific literature. Given this results, it was noted that the wearability and portability of such a system could be still achieved, though with a greater number of channels if compared to the reactive brain-computer interface. Moreover, after some preliminary tests, it was pointed out that conductive gel is needed to ensure proper contact with the scalp. Therefore, a commercial device with three bipolar channels and wet electrodes was exploited. Furthermore, neurofeedback was also considered to improve motor imagery detection by engaging the user during the task. Thus, the proposed design adds an extended reality multi-sensory feedback by means of a rolling ball on a screen and a haptic suit. Results of an experimental campaign conducted with eight subjects demonstrate that neurofeedback is effective in improving the detection of motor imagery for most subjects. Then, when considering all subjects together, the mean classification accuracy resulted higher when exploiting neurofeedback and compatible with 70 %, which is an empirical threshold for an acceptable performance of motor imagery brain-computer interfaces.

As a whole the work has demonstrated that reactive brain-computer interfaces are closer to daily-life applications. Indeed, the wearable and portable system discussed in this thesis mostly deserves an engineering phase. On the contrary, systems relying on motor imagery still need research and development, and the next step will probably involve a deeper study of neurofeedback as a means for enhancing the detection of these neurophysiological phenomena.

References

- [1] Hans Berger: dalla telepatia all'EEG. <https://cervelliacena.wordpress.com/2019/11/10/hans-berger-dalla-ricerca-della-telepatia-alla-nascita-delleeg/>. November 10, 2019.
- [2] George H Klem, Hans Otto Lüders, HH Jasper, C Elger, et al. The ten-twenty electrode system of the international federation. *Electroencephalogr Clin Neurophysiol*, 52(3):3–6, 1999.
- [3] Gareth James, Daniela Witten, Trevor Hastie, and Robert Tibshirani. *An introduction to statistical learning*, volume 112. Springer, 2013.
- [4] Texas Instruments. OPT101 Monolithic Photodiode and Single-Supply Transimpedance Amplifier (Rev. B). <https://www.ti.com/document-viewer/OPT101/datasheet/abstract#SBBS0022723>.
- [5] Pasquale Arpaia, Luigi Duraccio, Nicola Moccaldi, and Silvia Rossi. Wearable brain–computer interface instrumentation for robot-based rehabilitation by augmented reality. *IEEE Transactions on Instrumentation and Measurement*, 69(9):6362–6371, 2020.
- [6] Reinhold Scherer and Carmen Vidaurre. Chapter 8 - motor imagery based brain–computer interfaces. In Pablo Diez, editor, *Smart Wheelchairs and Brain-Computer Interfaces*, pages 171–195. Academic Press, 2018.
- [7] Pasquale Arpaia, Francesco Donnarumma, Antonio Esposito, and Marco Parvis. Channel Selection for Optimal EEG Measurement in Motor Imagery-Based Brain-Computer Interfaces. *International Journal of Neural Systems*, pages 2150003–2150003, 2020.
- [8] Jonathan R Wolpaw, Niels Birbaumer, Dennis J McFarland, Gert Pfurtscheller, and Theresa M Vaughan. Brain–computer interfaces for communication and control. *Clinical neurophysiology*, 113(6):767–791, 2002.
- [9] Thorsten O Zander and Christian Kothe. Towards passive brain–computer interfaces: applying brain–computer interface technology to human–machine systems in general. *Journal of neural engineering*, 8(2):025005, 2011.

- [10] Ke Lin, Andrea Cinetto, Yijun Wang, Xiaogang Chen, Shangkai Gao, and Xiaorong Gao. An online hybrid BCI system based on SSVEP and EMG. *Journal of neural engineering*, 13(2):026020, 2016.
- [11] Yuanqing Li, Jiahui Pan, Jinyi Long, Tianyou Yu, Fei Wang, Zhuliang Yu, and Wei Wu. Multimodal BCIs: target detection, multidimensional control, and awareness evaluation in patients with disorder of consciousness. *Proceedings of the IEEE*, 104(2):332–352, 2016.
- [12] Jonathan R Wolpaw, Niels Birbaumer, William J Heetderks, Dennis J McFarland, P Hunter Peckham, Gerwin Schalk, Emanuel Donchin, Louis A Quatrano, Charles J Robinson, and Theresa M Vaughan. Brain-computer interface technology: a review of the first international meeting. *IEEE transactions on rehabilitation engineering*, 8(2):164–173, 2000.
- [13] Gerwin Schalk, Dennis J McFarland, Thilo Hinterberger, Niels Birbaumer, and Jonathan R Wolpaw. BCI2000: a general-purpose brain-computer interface (BCI) system. *IEEE Transactions on biomedical engineering*, 51(6):1034–1043, 2004.
- [14] Minkyu Ahn, Mijin Lee, Jinyoung Choi, and Sung Chan Jun. A review of brain-computer interface games and an opinion survey from researchers, developers and users. *Sensors*, 14(8):14601–14633, 2014.
- [15] Brain-Computer Interfaces: the video game controller of the future. <https://www.factor-tech.com/feature/brain-computer-interfaces-the-video-game-controllers-of-the-future/>. February 27, 2017.
- [16] Benjamin Blankertz, Michael Tangermann, Carmen Vidaurre, Siamac Fazli, Claudia Sannelli, Stefan Haufe, Cecilia Maeder, Lenny E Ramsey, Irene Sturm, Gabriel Curio, et al. The Berlin brain-computer interface: non-medical uses of BCI technology. *Frontiers in neuroscience*, 4:198, 2010.
- [17] Luzheng Bi, Xin-An Fan, and Yili Liu. EEG-based brain-controlled mobile robots: a survey. *IEEE transactions on human-machine systems*, 43(2):161–176, 2013.
- [18] Clemens Brunner, Niels Birbaumer, Benjamin Blankertz, Christoph Guger, Andrea Kübler, Donatella Mattia, José del R Millán, Felip Miralles, Anton Nijholt, Eloy Opisso, et al. BNCI Horizon 2020: towards a roadmap for the BCI community. *Brain-computer interfaces*, 2(1):1–10, 2015.
- [19] Hans Berger. Über das elektrenkephalogramm des menschen. *Archiv für psychiatrie und nervenkrankheiten*, 87(1):527–570, 1929.
- [20] Elmer E Green, Alyce M Green, and E Dale Walters. Voluntary control of internal states: Psychological and physiological. *The Journal of Transpersonal Psychology*, 2(1):1, 1970.

- [21] David Rosenboom. Method for producing sounds or light flashes with alpha brain waves for artistic purposes. *Leonardo*, pages 141–145, 1972.
- [22] Jacques J Vidal. Toward direct brain-computer communication. *Annual review of Biophysics and Bioengineering*, 2(1):157–180, 1973.
- [23] Jacques J Vidal. Real-time detection of brain events in EEG. *Proceedings of the IEEE*, 65(5):633–641, 1977.
- [24] Theresa M Vaughan, WJ Heetderks, LJ Trejo, WZ Rymer, M Weinrich, MM Moore, A Kübler, BH Dobkin, N Birbaumer, E Donchin, et al. Brain-computer interface technology: a review of the second international meeting., 2003.
- [25] Ujwal Chaudhary, Bin Xia, Stefano Silvoni, Leonardo G Cohen, and Niels Birbaumer. Brain-computer interface-based communication in the completely locked-in state. *PLoS biology*, 15(1):e1002593, 2017.
- [26] Manuel Gomez-Rodriguez, Jan Peters, J Hill, Bernhard Schölkopf, Alireza Gharabaghi, and Moritz Grosse-Wentrup. Closing the sensorimotor loop: haptic feedback facilitates decoding of motor imagery. *Journal of neural engineering*, 8(3):036005, 2011.
- [27] Ana RC Donati, Solaiman Shokur, Edgard Morya, Debora SF Campos, Renan C Moiola, Claudia M Gitti, Patricia B Augusto, Sandra Tripodi, Cristhiane G Pires, Gislaine A Pereira, et al. Long-term training with a brain-machine interface-based gait protocol induces partial neurological recovery in paraplegic patients. *Scientific reports*, 6:30383, 2016.
- [28] Bojan Kerous, Filip Skola, and Fotis Liarokapis. EEG-based BCI and video games: a progress report. *Virtual Reality*, 22(2):119–135, 2018.
- [29] Yu-Te Wang, Yijun Wang, and Tzyy-Ping Jung. A cell-phone-based brain-computer interface for communication in daily life. *Journal of neural engineering*, 8(2):025018, 2011.
- [30] Fabien Lotte, Laurent Bougrain, Andrzej Cichocki, Maureen Clerc, Marco Congedo, Alain Rakotomamonjy, and Florian Yger. A review of classification algorithms for EEG-based brain-computer interfaces: a 10 year update. *Journal of neural engineering*, 15(3):031005, 2018.
- [31] Yi-Hsin Yu, Shao-Wei Lu, Chun-Hsiang Chuang, Jung-Tai King, Che-Lun Chang, Shi-An Chen, Sheng-Fu Chen, and Chin-Teng Lin. An inflatable and wearable wireless system for making 32-channel electroencephalogram measurements. *IEEE Transactions on Neural Systems and Rehabilitation Engineering*, 24(7):806–813, 2016.
- [32] Reza Abiri, Soheil Borhani, Eric W Sellers, Yang Jiang, and Xiaopeng Zhao. A comprehensive review of EEG-based brain-computer interface paradigms. *Journal of neural engineering*, 16(1):011001, 2019.

- [33] Peng Yuan, Xiaorong Gao, Brendan Allison, Yijun Wang, Guangyu Bin, and Shangkai Gao. A study of the existing problems of estimating the information transfer rate in online brain–computer interfaces. *Journal of neural engineering*, 10(2):026014, 2013.
- [34] Bci competitions - berlin brain-computer interface. <http://www.bbci.de/competition/>. 2000 - 2008.
- [35] Cybathlon 2020 global edition. <https://cybathlon.ethz.ch/en>. November 13-14, 2020.
- [36] Sarah N Abdulkader, Ayman Atia, and Mostafa-Sami M Mostafa. Brain computer interfacing: Applications and challenges. *Egyptian Informatics Journal*, 16(2):213–230, 2015.
- [37] Olivier David, James M Kilner, and Karl J Friston. Mechanisms of evoked and induced responses in MEG/EEG. *Neuroimage*, 31(4):1580–1591, 2006.
- [38] Thorsten O Zander, Christian Kothe, Sabine Jatzev, and Matti Gaertner. Enhancing human-computer interaction with input from active and passive brain-computer interfaces. In *Brain-computer interfaces*, pages 181–199. Springer, 2010.
- [39] Anupama A Ghodake and SD Shelke. Brain controlled home automation system. In *Intelligent Systems and Control (ISCO), 2016 10th International Conference on*, pages 1–4. IEEE, 2016.
- [40] Brendan Z Allison, Dennis J McFarland, Gerwin Schalk, Shi Dong Zheng, Melody Moore Jackson, and Jonathan R Wolpaw. Towards an independent brain–computer interface using steady state visual evoked potentials. *Clinical neurophysiology*, 119(2):399–408, 2008.
- [41] Rabie A Ramadan and Athanasios V Vasilakos. Brain computer interface: control signals review. *Neurocomputing*, 223:26–44, 2017.
- [42] Desney Tan and Anton Nijholt. Brain-computer interfaces and human-computer interaction. In *Brain-Computer Interfaces*, pages 3–19. Springer, 2010.
- [43] Michal Teplan et al. Fundamentals of EEG measurement. *Measurement science review*, 2(2):1–11, 2002.
- [44] Hermann Hinrichs, Michael Scholz, Anne Katrin Baum, Julia WY Kam, Robert T Knight, and Hans-Jochen Heinze. Comparison between a wireless dry electrode EEG system with a conventional wired wet electrode EEG system for clinical applications. *Scientific Reports*, 10(1):1–14, 2020.
- [45] Mehrdad Fatourechi, Ali Bashashati, Rabab K Ward, and Gary E Birch. Emg and eog artifacts in brain computer interface systems: A survey. *Clinical neurophysiology*, 118(3):480–494, 2007.

- [46] Sylvain Arlot, Alain Celisse, et al. A survey of cross-validation procedures for model selection. *Statistics surveys*, 4:40–79, 2010.
- [47] TD Sunny, T Aparna, P Neethu, J Venkateswaran, V Vishnupriya, and PS Vyas. Robotic arm with brain–computer interfacing. *Procedia Technology*, 24:1089–1096, 2016.
- [48] Inaki Iturrate, Javier M Antelis, Andrea Kubler, and Javier Minguez. A noninvasive brain-actuated wheelchair based on a p300 neurophysiological protocol and automated navigation. *IEEE transactions on robotics*, 25(3):614–627, 2009.
- [49] Leopoldo Angrisani, Pasquale Arpaia, Antonio Esposito, and Nicola Moccaldi. A wearable brain–computer interface instrument for augmented reality-based inspection in industry 4.0. *IEEE Transactions on Instrumentation and Measurement*, 69(4):1530–1539, 2019.
- [50] Robert Leeb, Felix Lee, Claudia Keinrath, Reinhold Scherer, Horst Bischof, and Gert Pfurtscheller. Brain–computer communication: motivation, aim, and impact of exploring a virtual apartment. *IEEE Transactions on Neural Systems and Rehabilitation Engineering*, 15(4):473–482, 2007.
- [51] Meng Wang, Renjie Li, Ruofan Zhang, Guangye Li, and Dingguo Zhang. A wearable SSVEP-based BCI system for quadcopter control using head-mounted device. *IEEE Access*, 6:26789–26798, 2018.
- [52] Open Source Brain-Computer Interfaces. <https://openbci.com/>.
- [53] Thea Radüntz. Signal quality evaluation of emerging EEG devices. *Frontiers in physiology*, 9:98, 2018.
- [54] Nima Bigdely-Shamlo, Scott Makeig, and Kay A Robbins. Preparing laboratory and real-world EEG data for large-scale analysis: a containerized approach. *Frontiers in neuroinformatics*, 10:7, 2016.
- [55] Vinay Jayaram and Alexandre Barachant. MOABB: trustworthy algorithm benchmarking for BCIs. *Journal of neural engineering*, 15(6):066011, 2018.
- [56] Marcello Ienca, Pim Haselager, and Ezekiel J Emanuel. Brain leaks and consumer neurotechnology. *Nature biotechnology*, 36(9):805–810, 2018.
- [57] Olimex Ltd. Schematics of the EEG-SMT device for electroencephalography. <https://www.olimex.com/Products/EEG/OpenEEG/EEG-SMT/resources/EEG-SMT-SCHEMATIC-REV-B.pdf>.
- [58] Ab-medica s.p.a. <https://www.abmedica.it/>.
- [59] Neuroconcise ltd. <https://www.neuroconcise.co.uk/>.

- [60] Leopoldo Angrisani, Pasquale Arpaia, Deborah Casinelli, and Nicola Moccaldi. A single-channel ssvep-based instrument with off-the-shelf components for trainingless brain-computer interfaces. *IEEE Transactions on Instrumentation and Measurement*, 2018.
- [61] Yijun Wang, Xiaorong Gao, Bo Hong, Chuan Jia, and Shangkai Gao. Brain-computer interfaces based on visual evoked potentials. *IEEE Engineering in medicine and biology magazine*, 27(5):64–71, 2008.
- [62] Kai Keng Ang, Zheng Yang Chin, Chuanchu Wang, Cuntai Guan, and Haihong Zhang. Filter bank common spatial pattern algorithm on BCI competition IV datasets 2a and 2b. *Frontiers in neuroscience*, 6:39, 2012.
- [63] Hakim Si-Mohammed, Jimmy Petit, Camille Jeunet, Ferran Argelaguet, Fabien Spindler, And  ol   vain, Nicolas Roussel, G  ry Casiez, and Anatole L  cuyer. Towards BCI-based Interfaces for Augmented Reality: Feasibility, Design and Evaluation. *IEEE transactions on visualization and computer graphics*, 2018.
- [64] Nicholas A Badcock, Kathryn A Preece, Bianca de Wit, Katharine Glenn, Nora Fieder, Johnson Thie, and Genevieve McArthur. Validation of the Emotiv EPOC EEG system for research quality auditory event-related potentials in children. *PeerJ*, 3:e907, 2015.
- [65] Jeffrey M Rogers, Stuart J Johnstone, Anna Aminov, James Donnelly, and Peter H Wilson. Test-retest reliability of a single-channel, wireless EEG system. *International Journal of Psychophysiology*, 106:87–96, 2016.
- [66] Wlodzimierz Klonowski. Everything you wanted to ask about EEG but were afraid to get the right answer. *Nonlinear biomedical physics*, 3(1):1–5, 2009.
- [67] Guangli Li, Sizhe Wang, and Yanwen Y Duan. Towards gel-free electrodes: A systematic study of electrode-skin impedance. *Sensors and Actuators B: Chemical*, 241:1244–1255, 2017.
- [68] Leonardo Casal and Guillermo La Mura. Skin-electrode impedance measurement during ECG acquisition: method’s validation. In *Journal of Physics: Conference Series*, volume 705, page 012006. IOP Publishing, 2016.
- [69] Zhichun Zhao, Kamen Ivanov, Ludwig Lubich, Olatunji Mumini Omisore, Zhanyong Mei, Nan Fu, Jinying Chen, and Lei Wang. Signal Quality and Electrode-Skin Impedance Evaluation in the Context of Wearable Electroencephalographic Systems. In *2018 40th Annual International Conference of the IEEE Engineering in Medicine and Biology Society (EMBC)*, pages 4965–4968. IEEE, 2018.
- [70] Fanny Grosselin, Xavier Navarro-Sune, Alessia Vozzi, Katerina Pandremenou, Fabrizio De Vico Fallani, Yohan Attal, and Mario Chavez. Quality assessment of single-channel EEG for wearable devices. *Sensors*, 19(3):601, 2019.

- [71] Bin Hu, Hong Peng, Qinglin Zhao, Bo Hu, Dennis Majoe, Fang Zheng, and Philip Moore. Signal quality assessment model for wearable EEG sensor on prediction of mental stress. *IEEE transactions on nanobioscience*, 14(5):553–561, 2015.
- [72] Mridu Sahu, Samrudhi Mohdiwale, Namrata Khorriya, Yogita Upadhyay, Anjali Verma, and Shikha Singh. EEG Artifact Removal Techniques: A Comparative Study. In *International Conference on Innovative Computing and Communications*, pages 395–403. Springer, 2020.
- [73] Sarah Blum, Nadine SJ Jacobsen, Martin G Bleichner, and Stefan Debener. A Riemannian modification of artifact subspace reconstruction for EEG artifact handling. *Frontiers in human neuroscience*, 13:141, 2019.
- [74] Saurabh R Sinha, Lucy R Sullivan, Dragos Sabau, Daniel San Juan Orta, Keith E Dombrowski, Jonathan J Halford, Abeer J Hani, Frank W Drislane, and Mark M Stecker. American clinical neurophysiology society guideline 1: minimum technical requirements for performing clinical electroencephalography. *The Neurodiagnostic Journal*, 56(4):235–244, 2016.
- [75] Maciej Labecki, Rafal Kus, Alicja Brzozowska, Tadeusz Stacewicz, Basab-datta S Bhattacharya, and Piotr Suffczynski. Nonlinear origin of ssvep spectra—a combined experimental and modeling study. *Frontiers in computational neuroscience*, 10:129, 2016.
- [76] IEEE Standards Association. Neurotechnologies for Brain-Machine Interfacing. <https://standards.ieee.org/industry-connections/neurotechnologies-for-brain-machine-interfacing.html>.
- [77] Alessandro Cultrera, David Corminboeuf, Vincenzo D’Elia, Ngoc Thanh Mai Tran, Luca Callegaro, and Massimo Ortolano. A new calibration setup for lock-in amplifiers in the low frequency range and its validation in a bilateral comparison. *Metrologia*, 2021.
- [78] IEEE Standards Association. IEEE 1057-2017 - IEEE Standard for Digitizing Waveform Recorders. <https://standards.ieee.org/standard/1057-2017.html>.
- [79] Marko Neitola. Four-Parameter Sinefit. <https://it.mathworks.com/matlabcentral/fileexchange/23214-four-parameter-sinefit>, 2021.
- [80] Peter Händel. Amplitude estimation using IEEE-STD-1057 three-parameter sine wave fit: Statistical distribution, bias and variance. *Measurement*, 43(6):766–770, 2010.
- [81] Joint Committee for Guides in Metrology (JCGM) - BIPM. Evaluation of measurement data — Guide to the expression of uncertainty in measurement. https://www.bipm.org/documents/20126/2071204/JCGM_100_2008_E.pdf/cb0ef43f-baa5-11cf-3f85-4dcd86f77bd6, 2008.

- [82] Dimitris Chatzopoulos, Carlos Bermejo, Zhanpeng Huang, and Pan Hui. Mobile augmented reality survey: From where we are to where we go. *Ieee Access*, 5:6917–6950, 2017.
- [83] Jens Grubert, Yuta Itoh, Kenneth Moser, and J Edward Swan. A survey of calibration methods for optical see-through head-mounted displays. *IEEE transactions on visualization and computer graphics*, 24(9):2649–2662, 2017.
- [84] Martin Klemm, Fabian Seebacher, and Harald Hoppe. High accuracy pixel-wise spatial calibration of optical see-through glasses. *Computers & Graphics*, 64:51–61, 2017.
- [85] Xincan Zhao, Chenyang Liu, Zongxin Xu, Lipeng Zhang, and Rui Zhang. Ssvep stimulus layout effect on accuracy of brain-computer interfaces in augmented reality glasses. *IEEE Access*, 8:5990–5998, 2020.
- [86] Volkan Çetin, Serhat Ozekes, and Hüseyin Selçuk Varol. Harmonic analysis of steady-state visual evoked potentials in brain computer interfaces. *Biomedical Signal Processing and Control*, 60:101999, 2020.
- [87] Martin Spüler. A high-speed brain-computer interface (BCI) using dry EEG electrodes. *PloS one*, 12(2):e0172400, 2017.
- [88] Anna Chabuda, Piotr Durka, and Jarosław Żygierewicz. High frequency SSVEP-BCI with hardware stimuli control and phase-synchronized comb filter. *IEEE Transactions on neural systems and rehabilitation engineering*, 26(2):344–352, 2017.
- [89] NJ Hill and Bernhard Schölkopf. An online brain–computer interface based on shifting attention to concurrent streams of auditory stimuli. *Journal of neural engineering*, 9(2):026011, 2012.
- [90] Christian Breitwieser, Vera Kaiser, Christa Neuper, and Gernot R Müller-Putz. Stability and distribution of steady-state somatosensory evoked potentials elicited by vibro-tactile stimulation. *Medical & biological engineering & computing*, 50(4):347–357, 2012.
- [91] Guangyu Bin, Xiaorong Gao, Yijun Wang, Bo Hong, and Shangkai Gao. Vep-based brain-computer interfaces: time, frequency, and code modulations [research frontier]. *IEEE Computational Intelligence Magazine*, 4(4):22–26, 2009.
- [92] Saba Ajami, Amin Mahnam, and Vahid Abootalebi. Development of a practical high frequency brain–computer interface based on steady-state visual evoked potentials using a single channel of EEG. *Biocybernetics and Biomedical Engineering*, 38(1):106–114, 2018.
- [93] Hubert Cecotti. A self-paced and calibration-less ssvep-based brain–computer interface speller. *IEEE transactions on neural systems and rehabilitation engineering*, 18(2):127–133, 2010.

- [94] Ming Cheng, Xiaorong Gao, Shangkai Gao, and Dingfeng Xu. Design and implementation of a brain-computer interface with high transfer rates. *IEEE transactions on biomedical engineering*, 49(10):1181–1186, 2002.
- [95] Yijun Wang, Ruiping Wang, Xiaorong Gao, Bo Hong, and Shangkai Gao. A practical vep-based brain-computer interface. *IEEE Transactions on neural systems and rehabilitation engineering*, 14(2):234–240, 2006.
- [96] Ivan Volosyak, Felix Gemblar, and Piotr Stawicki. Age-related differences in SSVEP-based BCI performance. *Neurocomputing*, 250:57–64, 2017.
- [97] Damien Lesenfants, Dina Habbal, Z Lugo, M Lebeau, Petar Horki, E Amico, Christoph Pokorny, F Gomez, A Soddu, Gernot Müller-Putz, et al. An independent ssvep-based brain–computer interface in locked-in syndrome. *Journal of neural engineering*, 11(3):035002, 2014.
- [98] Luis Fernando Nicolas-Alonso and Jaime Gomez-Gil. Brain computer interfaces, a review. *sensors*, 12(2):1211–1279, 2012.
- [99] Hakim Si-Mohammed, Ferran Argelaguet Sanz, Géry Casiez, Nicolas Roussel, and Anatole Lécuyer. Brain-computer interfaces and augmented reality: A state of the art. In *Graz Brain-Computer Interface Conference*, 2017.
- [100] Vojkan Mihajlović, Bernard Grundlehner, Ruud Vullers, and Julien Penders. Wearable, wireless EEG solutions in daily life applications: what are we missing? *IEEE journal of biomedical and health informatics*, 19(1):6–21, 2014.
- [101] Jesus Minguillon, M Angel Lopez-Gordo, and Francisco Pelayo. Trends in EEG-BCI for daily-life: Requirements for artifact removal. *Biomedical Signal Processing and Control*, 31:407–418, 2017.
- [102] Trung-Hau Nguyen and Wan-Young Chung. A Single-Channel SSVEP-Based BCI Speller Using Deep Learning. *IEEE Access*, 7:1752–1763, 2019.
- [103] Piotr Stawicki, Felix Gemblar, Aya Rezeika, and Ivan Volosyak. A novel hybrid mental spelling application based on eye tracking and SSVEP-based BCI. *Brain sciences*, 7(4):35, 2017.
- [104] Xiao Xing, Yijun Wang, Weihua Pei, Xuhong Guo, Zhiduo Liu, Fei Wang, Gege Ming, Hongze Zhao, Qiang Gui, and Hongda Chen. A high-speed SSVEP-based BCI using dry EEG electrodes. *Scientific reports*, 8(1):1–10, 2018.
- [105] An Luo and Thomas J Sullivan. A user-friendly ssvep-based brain–computer interface using a time-domain classifier. *Journal of neural engineering*, 7(2):026010, 2010.
- [106] Chi-Chun Lo, Tsung-Yi Chien, Jeng-Shyang Pan, and Bor-Shyh Lin. Novel non-contact control system for medical healthcare of disabled patients. *IEEE Access*, 4:5687–5694, 2016.

- [107] Michael Rüßmann, Markus Lorenz, Philipp Gerbert, Manuela Waldner, Jan Justus, Pascal Engel, and Michael Harnisch. Industry 4.0: The future of productivity and growth in manufacturing industries. *Boston Consulting Group*, 9, 2015.
- [108] Qing Gao, Xujun Duan, and Huaifu Chen. Evaluation of effective connectivity of motor areas during motor imagery and execution using conditional granger causality. *Neuroimage*, 54(2):1280–1288, 2011.
- [109] Ulrike Halsband and Regine K Lange. Motor learning in man: a review of functional and clinical studies. *Journal of Physiology-Paris*, 99(4-6):414–424, 2006.
- [110] Ou Bai, Dandan Huang, Ding-Yu Fei, and Richard Kunz. Effect of real-time cortical feedback in motor imagery-based mental practice training. *NeuroRehabilitation*, 34(2):355–363, 2014.
- [111] Gert Pfurtscheller and FH Lopes Da Silva. Event-related EEG/MEG synchronization and desynchronization: basic principles. *Clinical neurophysiology*, 110(11):1842–1857, 1999.
- [112] Niraj Bagh and M Ramasubba Reddy. Hilbert transform-based event-related patterns for motor imagery brain computer interface. *Biomedical Signal Processing and Control*, 62:102020, 2020.
- [113] D Thiyam and E Rajkumar. Common Spatial Pattern Algorithm Based Signal Processing Techniques for Classification of Motor Imagery Movements: A Mini Review. *IJCTA*, 9(36):53–65, 2016.
- [114] Johannes Müller-Gerking, Gert Pfurtscheller, and Henrik Flyvbjerg. Designing optimal spatial filters for single-trial EEG classification in a movement task. *Clinical neurophysiology*, 110(5):787–798, 1999.
- [115] Clemens Brunner, R Leeb, G Müller-Putz, A Schlögl, and G Pfurtscheller. BCI Competition 2008–Graz data set A. *Institute for Knowledge Discovery (Laboratory of Brain-Computer Interfaces), Graz University of Technology*, 16:1–6, 2008.
- [116] Berlin Brain Computer Interface (BBCI). Dataset IIIa: 4-class EEG data. http://www.bbc.de/competition/iii/desc_IIIa.pdf, 2006.
- [117] R Leeb, C Brunner, G Müller-Putz, A Schlögl, and G Pfurtscheller. BCI Competition 2008–Graz data set B. *Graz University of Technology, Austria*, pages 1–6, 2008.
- [118] Alois Schlogl, Julien Kronegg, J Huggins, and S Mason. 19 evaluation criteria for BCI research. *Toward brain-computer interfacing*, page 327, 2007.
- [119] Muhammad Zeeshan Baig, Nauman Aslam, and Hubert PH Shum. Filtering techniques for channel selection in motor imagery EEG applications: a survey. *Artificial intelligence review*, 53:1207–1232, 2020.

- [120] Sheng Ge, Ruimin Wang, and Dongchuan Yu. Classification of four-class motor imagery employing single-channel electroencephalography. *PloS one*, 9(6):e98019, 2014.
- [121] Luca Faes, Giandomenico Nollo, and Alberto Porta. Information-based detection of nonlinear Granger causality in multivariate processes via a nonuniform embedding technique. *Physical Review E*, 83(5):051112, 2011.
- [122] Douglas C Montgomery and George C Runger. *Applied statistics and probability for engineers*. John Wiley & Sons, 2010.
- [123] Alireza Ghaemi, Esmat Rashedi, Ali Mohammad Pourrahimi, Mehdi Kamandar, and Farhad Rahdari. Automatic channel selection in EEG signals for classification of left or right hand movement in Brain Computer Interfaces using improved binary gravitation search algorithm. *Biomedical Signal Processing and Control*, 33:109–118, 2017.
- [124] Praveen K Parashiva and AP Vinod. A New Channel Selection Method using Autoencoder for Motor Imagery based Brain Computer Interface. In *2019 IEEE International Conference on Systems, Man and Cybernetics (SMC)*, pages 3641–3646. IEEE, 2019.
- [125] Jing Jin, Yangyang Miao, Ian Daly, Cili Zuo, Dewen Hu, and Andrzej Cichocki. Correlation-based channel selection and regularized feature optimization for MI-based BCI. *Neural Networks*, 118:262–270, 2019.
- [126] H Henrik Ehrsson, Stefan Geyer, and Eiichi Naito. Imagery of voluntary movement of fingers, toes, and tongue activates corresponding body-part-specific motor representations. *Journal of neurophysiology*, 90(5):3304–3316, 2003.
- [127] Alyssa M Batula, Jesse A Mark, Youngmoo E Kim, and Hasan Ayaz. Comparison of brain activation during motor imagery and motor movement using fNIRS. *Computational intelligence and neuroscience*, 2017, 2017.
- [128] Camille Jeunet, Chi Vi, Daniel Spelmezan, Bernard N’Kaoua, Fabien Lotte, and Sriram Subramanian. Continuous tactile feedback for motor-imagery based brain-computer interaction in a multitasking context. In *IFIP Conference on Human-Computer Interaction*, pages 488–505. Springer, 2015.
- [129] Jonathan R Wolpaw, Dennis J McFarland, Gregory W Neat, and Catherine A Forneris. An EEG-based brain-computer interface for cursor control. *Electroencephalography and clinical neurophysiology*, 78(3):252–259, 1991.
- [130] Niels Birbaumer, Nimr Ghanayim, Thilo Hinterberger, Iver Iversen, Boris Kotchoubey, Andrea Kübler, Juri Perelmouter, Edward Taub, and Herta Flor. A spelling device for the paralysed. *Nature*, 398(6725):297–298, 1999.

- [131] Sangkyun Lee, Sergio Ruiz, Andrea Caria, Ralf Veit, Niels Birbaumer, and Ranganatha Sitaram. Detection of cerebral reorganization induced by real-time fmri feedback training of insula activation: a multivariate investigation. *Neurorehabilitation and neural repair*, 25(3):259–267, 2011.
- [132] Eltaf Abdalsalam, Mohd Zuki Yusoff, Aamir Malik, Nidal S Kamel, and Dalia Mahmoud. Modulation of sensorimotor rhythms for brain-computer interface using motor imagery with online feedback. *Signal, Image and Video Processing*, 12(3):557–564, 2018.
- [133] Christa Neuper, Reinhold Scherer, Selina Wriessnegger, and Gert Pfurtscheller. Motor imagery and action observation: modulation of sensorimotor brain rhythms during mental control of a brain–computer interface. *Clinical neurophysiology*, 120(2):239–247, 2009.
- [134] Takashi Ono, Akio Kimura, and Junichi Ushiba. Daily training with realistic visual feedback improves reproducibility of event-related desynchronisation following hand motor imagery. *Clinical Neurophysiology*, 124(9):1779–1786, 2013.
- [135] Athanasios Vourvopoulos, André Ferreira, and Sergi Bermudez i Badia. Neuro: an immersive vr environment for motor-imagery training with the use of brain-computer interfaces and vibrotactile feedback. In *International Conference on Physiological Computing Systems*, volume 2, pages 43–53. SCITEPRESS, 2016.
- [136] Karl A McCreddie, Damien H Coyle, and Girijesh Prasad. Is sensorimotor BCI performance influenced differently by mono, stereo, or 3-D auditory feedback? *IEEE Transactions on Neural Systems and Rehabilitation Engineering*, 22(3):431–440, 2014.
- [137] Thilo Hinterberger, Nicola Neumann, Mirko Pham, Andrea Kübler, Anke Grether, Nadine Hofmayer, Barbara Wilhelm, Herta Flor, and Niels Birbaumer. A multimodal brain-based feedback and communication system. *Experimental brain research*, 154(4):521–526, 2004.
- [138] Timothy R Coles, Nigel W John, Derek Gould, and Darwin G Caldwell. Integrating haptics with augmented reality in a femoral palpation and needle insertion training simulation. *IEEE transactions on haptics*, 4(3):199–209, 2011.
- [139] Seokhee Jeon and Seungmoon Choi. Haptic augmented reality: Taxonomy and an example of stiffness modulation. *Presence: Teleoperators and Virtual Environments*, 18(5):387–408, 2009.
- [140] Zhongpeng Wang, Yijie Zhou, Long Chen, Bin Gu, Shuang Liu, Minpeng Xu, Hongzhi Qi, Feng He, and Dong Ming. A BCI based visual-haptic neuro-feedback training improves cortical activations and classification performance during motor imagery. *Journal of neural engineering*, 16(6):066012, 2019.

- [141] Alexandre Gramfort, Martin Luessi, Eric Larson, Denis A. Engemann, Daniel Strohmeier, Christian Brodbeck, Roman Goj, Mainak Jas, Teon Brooks, Lauri Parkkonen, and Matti S. Hämäläinen. MEG and EEG data analysis with MNE-Python. *Frontiers in Neuroscience*, 7(267):1–13, 2013.
- [142] Bernhard Graimann, Jane E Huggins, Simon P Levine, and Gert Pfurtscheller. Visualization of significant ERD/ERS patterns in multichannel EEG and ECoG data. *Clinical neurophysiology*, 113(1):43–47, 2002.
- [143] bHaptics Inc. Tactsuit with forty vibration motors. <https://www.bhaptics.com/tactsuit/tactsuit-x40>.
- [144] Hohyun Cho, Minkyu Ahn, Sangtae Ahn, Moonyoung Kwon, and Sung Chan Jun. EEG datasets for motor imagery brain–computer interface. *GigaScience*, 6(7):gix034, 2017.
- [145] Stefano Federici and Marcia Scherer. *Assistive technology assessment handbook*. CRC Press, 2012.
- [146] Jaakko Malmivuo, Robert Plonsey, et al. *Bioelectromagnetism: principles and applications of bioelectric and biomagnetic fields*. Oxford University Press, USA, 1995.
- [147] Simon Musall, Veronika von Pförtl, Alexander Rauch, Nikos K Logothetis, and Kevin Whittingstall. Effects of neural synchrony on surface EEG. *Cerebral Cortex*, 24(4):1045–1053, 2014.
- [148] Sylvain Baillet, John C Mosher, and Richard M Leahy. Electromagnetic brain mapping. *IEEE Signal processing magazine*, 18(6):14–30, 2001.
- [149] David I Hoult and Balram Bhakar. Nmr signal reception: Virtual photons and coherent spontaneous emission. *Concepts in Magnetic Resonance: An Educational Journal*, 9(5):277–297, 1997.
- [150] Anton Nijholt, Desney Tan, Gert Pfurtscheller, Clemens Brunner, José del R Millán, Brendan Allison, Bernhard Graimann, Florin Popescu, Benjamin Blankertz, and Klaus-R Müller. Brain-computer interfacing for intelligent systems. *IEEE intelligent systems*, 23(3):72–79, 2008.
- [151] N Jeremy Hill, Thomas Navin Lal, Michael Schröder, Thilo Hinterberger, Guido Widman, Christian E Elger, Bernhard Schölkopf, and Niels Birbaumer. Classifying event-related desynchronization in EEG, ECoG and MEG signals. In *Joint Pattern Recognition Symposium*, pages 404–413. Springer, 2006.
- [152] D Puthankattil Subha, Paul K Joseph, Rajendra Acharya, and Choo Min Lim. EEG signal analysis: a survey. *Journal of medical systems*, 34(2):195–212, 2010.
- [153] Gert Pfurtscheller, Karin Pichler-Zalaudek, Britta Ortmayr, Josef Diez, et al. Postmovement beta synchronization in patients with parkinson’s disease. *Journal of clinical neurophysiology*, 15(3):243–250, 1998.

-
- [154] Benjamin Blankertz, Gabriel Curio, and Klaus-Robert Müller. Classifying single trial EEG: Towards brain computer interfacing. *Advances in neural information processing systems*, 14:157–164, 2001.
- [155] Satyajit Sen Purkayastha, VK Jain, and HK Sardana. Topical review: A review of various techniques used for measuring brain activity in brain computer interfaces. *Advance in Electronic and Electric Engineering*, 4:513–522, 2014.
- [156] Dean J Krusienski, Eric W Sellers, Dennis J McFarland, Theresa M Vaughan, and Jonathan R Wolpaw. Toward enhanced p300 speller performance. *Journal of neuroscience methods*, 167(1):15–21, 2008.
- [157] Gert Pfurtscheller and Christa Neuper. Motor imagery and direct brain-computer communication. *Proceedings of the IEEE*, 89(7):1123–1134, 2001.
- [158] Gert Pfurtscheller and Christa Neuper. Motor imagery activates primary sensorimotor area in humans. *Neuroscience letters*, 239(2-3):65–68, 1997.
- [159] Christoph Guger, Herbert Ramoser, and Gert Pfurtscheller. Real-time EEG analysis with subject-specific spatial patterns for a brain-computer interface (BCI). *IEEE transactions on rehabilitation engineering*, 8(4):447–456, 2000.

Appendix A

Measuring brain activity

The current Appendix furtherly discusses how brain activity can be measured, either in terms of neuroimaging techniques and measurand signals of interest. Indeed, the most relevant aspects are already treated in the chapters of this thesis to carry on a consistent discussion. Nonetheless, the interested reader can find more details hereafter.

A.1 Measurement techniques

The core of a BCI system is the acquisition and processing of brain signals. The choice of a proper approach for signal processing largely depends on the brain signals to analyze, and most of BCI literature has been focusing on algorithms of varying complexity for the analysis of specific brain activities [30]. Hence, it is of foremost importance to select a proper signal acquisition method in accordance with the requirements. In line with our current understanding of the human brain, the measurand brain activity is related to neurons, hundreds of billion nerve cells that communicate by means of electrical signals or chemical reactions. Typically, the activity of an entire brain area is measured, thus meaning that the average activity of a great number of neurons is considered at once. Each area is specialized for particular tasks, but concurrent tasks can be processed by the same area and many tasks are processed in multiple areas. Advancing technology and more deep brain function understanding allow to decipher with ever greater resolution the ongoing brain activity, but it is not (yet) possible to “read thoughts” [42]. Nowadays, one can

only measure general processes, and several challenges are posed by intra-subject and inter-subject variability in brain functionality.

The most common techniques for brain activity measurement are briefly described in the following. The aim is to help the reader understand the main advantages and disadvantages of each technique, and also to justify our focus on electroencephalography. Interestingly, multiple measurement techniques could also be used at once in order to improve BCI system performance [11].

A.1.1 Electroencephalography

Electroencephalography (EEG) is a technique used to record the electrical activity of the human brain by means of electrodes placed on the scalp [43]. The term 'EEG' typically refers to a non-invasive technique. The measurement setup is simple and safe. However, the electrical potentials detected with this technique must cross the tissues interposed between the scalp and the brain to reach the electrodes. Consequently, there is a considerable attenuation and the detection reliability decreases. Instead, in an electrocorticography (ECoG) the electrodes would be surgically positioned on the cerebral cortex, or they could be even implanted inside the cortex in intracortical techniques or electrograms. This would guarantee greater temporal and spatial resolution, as well as greater signal-to-noise ratios if compared to an EEG [36]. Usually, an EEG acquisition system is inexpensive, highly portable, and wearable. Clearly, this also depends on the number of electrodes, which can be more than one hundred. Electroencephalography guarantees a temporal resolution equal to 10 ms and 1 cm spatial resolution [42, 145]. Electrical signal amplitudes vary from $5 \mu\text{V}$ to $100 \mu\text{V}$ for EEG, while these signal amplitudes would reach 1 mV to 2 mV if the electrodes were implanted in the skull [146]. The signal bandwidth of usual interest spans the 0.1 Hz to 100 Hz range, and the amplitude decreases with increasing frequency. Recent studies also support the idea that EEG amplitudes correlate with the degree of neuron synchronization [147]. On the other side, EEG alone cannot detect brain area activation occurring in deeper regions. In this regard, techniques like fMRI and MEG can be employed.

A.1.2 Magnetoencephalography

Magnetoencephalography (MEG) is a technique allowing the detection of magnetic fields generated by the neurons' electrical activity. This technique guarantees deeper imaging if compared to the EEG, with a greater spatial resolution (about 1 mm) and a similar temporal resolution (1 ms to 10 ms) because the skull is almost completely transparent to magnetic fields [42, 145]. However, it is an expensive and not portable technology because it requires big magnets, and/or superconductivity, e.g. in superconducting quantum interference device [36]. Furthermore, MEG equipment can interfere with other instrumentation or suffer from electromagnetic interference. Therefore, MEG seems not very suitable for applications in every-day life. Nonetheless, magnetoencephalography is seen as complementary to EEG: a synergically employment of both techniques can provide important information about the dynamics of brain functions [148].

A.1.3 Functional magnetic resonance imaging

Magnetic resonance imaging (MRI) exploits nuclear magnetic resonance to reconstruct an image of a physiological process. A strong magnetic field is generated to make atoms absorb and release energy at radio frequency. In particular, hydrogen atoms are usually involved, which are abundant in water and fat. By localizing the signals emitted from the atoms, it is thus possible to obtain an image [149]. There are also other imaging techniques such as computed tomography scan (CT) or positron emission tomography (PET), but despite them MRI does not use X-rays or ionizing radiation. Functional Magnetic Resonance Imaging (fMRI) exploits the basic principles of MRI to detect changes in blood flow through changing blood magnetic properties, which are related to neural activity in the brain. Indeed, neurons need more oxygen and glucose when they communicate, thus causing an increase in blood flow to active regions of the brain [42]. fMRI is expensive and not portable because it requires cumbersome instrumentation, such as superconductive magnets [42, 145]. It provides data with high spatial resolution (even below 1 mm) but with a poor temporal resolution (few seconds) [145] due to the slow changes in blood flow. An hybrid system could, for instance, employ fMRI in conjunction with EEG or MEG to achieve both high temporal and spatial resolution [148]. Obviously, this

would require a proper fusion of the two measurement methods so to combine data and provide insight that could not be achieved with a single technique.

A.1.4 Functional near-infrared spectroscopy

Functional near-infrared spectroscopy (fNIRS) exploits light in the near-infrared range to determine the blood flow related to neuronal activity. It provides high spatial resolution (few millimeters), but poor temporal resolution (few seconds) [36, 145]. Compared to fMRI, fNIRS is portable and less expensive but it provides less imaging capabilities. The potential advantages of this technique include insensitivity to signal perception errors (artifacts) that are typically present in EEG [150]. Hence, a hybrid BCI would benefit from a proper combination of EEG and fNIRS.

A.1.5 Other techniques

In this last subsection, few notes are reported about further measurement techniques related to brain activity detection that go beyond the non-invasive techniques recalled above. As already mentioned above, neuroimaging techniques like electrocorticography (ECoG) or intracortical neuron recording are of great interest in the BCI field because they allow for a superior signal quality. ECoG is usually referred to as “partially-invasive” or “semi-invasive” to highlight its lower degree of invasiveness if compared to intracortical recording. However, the ECoG itself requires a craniectomy by which the electrodes are directly placed on the exposed surface of the brain [151]. Meanwhile, intracortical neuron recording exploits microelectrode arrays placed inside the gray matter of the brain in order to capture spike signals and local field potentials from neurons [98]. Invasive techniques also guarantee lower vulnerability to artefacts such as blinks and eye movement. Nevertheless, despite the advantages from the metrological point of view, there are evident difficulties in considering such techniques in daily-life applications.

Even the already mentioned CT and PET are noteworthy because they are of utmost importance for brain activity monitoring, notably in clinical applications. Computed Tomography (CT) is a technique that has much in common with PET, except that it uses X-rays and a camera to detect and record the activity of the brain. A similar technique is the “single-photon emission computed tomography

(SPECT)” which instead uses γ -rays [42]. Instead, positron emission tomography (PET) is a nuclear imaging technique based on the detection of blood flow and glucose consumption through a small amount of radioactive isotopes introduced into the blood. This technique has high spatial resolutions, down to 2 mm, while temporal resolution is again limited by the dynamics of [148]. In a certain sense, also CT and PET are invasive techniques and they are clearly unsuitable for a brain-computer interface. Indeed, they are poorly considered in the BCI community, unless they would be needed for a medical diagnosis. In conclusion, Tab. A.1 resumes the main

neuroimaging technique	physical property	temporal resolution	spatial resolution	advantages	disadvantages
EEG	electrical potential	10-100 ms	1 cm	low cost wearable portable	noisy sensible to artifacts electrodes placing
MEG	magnetic potential	10 ms	1 mm	deep imaging	expensive bulky
fMRI	blood flow	1 s	1 mm	deep imaging	expensive bulky
fNIRS	blood flow in cortical tissue	1 s	<1 cm	low cost wearable portable	no deep imaging low time resolution
ECoG	electrical potential	1 ms	1 mm	signal quality portable	(semi)invasive
Intracortical	local electrical field potential	1 ms	<1 mm	signal quality portable	invasive
SPECT	blood flow	1 s	1 mm	deep imaging	expensive bulky radiation
PET	blood flow	1 s	1 mm	deep imaging	expensive bulky radiation

Table A.1 Summary of the main characteristics concerning neuroimaging methods.

characteristics of the described neuroimaging techniques. A particular focus is given to the order of magnitudes for the respective temporal and spatial resolutions, and also to the advantages that make a technique suitable for daily-life applications, as well as the disadvantages that eventually make it unsuitable for that purpose.

As a final note, there are two other measurement techniques that are noteworthy for BCI application, but, strictly speaking, they do not measure brain activity. These are the electroculography (EOG), which measures the electric potential between the front and the back of the human eye, and the electromyography (EMG), i.e. the

measuring of the electrical activity of muscle tissue. EOG and EMG artifacts are indeed the most important sources of errors in neuroimaging, thus the measurement of ocular and/or muscular activity is exploited in many artifact removal techniques [45].

A.2 Measuring the electrical brain activity

An electroencephalographic signal, or EEG, is obtained as the potential difference over time between signals of measurement electrodes and the reference electrode signal [98]. Electrodes used for electroencephalography can be wet or dry. For wet electrodes, gel is needed between the electrode and the scalp to reduce the contact impedance down to $1\text{ k}\Omega$ to $10\text{ k}\Omega$. However, the main drawback of gels or electrolytic paste is the long preparation time of the subject and periodic refresh required for good quality signal [98]. Indeed, gel progressively dries out: this determines contact impedance and signal quality is negatively affected. Moreover, care must be taken to ensure that the gel does not slip between the electrodes since this would create a short circuit. On the other side, dry electrodes do not require any gel. These kinds of electrodes may be dry active electrodes, which have pre-amplification circuits for dealing with very high electrode-skin contact impedances, or dry passive electrodes, which have no active circuits, but are linked to EEG recording systems with ultra-high input impedance.

Usually, in multi-channel recordings, the 10/20 electrode system [2] is adopted. The measurement technique is based on standard landmarks of the skull, namely the nasion, which is a craniometric point placed in the midline bony depression between the eyes where the frontal and two nasal bones meet, theinion, other craniometric point that is an external occipital protuberance, and the left and right pre-auricular points. The pre-auricular points are felt as depressions at the root of the zygoma, which are behind the tragus [2]. The system's name is derived from the fact that electrodes are placed in determined positions at 10% intervals and 20% of the distances joining the nasion-inion points and the right and left pre-auricular points. To reduce preparation time of the subject, pre-assembled electrodes are generally already set in standard positions on the headset. The amplitude of oscillations at the brain surface can reach tens of mV, but amplitudes recorded on the scalp are about hundreds of μV [152]. Then, in EEG signal frequency of interest lies in the 0.5 Hz

to 100 Hz range, and specific sub-bands are related to physiological or pathological states [152, 98]. These sub-bands are known as *EEG rhythms* and five are typically distinguished:

- Delta (δ) rhythms: delta waves have frequencies in the 0.5 Hz to 4.0 Hz, and their amplitude is usually under $100 \mu\text{V}$. In adults, delta waves are associated with a state of deep sleep. Delta waves are mostly present in children. Their amplitude decreases with increasing age.
- Theta (θ) rhythms: theta waves have frequencies in the 4.0 Hz to 7.0 Hz, and their amplitude is below $100 \mu\text{V}$. As delta rhythm, theta waves are mostly present in children. In adults, theta waves are associated with states of sleep or meditation. In some adults, theta rhythm is also associated with emotional stress.
- Alfa (α) rhythms: alpha waves have frequencies in the 8.0 Hz to 13.0 Hz, and their amplitude is below $10 \mu\text{V}$. These waves can be recorded during waking state, but they indicate a state of relaxation. In the same range of the alpha waves, but in the motor cortex, the mu (μ) rhythm is also detected. This rhythm is interesting since it is strongly related both to movement, and to the observation of the movement executed by someone else (because of mirror neurons [153]), both to the imagination of the movement (after some training) [151, 154].
- Beta (β) rhythms: beta waves have frequencies in the 13.0 Hz to 30.0 Hz, and their amplitude is below $20 \mu\text{V}$. These waves appear during waking state, when the subject is occupied in a mental activity [151, 111]. Beta rhythms are also associated with motor activity. They are modulated either during real movement and during motor imagery.
- Gamma (γ) rhythms: gamma rhythms have frequencies over 30 Hz and they indicate a state of deep concentration. Some experiments have revealed a relationship in normal humans between motor activities and gamma waves during maximal muscle contraction. Gamma rhythms are less commonly used in EEG-based BCI systems, because artifacts or electrooculography are likely to affect them.

A.3 Measurand brain signals

With the different neuroimaging techniques reported in the previous section, it is possible to measure several types of brain signals. Indeed, there is a relation between the brain activity of interest and the neuroimaging method to employ for its detection. In the present section, the main focus will be on the brain signals measurable through the electroencephalography (EEG for short). However, this does not imply that EEG is the only possibility for such measurements, and surely hybrid approaches are often possible. Then, depending on the available signals and on the final application, a proper processing approach will be adopted.

In following a chronological order, it is convenient to start by introducing “evoked potential” (EP). EPs are variations of the EEG signals occurring as a result of a sensory stimulation. For instance, a largely treated class of EPs are the “visually evoked potentials” (VEP), where brain activity modulations occur in the visual cortex in correspondence of a visual stimulus [155]. Typical visual stimuli are flickering icons or light flashing. Therefore, the VEPs reflect the brain’s processing of visual information [61] and different types can be distinguished according to the kind of information they contain. An interesting distinction is proposed in [91] between transient VEPs (t-VEP), steady-state VEPs (SSVEP or f-VEP), and code-modulated VEPs (c-VEP). In t-VEPs, the frequency of visual stimulation is kept below 4 Hz to 6 Hz so that consecutive flashes do not overlap. The target flashes are mutually independent and they are typically detected by averaging over many signal epochs. Hence, successive epochs must be properly synchronized. Meanwhile, in frequency modulated VEPs (f-VEP), more commonly referred to as SSVEPs, the visual stimulus is a flickering icon with a frequency above 6 Hz. In such a case, the evoked potentials result from the overlapping of consecutive flashes, whose period is lower than a single t-VEP duration [61]. Different targets are therefore distinguished by means of different flickering frequencies and/or thanks to the phase information. Where the phase relation between targets is of interest for the SSVEP detection, a trigger signal is also needed for synchronization. Finally, c-VEPs rely on pseudo-random sequences of bits that modulate the duration of a flashing target. In detecting the response to a code-modulated stimulus, a synchronization of measured signals is needed and a template matching method is exploited to retrieve the code. Higher communication speeds are achievable with a c-VEP [91], but a more complex training of both the user and the algorithm is needed as well. Instead, a trainingless

BCI can be built, at least in principle, by considering SSVEPs. Another important difference between c-VEP and SSVEP is that the first has a broadband spectrum, while the second is characterized by narrow bands. Such considerations are crucial in choosing the processing approach. Generally speaking, evoked potentials recorded with EEG have relatively small amplitudes, so there is the need of proper filtering and amplification to extract the signal features of interest [98].

The discussion conducted for visually EPs can be extended to other evoked potentials, relying for example on auditory or somatosensory stimulation. As a whole, EPs are common measurands in reactive BCI paradigms and, thanks to the EEG, they can be exploited in building non-invasive, wearable and portable brain-computer interfaces for daily-life applications. In particular, the present thesis considers SSVEP-based BCI systems. Meanwhile, it is worth reporting further considerations about a largely exploited transient EP, which is the P300 potential. P300 EPs are positive peaks in the EEG elicited by infrequent visual, auditory, or somatosensory stimuli (flashes) [32]. The P300 wave is an endogenous response elicited about 300 ms after attending the stimulus. As already highlighted for SSVEPs, the use of P300-based BCIs does not necessarily require training. However, some studies have proven that the less probable the stimulus, the larger the amplitude of the response peak, and for that reason the system performance may be reduced if the user gets used to the flashes [98]. Also, P300-based BCIs speed is limited by the averaging process that is usually required in transient EP detection. On the other hand, it is possible to distinguish among many targets in a P300 paradigm, and for that reason these EPs are mostly exploited in building BCI spellers [156]. Despite this advantage, P300 was not considered in the present work, but it could be taken into account in a near future to furtherly investigate hybrid paradigms.

As further relevant measurand signals, sensorimotor rhythms comprise μ and β rhythms, which are oscillations in the brain activity localized in the mu band (7.0 Hz to 13.0 Hz), also known as the Rolandic band, and beta band (13.0 Hz to 30.0 Hz), respectively [98]. The amplitude of the sensorimotor rhythms varies when cerebral activity is related to any motor task although actual movement is not required to modulate the amplitude of sensorimotor rhythms. Similar modulation patterns in the motor rhythms are produced as a result of mental rehearsal of a motor act without any overt motor output. Sensorimotor rhythms have been used to control BCIs, because people can learn to generate these modulations voluntarily in the sensorimotor rhythms [98]. Studies [154] proved that, through the only imagination of the move-

ment (motor imagery), it is possible to start variations in sensorimotor rhythms like the ones associated with real movements [98]. Sensory stimulation, motor behaviour, and mental imagery can change the functional connectivity within the cortex and results in an amplitude suppression, the event-related desynchronization (ERD), or in an amplitude enhancement, the event-related synchronization (ERS), of mu and central beta rhythms. The dynamics of brain oscillations associated with sensory and cognitive processing and motor behaviour can form complex spatio-temporal patterns. Thus, a synchronization of higher frequency components embedded in a desynchronization of lower frequency components can be found on a specific electrode location at the same moment of time [157]. Voluntary movement induces ERD of μ and β sensorimotor rhythms [158]. Desynchronization begins in the contralateral hemisphere 2 s before the motor act, then it becomes symmetric during the execution of the movement [158]. The same ERD desynchronization can be revealed during motor imagery [158]. ERD desynchronization is often followed by ERS synchronization in the ipsilateral hemisphere, with similar frequency components [158]. One important feature of these beta oscillations is their strict somatotopic organization in MEG and EEG [157]. For this reason, patterns associated with the imagination of the movement of a hand can be distinguished with respect to the ones associated with the movement of the other hand. To properly record ERD and ERS, the EEG electrodes must be located close to the primary sensorimotor areas. Usually, the most interesting electrodes for these studies are C3 and C4. However, since two bipolar derivations are insufficient to describe the overall brain activity, it seems reasonable to assume that more EEG signals recorded over sensorimotor areas, which are sensitive to differences between left and right imagery, would improve the classification accuracy of the BCI [159]. Furthermore, although electrodes close to primary sensorimotor areas contain the most relevant information for discrimination, surrounding electrodes over premotor and supplementary motor areas also contribute some information to discriminate between brain states related to the motor imagery task [159]. Obviously, the more signals are recorded, the less BCI systems are portable because of the great number of electrodes and because of proportionally longer preparation times. Sensorimotor rhythms are utilizable for the design of endogenous BCIs, which are more useful than exogenous BCIs. Nevertheless, self-control of sensorimotor rhythms is not easy, and most people have difficulties with motor imagery. People tend to imagine visual images of related real movements, which is not sufficiently useful for a BCI system, because the patterns of these

sensorimotor rhythms differ from actual motor imagery [98]. Sensorimotor rhythms have been investigated extensively in BCI research. Well-known BCI systems such as Wadsworth, Berlin, or Graz BCIs employ sensorimotor rhythms as control signals [98].